Computational fluid dynamics (CFD) based approach to consequence assessment of accidental release of hydrocarbon during storage and transportation

by

© Muhammad Masum Jujuly

A thesis submitted to the School of Graduate Studies in partial fulfillment of the requirements for the degree of

Masters of Engineering

Faculty of Engineering and Applied Science

Memorial University of Newfoundland

May, 2016

St. John's Newfoundland

Abstract

This thesis investigated the risk of accidental release of hydrocarbons during transportation and storage. Transportation of hydrocarbons from an offshore platform to processing units through subsea pipelines involves risk of release due to pipeline leakage resulting from corrosion, plastic deformation caused by seabed shakedown or damaged by contact with drifting iceberg. The environmental impacts of hydrocarbon dispersion can be severe. Overall safety and economic concerns of pipeline leakage at subsea environment are immense. A large leak can be detected by employing conventional technology such as, radar, intelligent pigging or chemical tracer but in a remote location like subsea or arctic, a small chronic leak may be undetected for a period of time. In case of storage, an accidental release of hydrocarbon from the storage tank could lead pool fire; further it could escalate to domino effects. This chain of accidents may lead to extremely severe consequences. Analyzing past accident scenarios it is observed that more than half of the industrial domino accidents involved fire as a primary event, and some other factors for instance, wind speed and direction, fuel type and engulfment of the compound. In this thesis, a computational fluid dynamics (CFD) approach is taken to model the subsea pipeline leak and the pool fire from a storage tank. A commercial software package ANSYS FLUENT Workbench 15 is used to model the subsea pipeline leakage. The CFD simulation results of four different types of fluids showed that the static pressure and pressure gradient along the axial length of the pipeline have a sharp signature variation near the leak orifice at steady state condition. Transient simulation is

performed to obtain the acoustic signature of the pipe near leak orifice. The power spectral density (PSD) of acoustic signal is strong near the leak orifice and it dissipates as the distance and orientation from the leak orifice increase. The high-pressure fluid flow generates more noise than the low-pressure fluid flow. In order to model the pool fire from the storage tank, ANSYS CFX Workbench 14 is used. The CFD results show that the wind speed has significant contribution on the behavior of pool fire and its domino effects. The radiation contours are also obtained from CFD post processing, which can be applied for risk analysis. The outcome of this study will be helpful for better understanding of the domino effects of pool fire in complex geometrical settings of process industries. The attempt to reduce and prevent risks is discussed based on the results obtained from the numerical simulations of the numerical models.

Acknowledgements

First and foremost, I would like to express my profound gratitude to my supervisor, Dr. Faisal Khan, and co-supervisors Dr. Aziz Rahman and Dr. Salim Ahmed for their support, motivation, encouragement, supervision and suggestions throughout the research work. Their extensive guidance motivated me to complete my research work successfully. Besides my advisor, I would like to thank Dr. Premkumar Thodi for his continuous encouragement, insightful comments. His knowledge and technical suggestions helped me to develop the model successfully. I also acknowledge the support provided by INTECSEA Canada, MITACS at Memorial University of Newfoundland, Petroleum Research Newfoundland & Labrador (PRNL), Vale Research Chair Grant, Research & Development Corporation (RDC) of Newfoundland & Labrador and Natural Sciences and Engineering Research Council (NSERC) of Canada.

I would like to thank my fellow lab mates: Samith Rathnayaka, Junaid Hassan, Aminul Islam Khan, Dan Chen, Omit Mehfuz and all other members of Safety and Risk Engineering Group (SREG) for their valuable ideas, discussions and help in every aspect during this time. Finally, I would like to specially thank my parents, relatives and friends for their support and encouragement to pursue this degree.

Table of Contents

List of Tables

List of Figures

List of Symbols and Abbreviations

Symbol	Definition
ρ	Density of fluid in kg/m^3
P	Static pressure in Pa
T	Temperature in K
k	Turbulent kinetic energy in j/kg
σ_ω	Prandtl number for ω
g	Gravitational acceleration in m/s^2
v	Velocity vector in m/s
μ	Viscosity of fluid in m^2/s
ϵ	Eddy dissipation rate in m^2/s^3
σ_k	Prandtl number for k
ϕ	Volume of fraction
A	Leak orifice area in m^2
ΔP	Differential pressure in psi
N	Coefficient factor
dP/dX	Pressure gradient in Pa/m
PSD	Power spectral density

FFT	Fast Fourier transformation
LES	Large eddy simulation
DO	Discrete ordinates
Y_α	Mass fraction of species α
RTE	Radiative transfer equation
σ	Stefan-Boltzmann constant ($5.67 \times 10^{-11} kW/m^2K^4$)
$\widetilde{Y_s}$	Soot mass fraction in kg/kg
X_N	Specific concentration of radical nuclei in mol/kg
$\dot{m}$	Mass burning rate of fuel in kg/m^{2}s
RAM	Random-access memory
SEP	Surface emitting power in kW/m^2
L/D	Mean ration of pool fire length and diameter
u_w	Wind speed in m/s
PRV	Pressure relieving valve
CFD	Computational fluid dynamics
LNG	Liquefied natural gas
RANS	Reynold's Average Navier-Stokes
DES	Direct numerical simulation

Chapter 1

Introduction

1.1 Overview of Storage and Transportation Risks

Risks of hydrocarbon storage and transportation are evaluated in this study. There are numbers of incidents in hydrocarbon storage and transportation occurred including LaSalle, Quebec (1965); Bucheon LPG filling station, Korea (1998); Ath, Belgium (2004); Buncefield, UK (2005); Puerto Rico, USA (2009); Sitapura, India (2009); Oakville, Ontario (2010); Nirobi pipeline fire, Kenya (2011); Sinopec Corp pipeline explosion in China (2013) and most recently Tianjin, China (2015); where not only property losses were high, the death tolls were also enormous. In addition to asset and human loss, the reputation of the operating companies were plunged down. Conducting experiments to simulate an industrial hydrocarbon fire scenario at this magnitude are extremely difficult and time consuming. Thus, to evaluate possible risks of nearby storage and transportation area a numerical approach is employed. The small scale fire and explosions can be studied by experiments but the extrapolations of small scale fire and explosion model to large industrial scale accident scenario is a challenge. Therefore, the numerical approach is required to develop computational fluid dynamics modeling which is capable to model both experimental and real case accidental fire scenario with complex combustion process, and with complex geometry.

A computational fluid dynamics software ANSYS platform is used to quantify the risks involved. It gives wide degree of freedom to the users regarding the three dimensional hazard scenario for actual visualization. Moreover, numerical methods provide more spatial and temporal fidelity than analytical solutions. Analytical solution of a mathematically defined problem is possible but the simplistic analytical models based on limited boundary conditions and poor assumptions often lead to model error. Complex analytical models are time consuming and highly non-linear equations are not even possible to solve with analytical techniques. For instance, there are two major types of analytical models of pool fire, the point source model and the solid flame model. The point source thermal radiation models are based on the assumptions that the flame is a single point source of thermal energy and the thermal radiation intensity varies inversely with the square of the distance. The point source model can predict radiation in larger distances from the flame but in closer distances it underestimates the thermal radiation. In the solid flame model a cylindrical shaped flame zone is considered as a radiating object. This model assumes similar irradiance of fire throughout the solid circle zone. Advanced turbulence model is not used in these models to capture the full dynamics of pool fire in eddy scale. During the wind scenario the tilt of the flame as a solid cylinder is practically not valid. In case of complex geometries these models cannot predict the exact behavior of pool fire. Moreover, with analytical methods the domino effect cannot be fully captured. Although numerical methods are relatively complex, but they can reliably predict radiation hazard [1].

There are a number of risk scenarios involved in hydrocarbon storage and transportation operation. Many of these can be anticipated but not all of these are accounted for catastrophic disaster. The possible risk scenarios are [2]:

- Subsea pipelines and subsea blowouts will result in dispersion of hydrocarbon release in aquatic environment
- Leakage when loading the crude hydrocarbon to the processing unit
- Leakage from the storage tanks results pool fire or toxic release
- Leakage from the pipelines attached to the storage tanks results fire and explosion
- Traffic accidents within or outside of the perimeter leads fire and explosion
- Natural disasters (i.e. earthquake or lightening) could cause toxic release or fire and explosion
- Terrorism or vandalism causing toxic release or fire and explosion

There could be more unforeseen events which can lead to a major incident during hydrocarbon handling. Only two major scenarios will be considered in this thesis, leakage from the subsea export pipelines and the leakage from the storage tanks. Consequences of these two scenarios will lead toxic dispersion at aquatic environment and the result of fire and explosions which are the most frequent accident scenarios [3, 4].

1.1.1 Overview of Storage Facilities Risks

The largest quantities of hazardous material are found in storage facilities; consequences of the storage accident are also severe. The hazard of toxic release and fire and explosion in storage may cost both financial losses and the loss of life. Smokes, heat radiation and toxic fluid dispersion resulting from fire and explosion of storage and transportation lines are the largest threat for the whole operation of petroleum industries [1].

The leakages at the storage tanks and the transportation pipelines are also very common phenomena. The probabilities of fire and explosion risk are higher if there is a leakage in the storage tanks or the transportation pipelines. The leakage from the loading, storage tanks or the adjunct pipelines can cause fire and explosions. Since the 1950's more than 450 tank fire incidents have been identified worldwide. Tank fires are estimated to be around 15-20 every year [5].

One of the main reasons of fire and explosions is the discharge of gasoline from the leakage of storage tank and from the adjacent pipelines of the tank. Pipelines are used to transport the hydrocarbons from the tanker to the reservoir or vessel for storage and from the tanks to the transportation trucks via the loading racks. There are thousands of connections, joints and valves between pipes and tanks. According to the design specification, those connections have to be tight enough to avoid any leakages but that is not the case all the time. Corrosion, metal fatigue due to external stresses, erosion in welding joints are the problems that brought up since tanks and pipelines are made of metals [2]. A minor spark from the static electricity could ignite the hydrocarbons. There

could be some other sources of ignitions for instance ignition due to explosion energy, external heat from the surroundings, or flash ignition from flammable vapour-could mixtures [6].

1.1.2 Overview of the Pipeline Transportation Risks

Pipeline is one of the major mode of transportation of hydrocarbons. Pipeline carrying hydrocarbons and other flammable materials can be exposed by jet fire or flammable vapour cloud, leading flash fire or vapour cloud explosion (VCE). Another major accident scenario for pipeline transportation is the liquid spillage, which can lead to pool fire or the toxic liquid dispersion. The older pipelines were made of mild steel or cast iron, however, the standards of construction and protection of pipelines have been improved to prevent catastrophic accidents. In order to minimize the external corrosion cathodic protection is utilized with combination of wrapping the pipeline by tar or glass fiber. Intelligent pigging is introduced to inspect the internal corrosion in order to prevent the pipeline leakage [1].

Table 1-1: Cause of failure of inter-state natural gas transmission pipelines in USA 1950-1965 [1].

Hazardous events	**Frequency of occurrence**
Pipelines punctured by plough, bulldozer, excavating shovel, road grader or any other equipment	279
Corrosion: Corrosion at external pipe surface Corrosion at internal pipe surface	 148 45
Welding failure	190
Action of the elements	84
Coupling failures	65
Damage during installation	58
Fatigue failures	35
Defective pipe	26
Thermal stress	21
External explosion	14
Miscellaneous	38
Unknown/unreported	55
Total	**1058**

Table 1-2: Hazardous events for the storage of toxic and flammable materials [1]

Hazardous events			
Materials	**State**	**Storage condition**	**Hazardous events**
Flammable	Liquid	Atmospheric	Liquid release, tank fire, tank explosion
	Liquefied gas	Pressure	Flashing liquid release - flammable vapour cloud, liquid pool, pool fire, jet fire, VCE, jet fire, BLEVE
	Liquefied gas	Refrigerated	Flashing liquid release - flammable vapour cloud, liquid pool, tank fire, VCE, fire engulfed tank, tank fire, bund pool fire, running fire
Toxic	Liquid	Atmospheric	Liquid release, toxic gas could, tank explosion, toxic gas cloud
	Liquefied gas	Pressure	Flashing liquid release - flammable vapour cloud, liquid pool, toxic gas cloud
	Liquefied gas	Refrigerated	Flashing liquid release - flammable vapour cloud, liquid pool, toxic gas cloud, fire engulfed tank.

Table 1-1 shows the cause of failure of natural gas transmission pipeline in the USA from 1950-1965, during this fifteen years only there were 1058 failures causing 64 deaths and 135 injuries. According to conservation of clean air and water in Europe (CONCAWE), during the period of 1972-76 there were 93 spillages by pipeline in Europe and the failure rate is 1.05×10^{-3} /km-year. The failure rate was 0.5×10^{-3} /km-year for the period 1987-1991. Table 1-2 shows the consequences of the failures described in Table 1-1.

In case of subsea pipelines the main hazard is the leakage. The subsea condition may likely be harsh as well as remote and inaccessible. Arctic marine pipelines can be damaged by contact with drifting iceberg. Intense deformations could occur beneath a gouge, and a trenched pipeline might still be damaged. Pipeline can also be plastically deformed by seabed shake down event as a consequence of ice gouging. It can lead to catastrophic events and can have adverse effects on wildlife, environment, economy and the reputation of the company since it is very difficult and expensive to clean up oil spill in harsh environment like arctic and subsea [3].

1.2 Motivation of the Research

Pipeline failure during transportation and vessel failure during storage of hydrocarbons or flammable materials are the most frequent accidents. Thus, the risk of the leakage from the subsea export pipelines and pool fire due to vessel failure is immense. There are numbers of studies conducted on safer process plant design in order to maintain safe workplace and several safety codes are available in contemporary literatures. A number of safety guidelines have been proposed to prevent accidents. Still storage tank and pipeline transportation are considered as a serious threat for the industries dealing with hydrocarbons and flammable materials; and this is the primary motivation to conduct numerical modeling of the subsea pipeline leak and the pool fire from the storage tank.

According to Khan and Abbasi (1999), of the 3222 accidents from 1926-1997, 54% are fixed installation, 41% are transportation and 5% miscellaneous accidents. Further, 18% of the 1320 transportation accidents can be classified during pipeline transport which are 228 cases. The same study also revealed that there are 1744 significant accidents occurred during 1928-1997 due to the vessels or equipment failure. 25% of the 1744 accidents involve fire and explosions and the rest involves toxic release or the combinations of fire, explosion and toxic release [7].

1.2.1 Research Motivation of Numerical Simulation of Pipeline Leakage

Numerical simulation of pipeline leakage in subsea condition is relatively new and very promising research area. From research perspectives, it is difficult to conduct experiments on subsea pipelines. In some events, the pipeline fluid transfer has to shut down to conduct a proper experiment. Furthermore, because the industrial full-scale pipeline is large in diameter, pipeline hydrodynamics cannot be captured accurately in a small-scale, lab environment. Thus, a numerical simulation can provide a better understanding of pipeline flow and the consequences of pipeline leaks in different scales, reducing the cost and number of experiments. ANSYS computational fluid dynamics software can be used to serve this purpose. ANSYS workbench provides integrated modular design, meshing technology, and large degree of freedom for pre- and post-processing for the fluid flow simulation in pipeline. Most importantly, ANSYS is highly interactive which will allow for better visualization of the problem and its solution.

1.2.2 Research Motivation of Numerical Simulation of Hydrocarbon Pool Fire

Like the subsea pipelines, it is also very challenging to conduct experiments involving pool fire resulting from vessel failure; especially experiments to study domino effects. There are several analytical and semi-empirical methods to calculate the radiation intensity and overall risk evaluation, however, those methods have limitations in case of complex three dimensional geometry. Under valid assumptions and boundary conditions, CFD models have much better temporal and spatial dependability than point source or

solid flame models. The three dimensional simulation of complex geometrical structure of a process plant can be performed by CFD. Apart from some constraints like simulation time and valid boundary conditions, CFD is the most reliable and realistic method for calculating risk from fire hazard [25].

1.3 Objectives of the Research

There are two major objectives of this research. The first one is to perform numerical investigations of subsea pipeline leakage. The pressure noise data generated for the leak at the pipeline was processed through FFT (Fast Fourier Transform) and presented data for different leak locations around the leak. The response of pressure and temperature frequency domain to input perturbations will be calculated from a steady state simulation. The local pressure and temperature contours will also be generated and these contours will help to identify the position of the leak. Thus, the flow in a pipe and response to a leak will be studied. The influence of size of the leak on the test fluid pressure and temperature distribution will also be investigated. Leaks create acoustic signatures due to the high turbulence and high pressure around the vicinity. A transient simulation using large eddy simulation (LES) will be used for simulating acoustic signature of the leakage. Another objective is to investigate the fate of the fluid after its release. CFD method is able to perform proper consequence modeling as a part of a risk assessment. Simplified method for dispersion prediction is generally not very useful, however, CFD tools have the potential to model the relevant physics and predict the dispersion pattern well. Not

many numerical studies are currently available on the dispersion of hydrocarbon from a small leakage in subsea environment; this study can be a potential milestone. Leakages from a pipe can result in damage to the ambient environment depending on the total amount of released hydrocarbon and the concentrations in the proximity of the leakage, even there is a chance that hydrocarbons will dissipate or ignite and explode. The pipeline leakage consequence model would quantify the hydrocarbon volume released during the chronic small leakage. The vector plot and the velocity profile of the leaked fluid would accurately provide the information on the fluid dispersion and its migration path. Plume trajectory as well as mixing behavior with the initially stagnant atmosphere will be analyzed and presented in the form of space–time concentration distribution and distances to a given concentration. The leakage flow patterns along with the leakage diameters can also be observed using this study.

The second objective of this research is to develop a numerical model for pool fire. Liquefied natural gas (LNG) is used as the fuel. In this work, the computational fluid dynamics approach is used to evaluate the effects of environmental conditions on the domino effects of an LNG pool fire. Another important feature of this study is the analysis of the effects of pool fire on the surrounding processing units using the CFD post-processing results. From the effect of local temperature of the processing units the safe distance of the adjunct tank with flammable liquids can be determined. The domino effect accident scenarios have been discussed. The radiation contours and the local temperature distribution can be used to calculate risk of the domino effect escalation. The

maximum thermal radiation intensity and the temperature received by the processing units can be used to perform hazard analysis.

1.4 Contributions

The key contributions of this thesis are described below:

i. A numerical investigation has been performed to determine the patterns of fluid flow inside the pipeline and particle dynamic study of local parameters (i.e. pressure, temperature, turbulence kinetic energy, pressure gradient, velocity vectors, etc.). The sensitivity study of local parameters using different fluids and leak sizes provided deeper insight into the leakage flow. A general correlation among the pressure, leak size and flow rate from leak orifice for different test fluids have been established. A transient simulation model has been developed to generate the acoustic signal from the leak orifice. The acoustic signal generated for the pipelines, with small chronic leak, indicated that the influence of leakage on the generated acoustic signal is significant. Further analysis is needed to explain the acoustic signal with respect to the leak characterization. Fluid dispersion trajectories to the ambient were studied as well, and it revealed the fate of fluid (i.e. dispersion) after leakage.

ii. The pool fire characteristics and hazard analysis has been performed using numerical approach. CFD simulations of unconfined pool fire with temperature and thermal radiation profiles of the flame in quiescent and in present of wind condition are studied in order to observe the effect of wind to the pool fire. Thermal radiation contour plots of the

pool, maximum heat flux received by the units (e.g. tank), and maximum temperature distribution of flame and units in quiescent and in the presence of wind provide the information about the threshold value for the failure of the units due to the thermal radiation. Relation between the flame tilt angles (from vertical) and the flame drag with wind speed has also been established. The temperatures and irradiances received by the tanks due to the flame tilt and drag have been observed. Taking all these into consideration, a safe distance between vessels filled with flammable material with a property value has been suggested. In order to prevent the secondary accident scenario the impounding between vessels are necessary. This study also suggested that the impounding can be either done by increasing the spacing between the neighboring vessels or using a dike. Simulation results showed that the temperature is higher at the upper portion of the tank as the flame tilted by the wind. Thus the height of the dike, painted with thermal radiation reflective colors, should be higher which not only control the spill, also resist from the thermal radiation of any accident scenario.

1.5 Organization of the Thesis

This thesis is written in manuscript format. Outline of each chapter is explained below:

Chapter 1 is a brief introduction of the risks associated with storage and transportation of hydrocarbons. The research objectives and the contributions of the research are mentioned in this section.

Chapter 2 is the literature review part of this thesis. Existing methodologies of evaluating pool fire hazard and risk of the exposure of hydrocarbons at subsea conditions are discussed in this chapter.

Chapter 3 presents the subsea pipeline leak modeling using computational fluid dynamics simulations. Two different models have been developed. A model of flow inside the pipeline with leakage as well as a dispersion model of escaped fluid flow outside of the pipeline are developed. This chapter is submitted to the Process Safety and Environmental Protection (PSEP) journal.

Chapter 4 presents the liquefied natural gas pool fire simulation for domino effect analysis. Two different scenarios have been considered in this study, the temperature and radiation intensity of the burned hydrocarbon in presence of wind and in quiescent condition. This chapter has been published in Reliability Engineering and System Safety journal on March, 2015 (Ref. No.: RESS-D-14-00570R1).

Chapter 5 is the overall conclusion of the study and further potential research scope in this area.

Chapter 2

Literature Review

2.1 Preface

In this section a literature review on pipeline leakage modeling, consequences of the pipeline leakage, pool fire and the analytical and computational modeling approach of pool fire and fluid dispersion from pipeline leakage has been discussed. The purpose of the literature survey is to briefly recapitulate the updated research.

Fire, explosion and toxic fluid dispersion due to the damage of the storage tank and pipelines are most common accidents and considered as serious threats for the industries that store and/or transport hydrocarbons and relevant flammable and toxic materials. To protect the industries from such catastrophic incidents, advanced research and development is required. A substantial work on accident modeling and probabilistic approach of risk assessment has been done already [6,7]. Industries always require a practical solution for process safety which can be implemented easily and the probabilistic analysis provides good quantification numbers which relevant industries can follow and implement. However, employing numerical method could provide more insights of the problems and the quantification of risk involved in a process can be estimated more accurately.

In this study a computational fluid dynamics approach is used to study subsea pipeline leakage and resulting fluid dispersion. The characteristics of pool fire resulting from storage tank failure and its consequences, i.e. domino effect are also studied.

2.2 Pipeline Leakage

Pipeline leak modeling through numerical approach or computational fluid dynamics (CFD) simulation is relatively a new area. Handful amount of literatures are available on this topic. Ben-Mansour et al. (2012) developed a 3D turbulent flow model with 10 cm diameter pipeline to detect the small leakage (1mm x 1mm) for a water distribution pipeline using ANSYS FLUENT. Both steady state and transient simulations were performed in this study. For the turbulence model authors used κ-ε for steady state and DES (Detached Eddy Simulation) for transient simulation. The pressure noise signals were measured for different locations around the leak and processed through FFT (Fast Fourier Transform). The results indicated that the presence of leak at the pipeline cause measurable difference in the magnitude and frequency of the pressure signal spectrum. An important conclusion from this literature, FLUENT package is preferable in order to simulate the acoustic signatures in ANSYS because FLUENT supports acoustic sub-model based on FFT theorem. However, only the noise due to pressure is discussed in this study. The effect of temperature is not discussed. No sensitivity study has been performed varying the leak size and shape. Also, no comparative study on different fluids has been performed as part of this work [10]. Olivares et al. (2009) presented the effect of

temperature and pressure to the leak noise at a district water heating pipeline but no sensitivity studies has been performed in this study either [11]. Liang Wei et al. (2013) developed a leak detection system based on the acoustic technology. The acoustic field is estimated with several pipeline pressures, and with a 4 mm diameter leak orifice. The vibration signal data caused by leak has been presented [12]. A hydrodynamic study of pipeline with oil leakage is performed by de Vasconcellos Araújo et al. (2014). In this study a model with two leaks including a Tee junction were developed. The influence of the leak in the flow dynamics parameters and the behavior of the fluid were analyzed using velocity vectors and pressure fields [13]. The ANSYS CFX software was used for the numerical simulation. Zhu et al. (2014) developed a numerical model to simulate oil leakage from damaged submarine pipeline. In this study, the effects of oil properties, leak rate and leak size has been examined. The FLUENT package to model 2-D transient simulation has been used [14]. Another similar work of subsea gas dispersion model was developed by Cloete et al. (2009). The volume of fluid (VOF) model was used for the simulation. In both models, the migration pattern of the spilled oil and the time required for the migration was identified [15]. There is no combined study on leak characteristics based on acoustic model and the consequences has been performed which are the primary goal of this current study.

2.3 Pool Fire

Fire and explosions are among the most dangerous accidents in process facilities; especially pool fire is the most frequent incident. Pool fire is responsible for triggering 44% of all physical accidental scenarios which escalate domino effect [16]. Pool fire characteristics largely depend on the fuel mass burning rate which is a function of the fuel properties, pool diameter and wind speed. Zabetakis and Burgess et al. (1961) proposed their correlation of mass burning rate for radiation prevailing heat transfer region by modified Hottel (1951) work [17]. However, they have ignored the convective heat transfer to the pool and the effect of the heat of combustion. Mudan et al. (1984) developed an expression for the mass burning rate that gives better results for liquefied gases (e.g. LNG, LPG) but less accurate for predicting the burning rate of other fuels [18]. Fay et al. (2006) considered convection as a major mode of heat transfer to the liquid pool as Hottel (1951) suggested for the pool burning rate but ignored the radiative mode of transmission [19]. There are several experimental studies e.g. Koseki et al. (2000) used crude oil, Chatris et al. (2001) used gasoline and diesel, T. Blanchat et al. (2008) used JP8 fuel and Mishra et al. (2008) used kerosene and peroxides as fuel but all experimental studies are based on small pool diameters (less than 10 m) [20-23].

In order to describe thermal radiation from a large pool fire, point source model and different semi-empirical models has been developed such as: zone model, field model, integral model etc. Zone models are based on the differential equations for mass and energy balance. Field models are stationary model, based on solving the time average Navier-Stokes PDE with some empirical sub models. Moorehouse and Pritchard (1982)

calculated the maximum surface emitting power (SEP) from a point source model [24]. The point source model can predict radiation in from the flame but since it underestimates the thermal radiation so in closer distance this model is ineffective. Solid flame models and the modified solid flame models are widely used as alternatives of the point source model. The solid flame radiation method has certain limitation on determining the grey gas emission value and this method gives very conservative values. Solid flame model can be modified to get better result. In case of complex geometries these models cannot predict the exact behavior of pool fire [25]. Analytical methods are easy to calculate the radiation hazard because of their simplicity. However, analytical methods are very case specific and cannot be applied to complex geometries. Moreover, with analytical methods the domino effect cannot be fully captured. Although numerical methods are relatively complex, they can reliably predict radiation hazard. Few studies have been performed using computational fluid dynamics (CFD) for numerical investigation of fire related hazard. These are explained in details in the section 4.1.

2.4 Consequence Analysis of Fire, Explosion and Fluid Dispersion

The consequences of fire and explosions are severe for both on-shore and offshore process facilities and the transportation pipelines. Although there are safety systems installed but to envisage the accidents are highly uncertain. A process area is never free of risk and there is always rooms for improvements. Among all other types of accidents, fire and explosions and the toxic fluid dispersion from pipeline or storage tanks are the most frequently reported accidents. These types of accidents have the potential to cause deaths

or serious injuries as well as to cause major damage to equipment and disruption of operations. Pula et al. (2006) proposed a grid based approach for fire and explosion consequence analysis. In this study a review of existing consequence models, such as, source models, dispersion models, ignition models and fire as well as fire and explosion models were discussed in case of offshore operations. Results from this study could be useful to design the protective layers (the barriers between the accidents and receptors). However, the grid based consequence study is two dimensional analysis and the pool fire characteristics is not discussed in this study [53]. Mohammad et al. (2013) proposed an integrated approach for fire and explosion consequence modeling using specialized computational fluid dynamics codes FLACS and FDS. These CFD codes were used to simulate the potential liquid and gas release incidents. The results were then analysed and presented in the form of injuries/death ratio of the accident. Both pool fire and explosions have been considered in this study but the effect of the wind velocity on fire and explosion has not been considered in this study [54]. Koo et al. (2009) conducted study on accident scenario of LNG terminal using PHAST software. This study showed that the accident would have an impact on areas outside the plant boundary and secondary pool fire is more catastrophe than primary pool fire [9]. Gavelli et al. (2011) analyzed the consequences resulting from the ignition of LNG vapor cloud dispersion during the offloading process. FLACS CFD codes were used to model the vapor cloud dispersion and ignition. The study showed that the sequences of events led to a pool fire after the release of LNG and ignition [55, 56]. Recently ANSYS CFX and FLUENT are becoming more popular for the numerical investigation of fire, explosion, fluid dispersion and consequence analysis. Ruifeng et al. (2010) used ANSYS CFX-11 to perform simulations

of LNG vapour dispersion and its consequences; a parametric study was performed to study the effects of atmospheric conditions, LNG pool diameter and turbulence intensity, and the presence of obstacles [57]. Sun, B. et al. (2014) conducted a 3-D CFD simulation of LNG pool fire using ANSYS FLUENT-14; an advanced turbulence model large eddy simulation (LES) was used to simulate the pool fire with additional sub-models for combustion and radiation. The model outcomes were then compared with experimental results for validation [47].

There are several studies on the pipeline risk consequence analysis. Dinovitzer et al. (2004) conducted a risk assessment on offshore arctic pipeline oil spill. In this study consequence model of a pipeline was developed to quantify the oil volume released during pipeline failure events associated with pipeline leakage, rupture and crack. The model also considered leak detection and the time to detect the leak, shutdown and line evacuation. The consequences of oil spill at the ocean are analyzed and also the hazard study has been performed to quantify the risks in terms of the volume of oil spill. However, in this study the gas pipeline leakage and the sensitivity study of spill depending on the leak size has not been discussed [26]. Zhu et al. (2014) proposed a two dimensional model of the oil leakage from the damaged submarine pipelines. In this study a two dimensional domain is used to observe the effect of leak size and water velocity to the leak rate and the migration time of the dispersed oil to the sea surface [34]. A similar study has been performed by Li et al. (2012) using FLUENT software package [27]. But none of these studies provides integrated approach on the leak detection and the fate of the fluid using numerical method.

Chapter 3

Subsea Pipeline Leak Modeling using Computational Fluid Dynamics

Muhammad Masum Jujuly, Premkumar Thodi, Aziz Rahman, Faisal Khan

Safety and Risk Engineering Group
Faculty of Engineering & Applied Science,
Memorial University of Newfoundland, NL, St. John's, A1B 3X5, Canada.

Preface

A version of this manuscript is submitted in the Process Safety and Environmental Protection (PSEP), August 2015. The co-authors of this research work, Dr. Thodi and Dr. Rahman supervised the principal author M. Masum Jujuly to develop the research methodology on the entitled topic and helped him to conceptualize the techniques and theories available for this topic. Corresponding author Dr. Khan was the principal supervisor of this work and provided knowledgebase support to the author and co-authors.

Abstract

Leakage of pipelines in subsea environment can have severe consequences. Leak detection and location identification in a timely manner is crucial because of the economic impact of a hydrocarbon spill to its stakeholders can be huge. Pipeline leakage could have an adverse impact on life, the environment, the economy and corporate

reputation. In this paper, a numerical modeling of a subsea pipeline leakage is performed using a 3-D turbulent flow model in computational fluid dynamics (CFD). Four different types of fluids are tested in this study, with specified operating conditions. The CFD simulations showed that the flow rate of the fluid escaping from the leak increases with pipeline operating pressure. The static pressure and pressure gradient along the axial length of the pipeline have been observed to have a sharp signature variation near the leak orifice. This signature has been captured using pressure gradient curves. The temperature profiles near leak orifice indicate that the temperature is observed to increase slightly in the case of incompressible fluids; however, temperature drops rapidly for the compressible fluids. Transient simulation is performed to obtain the acoustic signature of the pipe near leak orifice. The power spectral density (PSD) signal is strong near the leak orifice and it dissipates as the distance and orientation from the leak orifice increase. The high-pressure fluid flow generates more noise than the low-pressure fluid flow. In order to model the turbulence, large eddy simulation (LES) was used and Ffowcs-Williams and Hawking (FW-H) model in FLUENT was activated to generate acoustic data. Time step of the simulation was selected $\Delta t = 0.0005$ s and the number of iteration was 20000 to get higher frequency noise signal.

Keywords: Computational fluid dynamics (CFD), pipeline leak modeling, acoustic model, subsea pipeline, dispersion model.

3.1. Introduction

3.1.1 Background

The purpose of this study is to investigate subsea pipeline leaks and their impact on the surroundings. A numerical approach using a computational fluid dynamics (CFD) software package ANSYS FLUENT is employed. The subsea condition may likely be harsh due to the remoteness and inaccessibility. Arctic marine pipeline can be damaged by contact with drifting iceberg. Trenched pipeline is at risk as well, as it may be damaged by corrosion or it could be plastically deformed by the resulting seabed shake down event [28] or dropped objects. Furthermore, due to the remoteness and harsh environment of the ocean, it may be difficult to conduct regular repair procedures. It is imperative to take additional precautions while operating in the subsea region, so rapid leak detection and location identification is crucial. Failure to do so may result in catastrophic incidents; cleaning up an oil spill in a harsh environment would be difficult and expensive, and also it could have an adverse effect on wildlife, environment, economy, and the corporate reputation. Evidence comes from the 2.5% drop in the price of BP shares that followed the Trans-Alaska pipeline leak in 2006 [38]. Although these pipelines are precisely designed not to leak, leaks may still occur due to aforementioned reasons. Development of a method for detecting small, chronic leaks will allow operators to reduce risks involved with hydrocarbon spillage [29].

Traditional approaches to detect subsea pipeline leaks are based on internal flow condition measurements (e.g. internal pressure, flow rate, mass/volume balance), which

are good for detecting large and small pipeline leakage in normal environmental condition. However, subsea pipelines require special and improved systems to detect very small chronic leaks reliably. Without this, a small chronic leak that is below the threshold of current leak detection systems might continue undetected for a long period of time, potentially releasing a significant amount of hydrocarbon to the environment. Distributed fiber optic cable systems are able to identify small chronic leaks by detecting local temperature changes, longitudinal strains and vibrations. These systems can detect very small multiple leak events and the leak locations accurately, and can reduce false alarms [29]. Fiber optic cable systems are applicable in harsh environments.

It is difficult to conduct small-scale experiments on subsea pipeline with leakage, mainly because, the pipeline may need to release hydrocarbons to the environment. Further, since the industrial full-scale pipeline is large in diameter, fluid thermodynamics cannot be captured accurately in a small-scale, laboratory environment. Thus, a numerical simulation can provide a better understanding of pipeline internal flow and the consequences of pipeline leaks in different scales, reducing the cost and number of experiments. Commercially available ANSYS FLUENT computational fluid dynamics software is used to serve this purpose. ANSYS workbench provides integrated modular design, meshing technology, and large degree of freedom for pre- and post-processing for the fluid flow simulation in pipeline. In this paper, a literature survey has been performed to review the various numerical and experimental techniques using for leak detection presented in section 3.1.2. The theoretical background of the CFD simulation is briefly explained with the sub-models used in this literature such as: the sub-models for

turbulence and acoustics are showed in section 3.2. In section 3.3, the leakage simulation geometry creation, meshing, boundary conditions and overall simulation methodology is described. Two different simulation models have been used in this work, one is the modeling of flow inside the pipeline with leakage. The other model is the fluid dispersion model which is the model of escaped fluid flow outside the pipeline from leakage to the atmosphere (water in sub-sea condition). Results from the first model are compared with the available literature [30] and presented in section 3.4. Both steady-state and transient simulations have been performed to obtain the results. Steady state simulations are performed in the section 3.5.1 to observe the deviation of local parameters (e.g. pressure, temperature) near at the leak orifice for four different fluids used in this study, which are water, crude oil, nitrogen and methane. In the section 3.5.2 the transient simulations have been performed in order to capture the acoustic signatures generated from the leakage. The results from the fluid dispersion models are explained in the section 3.5.2.2.

3.1.2 Literature review

Pipeline leak modeling through numerical approach is relatively a new area. A few literatures are available on this topic. Ben-Mansour et al. (2012) developed a 3D turbulent flow model with 10 cm diameter pipeline to detect the small leakage (1mmx1mm) for a water distribution pipeline [30]. Length of the pipeline modeled was 2 m. ANSYS FLUENT 6.2 was used to model the pipeline leakage. Both steady state and transient simulations were performed employing DES (Detached Eddy Simulation) model. The

pressure noise data was processed through FFT (Fast Fourier Transform) and presented data for different leak locations around the leak. The pressure and pressure gradient variations along the pipe have been showed using steady state simulations. The results indicated that the presence of leak cause measurable difference in the magnitude and frequency of the pressure signal spectrum. However, the temperature effect was not discussed in the paper. Olivares (2009) presented the effect of temperature and pressure to the leak noise at the district water heating pipeline [31]. Since the temperature has effect on viscosity, at low temperature the viscosity of water is high. In the paper, it has been showed that the high viscous flow at low temperature created noise in low frequency zone. Liang Wei et al. (2013) developed a leak detection system based acoustic technology. The acoustic field is estimated with several pipeline pressures, and with a 4 mm diameter leak orifice. The vibration signal data caused by leak has been presented [32]. A hydrodynamic study of pipeline with oil leakage is performed by de Vasconcellos Araújo et al. (2013). In this paper a model with two leaks including a Tee junction was developed. The influence of the leak in the flow dynamics parameters and the behavior of the fluid were analyzed using velocity vectors and pressure fields [33]. The ANSYS CFX software was used for the numerical simulation. Zhu et al. (2014) developed a numerical model to simulate oil leakage from damaged submarine pipeline. In this study, the effects of oil properties, leak rate and leak size have been examined. The FLUENT package to model 2-D transient simulation has been used [34]. Another similar work of subsea gas dispersion model was developed by Cloete et al. (2009). The volume of fluid (VOF) model was used for the simulation. In both models, the migration pattern of the spilled oil and the time required for the migration were identified [35].

3.2. Theoretical Framework for CFD Simulation

The numerical simulations were carried out with the commercially available computational fluid dynamics (CFD) software ANSYS FLUENT. It uses element based finite volume method (FVM) to discretize computational domain utilizing fine meshing. The mesh creates finite volumes which are used to solve the mass, and momentum, equations. Discretization helps to linearize a large system of non-linear algebraic conservation and transport equations. The flow in a pipe and the influence of small leakage is a complex problem, including buoyancy driven flow, turbulence, acoustics associated. These physical processes are modeled as a set of partial differential equations with boundary conditions. The theoretical framework of a CFD simulation is based on the solution of the conservation equations, namely, mass, and momentum conservations [3.9].

The overall conservation equation is:

$$\frac{\partial(\rho\Phi)}{\partial t} + \nabla.(\Phi\rho\vec{v}) = \nabla.\left(D^{(\Phi)}\nabla\Phi\right) + S_{\Phi} \qquad (3\text{-}1)$$

where, ρ is the density of the fluid in (kg/m^3) and $\vec{v}$ is the velocity vector in m/s. The general exchange coefficient $D^{(\Phi)}$ is determined through local sources S_{Φ} and the temporal change of variable property Φ. Pipe flow simulation requires the conservation equation. These equations are given bellow:

Continuity equation ($\Phi = 1$)

$$\frac{\partial\rho}{\partial t} = -\nabla.(\rho\vec{v}) \qquad (3\text{-}2)$$

here ρ is the density and $\vec{v}$ is the velocity vector in a fluid depends on the coordinate x,y, and z. It can be written as, $\vec{v} = u\hat{\imath} + v\hat{\jmath} + w\hat{k}$.

Momentum conservation equation ($\Phi = \vec{v}$) is known as Navier-Stokes equations which is a general equation to describe the motion of compressible or incompressible viscous fluids.

$$\frac{\partial(\rho\vec{v})}{\partial t} + \nabla.(\rho\vec{v}\vec{v}) = -\nabla p + \nabla.\tau \quad (3\text{-}3)$$

where p is static pressure, τ is stress tensor which can be written as

$$\tau = \mu_{eff}\,(\nabla\vec{v} + \nabla(\vec{v})^T - \frac{2}{3}\delta\nabla.\vec{v}) \quad (3\text{-}4)$$

here μ_{eff} is effective viscosity. The detailed on turbulence model is discussed on 3.2.1.1 section below.

Equation (3-4) contains four scalar components. In order to solve ρ an equation of state must be added. The equation of state is a thermodynamic equation which describes the state of the fluid under certain boundary conditions. The equation of state for ideal gas is $p = \rho RT$, where R is the gas constant and T is temperature [31]. For incompressible fluids the density is assumed constant for any value of pressure and temperature but for compressible fluids the density requires correction, especially at high pressure and low temperature conditions. The compressibility factor of a species i according to Peng-Robinson equation is $z^v = \frac{x_i^v}{C_{i,s}}(\frac{p}{RT})$, where z^v is the vapor phase compressibility, $C_{i,s}$ is the vapor concentration and x_i is mole fraction of the species i [36].

Energy conservation equation ($\Phi = E$)

$$\frac{\partial(\rho \mathrm{E})}{\partial t} - \frac{\partial p}{\partial t} + \nabla.(\mathrm{E}\rho\vec{v}) = \nabla.(\lambda \nabla T) + \nabla.(\vec{v}.\tau) + \vec{v}.S_{\mathrm{M}} + S_E \quad (3\text{-}5)$$

$$E = h + \frac{v^2}{2} \quad (3\text{-}6)$$

where E is total energy, λ is thermal conductivity and S_E is energy source term. The term $\vec{v}.S_{\mathrm{M}}$ is the work due to external moment source and ignored. The main energy source of the fluid flow in a pipeline is the eddy dissipation. The large eddies gain energy from the mean flow and small eddies gain energy from the large eddies. At one stage the smaller eddies dissipates their energy and convert the kinetic energy to thermal energy [31].

3.2.1 Sub-models

To simulate a pipe flow with leak orifice and generate the acoustic signal, turbulence and acoustic sub-models have been used. The volume of fluids (VOF) model is used to model the fluid dispersion from the submarine pipeline.

3.2.1.1 Turbulence Sub-model

Two major turbulence sub-models are available in FLUENT; the RANS (Reynold's Average Navier-Stokes) equation based $k - \epsilon$ model and hybrid model. Hybrid model is based on the compromise between the direct numerical simulation (DNS) and the RANS.

Large Eddy Simulation (LES) is widely used as a turbulent model, especially for transient simulations. The only drawback of LES is its large time requirement to converge to exact solution. In LES turbulence model, large eddies are resolved directly and small eddies are modeled. Thus, it can be said that LES is a hybrid model of DNS and RANS in terms of the fraction of the resolved scales. The mass, momentum and energy, which transports during the flow are treated as large eddies. The small eddies are less dependent on the geometries, these are solved by using RANS based models [36]. For steady-state simulation $k-\epsilon$ model provides fairly reasonable result, however, for transient simulation, LES is the efficient model.

3.2.1.1.1 Turbulence Sub-model for Steady-State Simulation Inside the Pipeline

RANS equation based models are used to model steady-state turbulent flow simulations. Two equations model such as the standard $k-\epsilon$ model is most widely used in engineering turbulence modeling for industrial applications based on RANS turbulence equation. In this model, two transport equations, turbulent kinetic energy, k, and the dissipation rate of turbulent kinetic energy, ϵ, are solved. The $k-\epsilon$ model is based on the eddy viscosity concept where the effective viscosity, μ_{eff}, accountable for turbulence is modeled as:

$$\mu_{eff} = \mu + \mu_t \tag{3-7}$$

where, μ_t is the turbulent viscosity and $k-\epsilon$ model assumes that the turbulent viscosity is linked to the turbulence kinetic energy and dissipation via Equation 6. Fluid density ρ and C_μ is a constant [36]. The $k-\epsilon$ model is numerically robust and proven to be stable. It has well established regime of predictive capability and it offers good accuracy. The implementation of RANS turbulence model into CFD is easy and computationally least expensive with satisfactory results for engineering applications [3.10].

The turbulent or eddy viscosity μ_t is computed by combining the k and ϵ as follows:

$$\mu_t = \frac{\rho C_\mu k^2}{\epsilon} \tag{3-8}$$

here C_μ is a model constant. The default value of $C_\mu = 0.09$ will be used in this study which is used for high Reynolds number. The kinetic energy of turbulence k and dissipation rate ϵ are obtained by solving their conservation equations. The conservation equation of renormalization group (RNG) turbulence model is given below.

The kinetic energy of turbulence model can be described as

$$\frac{\partial(\rho k)}{\partial t} + \frac{\partial(\rho k u_i)}{\partial x_i} = \frac{\partial}{\partial x_j}\left(\frac{\mu_{eff}}{\sigma_k}\frac{\partial k}{\partial x_j}\right) + G_k - \rho_\epsilon \tag{3-9}$$

The dissipation rate of kinetic turbulent energy can be modeled as

$$\frac{\partial(\rho \epsilon)}{\partial t} + \frac{\partial(\rho \epsilon u_i)}{\partial x_i} = \frac{\partial}{\partial x_j}\left(\frac{\mu_{eff}}{\sigma_\epsilon}\frac{\partial \epsilon}{\partial x_j}\right) + C_{1\epsilon}\frac{\epsilon}{k}(G_k + C_{3\epsilon}G_b) - C_{2\epsilon}\rho\frac{\epsilon^2}{k} \tag{3-10}$$

here G_k and G_b represents the generation of turbulence kinetic energy due to the mean velocity gradient and due to buoyancy respectively. The buoyancy effects on ϵ are often neglected in the transport equation for ϵ.

$$G_k = -\rho\overline{u_\iota u_J}\frac{\partial u_j}{\partial x_i} \tag{3-11}$$

The model constants for $C_{1\epsilon}$, $C_{2\epsilon}$, σ_k, and σ_ϵ have the following default values [3.9]:

$C_{1\epsilon} = 1.44$, $C_{2\epsilon} = 1.92$, $\sigma_k = 1.0$, and $\sigma_\epsilon = 1.3$.

3.2.1.1.2 Turbulence Sub-model for Transient Simulation Inside the Pipeline

Large eddy simulation (LES) is considered as the most suitable turbulence model for acoustic application [31]. The governing equations employed for LES are obtained by filtering the time-dependent Navier-Stokes equations in such way that only larger eddies are resolved by direct numerical analysis and smaller eddies are modeled. The larger eddies carry the mass, momentum and other fluid quantities and these eddies are dependent on geometry, mesh and boundary conditions where smaller eddies are less dependent on geometry [3.9]. A filtered variable of LES is defined by,

$$\overline{\phi}(\mathrm{x}) = \int_{\mathrm{D}} \phi(\mathrm{x}')\mathrm{G}(\mathrm{x},\mathrm{x}')\mathrm{d}\mathrm{x}' \tag{3-12}$$

here *D* is the filter domain and *G* is filtered function determines the scale of the resolvable eddies. The filter function implied,

$$G(x,x') = \begin{cases} 1/V, & x' \epsilon v \\ 0, & \text{otherwise} \end{cases}$$

where V is the volume of computational cell. Filtering the Navier-Stokes equations, the governing equations of incompressible flows are obtained as,

$$\frac{\partial \rho}{\partial t} + \frac{\partial (\rho \overline{u_i})}{\partial x_i} = 0 \tag{3-13}$$

$$\frac{\partial (\rho \overline{u_i})}{\partial t} + \frac{\partial (\rho \overline{u_i}\,\overline{u_j})}{\partial x_j} = \frac{\partial \sigma_{ij}}{\partial x_j} - \frac{\partial \overline{p}}{\partial x_i} - \frac{\partial \tau_{ij}}{\partial x_j} \tag{3-14}$$

where σ_{ij} is the stress tensor due to molecular viscosity and τ_{ij} is the sub-grid scale stress which are defined as,

$$\sigma_{ij} \equiv [\mu \left(\frac{\partial \overline{u_i}}{\partial x_j} + \frac{\partial\, \overline{u_j}}{\partial x_i} \right)] - \frac{2}{3} \mu \frac{\partial \overline{u_l}}{\partial x_l} \delta_{ij} \tag{3-15}$$

$$\tau_{ij} \equiv \rho \overline{u_i u_j} - \rho \overline{u_i}\,\overline{u_j} \tag{3-16}$$

The sub-grid scale stresses τ_{ij} result from the filter operations are unknown and require modeling. This sub-grid scale models employ Boussineq hypothesis like RANS model as,

$$\tau_{ij} - \frac{1}{3} \tau_{kk} \delta_{ij} = -2 \mu_t \overline{S}_{ij} \tag{3-17}$$

here μ_t is the sub-grid turbulent viscosity and $\overline{S}_{ij}$ is the rate of strain tensor defined by,

$$\overline{S}_{ij} \equiv \frac{1}{2} \left(\frac{\partial \overline{u_i}}{\partial x_j} + \frac{\partial\, \overline{u_j}}{\partial x_i} \right) \tag{3-18}$$

In this work, Smagorinsky-Lilly model is selected in order to avoid numerical instability. In this model the eddy viscosity is modeled as,

$$\mu_t = \rho L_s^2 \overline{|S|} \tag{3-19}$$

where L_s is the mixing length of the sub-grid scale and $\overline{|S|}$ is defined as, $\overline{|S|} \equiv \sqrt{2\overline{S}_{ij}\overline{S}_{ij}}$.

In ANSYS FLUENT the mixing length L_s is computed as,

$$L_s = \min(\kappa d, C_s \Delta) \tag{3-20}$$

where κ is the von Karman constant and d is the distance at the closest wall. C_s is the Smagorinsky constant and the value is derived is 0.17 for homogeneous isotropic turbulence. Δ is the local grid scale and defined as, $\Delta = \mathrm{V}^{\frac{1}{3}}$.

3.2.1.1.3 Turbulence Sub-model for Transient Simulation of Fluid Dispersion

The sear-stress transport (SST) $k-\omega$ turbulence model is used for the fluid dispersion. In SST $k-\omega$ model the turbulent viscosity is modified to account for the transport of the turbulent shear stress and that makes this model more reliable for wider class of flows like, adverse pressure gradient flows [36]. The turbulence kinetic energy k and specific dissipation rate ω are obtained from following equations for SST $k-\omega$ model,

$$\frac{\partial(\rho k)}{\partial t} + \frac{\partial(\rho k u_i)}{\partial x_i} = \frac{\partial}{\partial x_j}\left(\Gamma_k \frac{\partial k}{\partial x_j}\right) + \widetilde{G_k} - Y_k \tag{3-21}$$

$$\frac{\partial(\rho \omega)}{\partial t} + \frac{\partial(\rho \omega u_i)}{\partial x_i} = \frac{\partial}{\partial x_j}\left(\Gamma_\omega \frac{\partial \omega}{\partial x_j}\right) + G_\omega - Y_\omega + D_\omega \tag{3-22}$$

In these equations, $\widetilde{G_k}$ is the turbulence kinetic energy generation due to mean velocity gradient, and G_ω represents the generation of ω. Y_k and Y_ω represents the dissipation of k and ω due to turbulence, and D_ω represents the cross-diffusion term. Γ_k and Γ_ω are the effective diffusivity of k and ω respectively, and these can be expressed as, $\Gamma_k = \mu + \frac{\mu_t}{\sigma_k}$ and $\Gamma_\omega = \mu + \frac{\mu_t}{\sigma_\omega}$. Here σ_k and σ_ω are the turbulent Prandtl number for k and ω respectively. The model constants for this model are, $\sigma_{k,1} = 1.176$, $\sigma_{k,2} = 1$, $\sigma_{\omega,1} = 2$, and $\sigma_{\omega,2} = 1.168$.

3.2.1.2 Acoustic sub-model

There are several models exist to calculate the acoustic data from the leakage, such as: Computational Aeroacoustics (CAA) and Ffowcs-Williams and Hawking (FW-H) methods. The CAA method is presented by Lighthill (1952), where Navier-Stokes equations are recast into an inhomogeneous wave equation,

$$\frac{\partial^2 \rho'}{\partial t^2} - c_0^2 \nabla^2 \rho' = \frac{\partial^2 T_{ij}}{\partial y_i \partial y_j} \tag{3-23}$$

$$\rho' = \rho - \rho_0 \tag{3-24}$$

$$T_{ij} = \rho u_i u_j - e_{ij} + \delta[(p - p_0) - c^2(\rho - \rho_0)] \tag{3-25}$$

where T_{ij} is the Lighthill stress tensor, e_{ij} is the viscous stress tensor. ρ' and c_0 are the fluid density used in the acoustic field and velocity of the sound. ρ and ρ_0 are fluid density, and p and p_0 are fluids pressure after and before perturbation.

FW-H method is more appropriate for the stationary surfaces like pipeline leakage. It gives,

$$\frac{1}{a_0^2}\frac{\partial^2 p'}{\partial t^2} - \nabla^2 p' = \frac{\partial^2 [T_{ij} H(f)]}{\partial x_i \partial x_j} - \frac{\partial}{\partial x_j}\left[\{P_{ij} n_j + \rho u_i\,(u_n - v_n)\}\delta(f)\right]$$

$$+ \frac{\partial}{\partial t}[\{P_0 v_n + \rho(u_n - v_n)\}\delta(f)] \qquad (3\text{-}26)$$

$$H(f) = \begin{cases} 0, & f = 0 \\ 1, & elsewhere \end{cases}; \quad \delta(f) = \frac{d}{df}[H(f)] \qquad (3\text{-}27)$$

here u_i and u_n are the fluid velocity components at x_i and normal directions respectively; v_i and similarly, v_n are the surface velocity components at x_i and normal directions. $\delta(f)$ is the Dirac delta function and $H(f)$ is the Heaviside function [39].

The approaches available in FLUENT for computing noise data are given in Table 3-1. Although FW-H method got certain limitations, still the accuracy of this method is quite reasonable. Another advantage of using FW-H acoustics model in FLUENT is that it allows to select multiple source surfaces and receivers. The acoustic signals obtained from the source can be post-processed using the FFT. In order to use FW-H method, a high quality unsteady LES model is required for transient solution [31].

Table 3-1: Acoustic sub-models comparison [31]

	CAA	**FW-H**
Computational effort	Very high	High
Reflection/scattering at the pipe wall	Yes	No

Sound propagation through pipe wall	No	No
Account the effect of flow on sound	Yes	No
Solution required	Transient	Transient
Accuracy	Good	Good

3.2.1.3 Volume of Fluid (VOF) Model

The VOF method is based on the solution of the momentum equation for the mixture of two or more immiscible fluids and the volume fraction of each of the fluid throughout the domain [34]. In this work, the volume of fraction of water and hydrocarbon are defined as ϕ_1 and ϕ_2 respectively. The two-dimensional transport equations for the fractions are presented as,

$$\frac{\partial \phi_1}{\partial t} + \frac{\partial u\phi_1}{\partial x} + \frac{\partial v\phi_1}{\partial y} = 0 \quad (3\text{-}28)$$

$$\frac{\partial \phi_2}{\partial t} + \frac{\partial u\phi_2}{\partial x} + \frac{\partial v\phi_2}{\partial y} = 0 \quad (3\text{-}29)$$

The density and viscosity can be expressed as,

$$\rho = (1 - \phi_1 - \phi_2)\rho_{air} + \phi_1\rho_1 + \phi_2\rho_2 \quad (3\text{-}30)$$

$$\nu = (1 - \phi_1 - \phi_2)\nu_{air} + \phi_1\nu_1 + \phi_2\nu_2 \quad (3\text{-}31)$$

here ρ_1 and ρ_2 are the density, and ν_1 and ν_2 are the viscosity of water and hydrocarbon respectively.

3.3. Simulation Methodology

3.3.1 Flow Inside the Pipeline Model

The main purpose of CFD model of the fluid inside the pipeline was to predict the local pressure and temperature change contours for different leak sizes and fluids. Further, the acoustic signatures were generated from the transient simulation. The flow domain of the pipe length was L = 8 m, diameter D = 0.322 m. The leak was positioned at (x = L/2, y = D/2, z = 0) as shown in Figure 3-1.

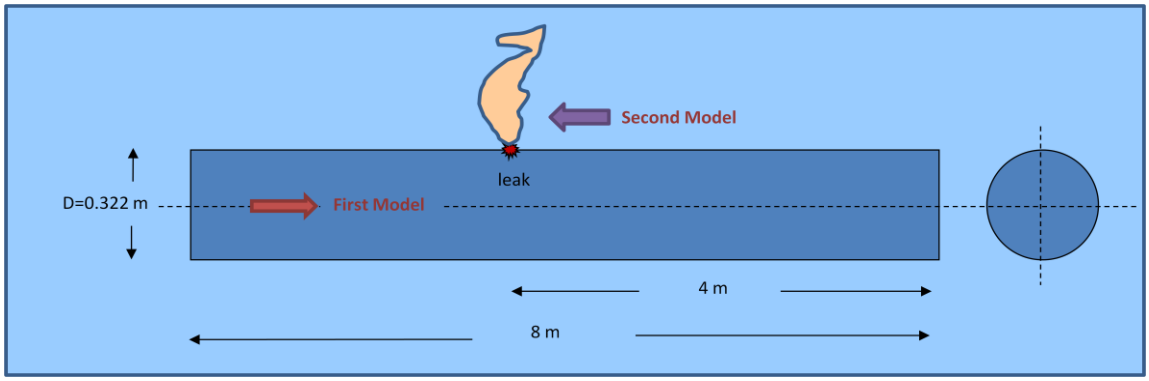

Figure 3-1: Pipeline physical model and leakage position

The leak orifice size varied from 4 mm to 8 mm, and assumed as circular shape cavity. Although the size and shape of the leakage of subsea oil and gas pipeline can be in wide range, but in this study the shape of the hole is considered circular shape for the compatibility of the results. The geometry of the pipeline was created using SolidWorks 2014 and imported to the ANSYS workbench, as shown in Figure 3-2. Since the leak orifice was very small, a refined mesh was used in order to capture the features around the leak hole, total 32 cells area were included as shown in Figure 3-3. The turbulent

eddies near wall are very small and a special is consideration required to obtain good results in CFD. It is recommended that the mesh near walls need to be fined enough to resolve the small eddies. An dimensionless quantity y^+ is a powerful tool provided by FLUENT to check the near wall mesh treatment. For a standard wall function, the value of y^+ for the first cell should be within the range of $30 < y^+ < 150$. In this study, the value of y^+ was 115, which is in the acceptable region. Although, more fine treatment would give better y^+ value but increase the computational cost. The LES turbulent model also require finer mesh size to resolve the high energy content eddies. The largest eddies of a flow in a pipe is 7% of the characteristics length of a duct, which is the diameter of a pipe [31].

The computational domain of this simulation consisted of 3-D unstructured triangular mesh. The numbers of element generated were 2924352 and numbers of nodes generated were 543069. The optimum number of mesh elements found from the mesh independent study is 1.5 millions where in this case around 3 millions of mesh elements were used. The reason is, smaller grids are sufficiently small enough to capture the hydrodynamic features at the near leak region.

Since, in this study the pipe diameter was 0.322 m, the largest turbulent length scale would be 22.54 mm. Assuming 80% of the total kinetic turbulent energy need to be calculated, the eddies of approximately half size must be resolved, which is 11.27 mm. The minimum cell size at the coarse region of the pipe is 4mm and at the leak is 0.5 mm which are fine enough to resolve the eddies. The domain was named into different sub-sections; inlet, outlet, leak orifice and the wall. The inlet boundary condition was set as

velocity inlet with velocity of the fluid 9 m/s for throughout the pipeline and outlet boundary condition was set as pressure outlet. The leak was also set as pressure outlet, however, the pipe was assumed to be submerged underwater. Thus, the leak outlet releases fluid into the water and the pressure outlet boundary at the leak orifice was considered to be equal to 100 m of water column, i.e. P_{leak} = 150 psi. This remaining boundary was set as solid wall with no slip condition. Two different boundary conditions for the temperature of the fluid inside pipe was set, 2^{o}C and 50^{o}C to capture the extreme deviation of the temperature. The ambient temperature was set at 4^{o}C, which is considered as the temperature of the sub-sea water. The steady-state simulations have been carried out by using standard *k*-ε model and the transient simulations have been performed with large eddy simulation model. The model parameters and boundary conditions are summarized in Table 3-2. For the incompressible fluids the density was assumed constant throughout the pipe, however, for compressible fluids the density was determined by employing Peng-Robinson EOS [36]. A standard $k-\epsilon$ turbulence model was utilized to perform the steady-state simulations and LES model for the transient simulations. In order to avoid any numerical instability, Smagorinsky-Lilly sub-grid scale model was employed with LES. The pressure-implicit with splitting of operators (PISO) pressure-velocity coupling solver scheme was used. In addition, in order to ensure accurate numerical solution a second order upwind scheme was considered.

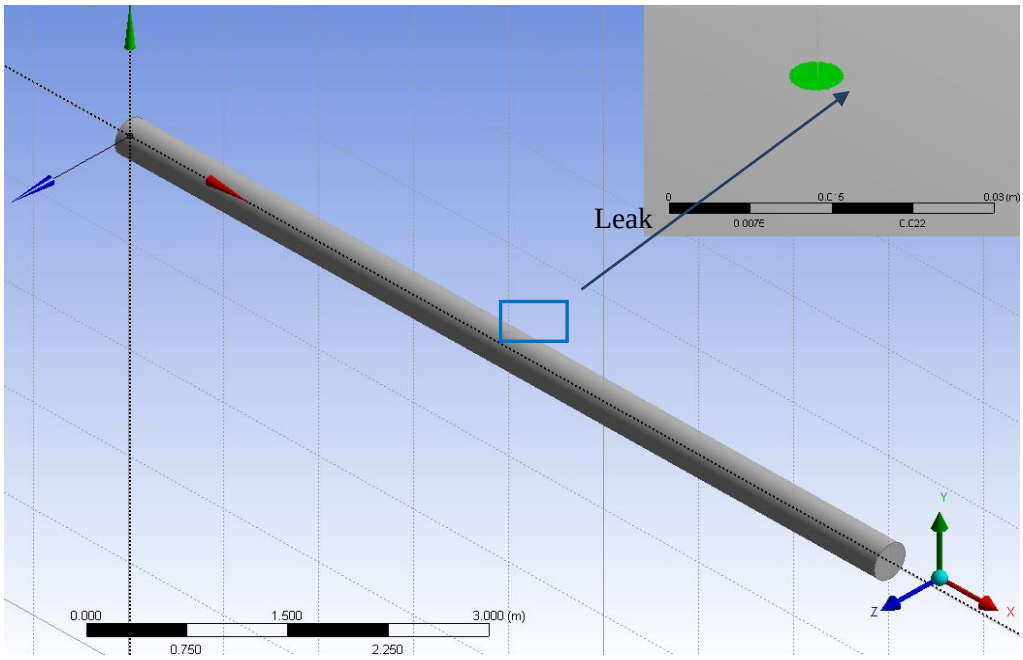

Figure 3-2: Isometric view of the pipeline model geometry (zoomed view: leak hole)

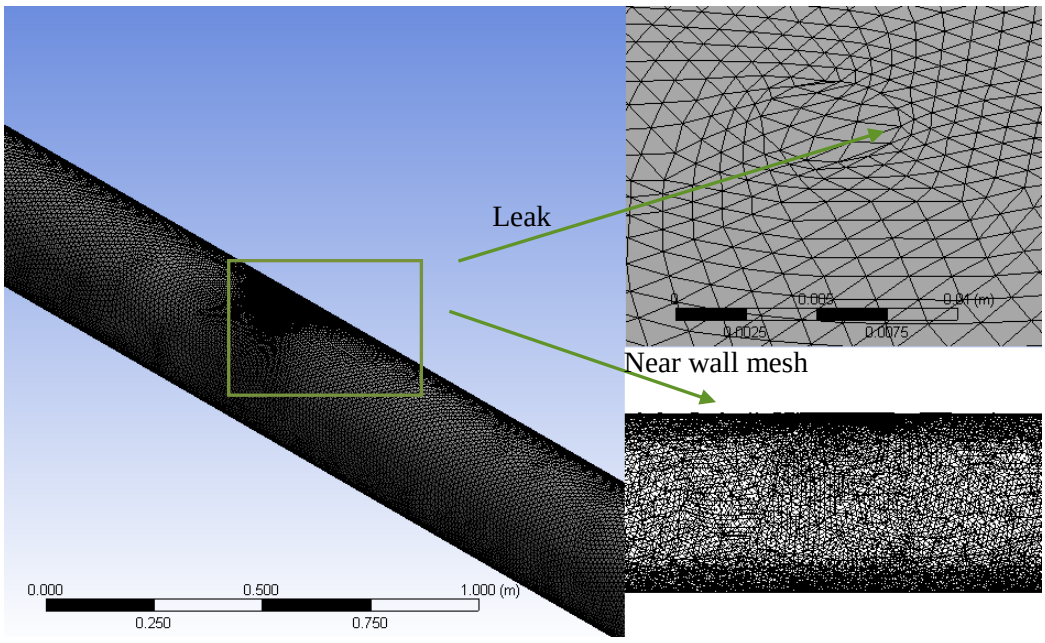

Figure 3-3: Refined meshing of pipeline at the near wall and leak (zoomed view: leak hole)

Table 3-2: Boundary conditions for the CFD simulation of flow inside the pipeline and dispersion model

Boundary conditions	**Flow inside the pipeline model**	**Fluid dispersion model**
Domain	Three dimensional	Two dimensional
Meshing	Triangular unstructured with refinement	Hexahedral unstructured with refinement
Simulation type	Steady-state and transient	Transient
Turbulence model	Standard $k-\epsilon$ for steady-state and LES for transient simulation	SST $k-\omega$
Fluids	Water, crude oil, nitrogen and methane	Crude oil and methane
Pipe pressure (psi)	200 - 5800	5800
Pipe temperature (K)	277 and 320	320
Ambient pressure (psi)	150	150
Inlet velocity (m/s)	9	Result from the flow inside the pipeline model
Pipe wall	No slip conditions	-
g (m/s^2)	9.8	9.8
Real gas properties	Peng-Robinson correlation	Peng-Robinson correlation

3.3.2 Fluid Dispersion Model

In order to simulate the fate of the released fluids, a 2-D transient model was developed to quantify the fluid volume released during the small leakage. The fluid dispersed from the damaged submarine pipeline can reach maximum horizontal migration distance since there is no action of current in subsea water is assumed. As a result, 2-D flow simulation is accurate enough to capture the migration pattern. The size of the domain is assumed square 30 m x 30 m and leak size is only 5 mm which is situated at the center of the domain. Having a time step of 10^{-4} second for 15 seconds long simulated flow time, resulting in 150,000 iterations. Assuming that one iteration with SST $k-\omega$ turbulence model takes 2 seconds for two dimensional flow and 15 seconds for three dimensional flow, the total time is 3.4 and 26 days respectively, thus three dimensional flow model in this system is not feasible. The escape velocity profile of the leaked fluid provides the information on fluid dispersion and its migration path. Plume trajectory as well as mixing behavior with the subsea stagnant atmosphere was analyzed and presented in the form of a space–time concentration distribution and distances to a given concentration. A volume of fluid (VOF) model was developed to study the fluid dispersion pattern from the subsea pipeline leakage. Since LES couldn't be used in case of two dimensional model, the turbulence was modeled using SST $k-\omega$ model. In order to ensure the accuracy, second order upwind scheme was used. The inlet of the leakage domain was selected as velocity inlet, the inlet boundary conditions were basically obtained from the outlet flow of the simulation inside pipeline. The subsea water domain was considered as the pressure outlet. The model parameters and boundary conditions are mentioned in Table 3-2.

3.4. CFD Code Validation

The CFD codes used in this study has been validated with the codes available in the literature. R. Ben-Mansour et al. (2012) performed a CFD study on the simulation of small leaks in water pipelines [30]. The calculations were performed with 2 m pipe length and 0.1 m outside diameter, and a with square- shaped leak hole. Leak was placed at the top-middle section of the pipeline. Velocity of the fluid was 1 m/s and line pressure was 1 - 6 bar for different leak sizes. The pressure outlet at the leak hole was taken same with atmospheric gage pressure P_{leak} = 0 bar. Results shown in Figure 3-4 illustrate the close match with the results published in [30]. and the current modeling work.

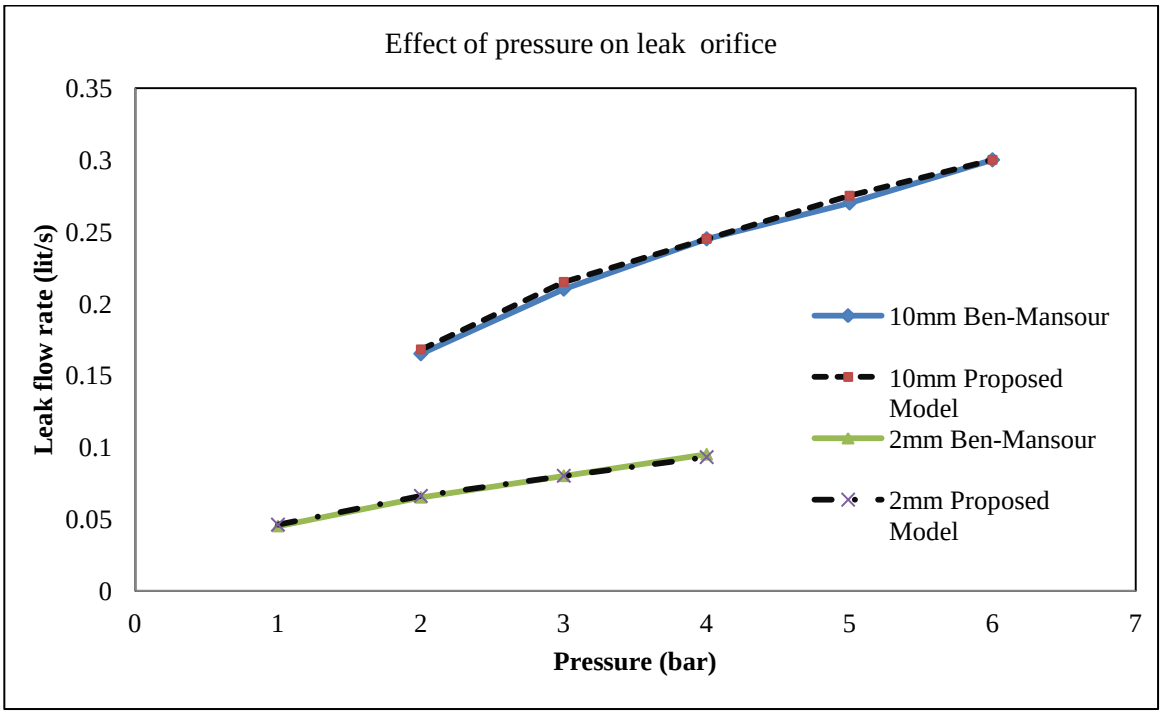

Figure 3-4: CFD code validation with literature (pipe length 2 m, velocity 1 m/s, pressure 1 bar) [30]

3.5. Results and Discussions

The inlet fluid velocity was assumed to be 9 m/s as per an operating subsea pipeline data. The line pressure and temperature varies between 200 - 5800 psi, and 2 and 50 ^{o}C, respectively. The pipeline is assumed at 100 m below under the sea, where the ambient pressure is 150 psi. The results presented below are based on the steady-state and transient simulations.

3.5.1 Steady-State Simulations

A set of steady state simulations have been performed in order to validate the proposed model. Steady state simulation results provide valuable information on the flow velocity and the effect of pressure variation and flow pattern inside the pipeline near leak orifice. Also the variation of turbulence kinetic energy and temperature is observed from steady state simulation.

3.5.1.1. Model Validation

The effects of pressure on leak size and fluids have been observed to validate the CFD model. Total forty simulations have been performed in order to validate the CFD model for the flow inside the pipeline. The results are presented in Figures 3-5 and 3-6.

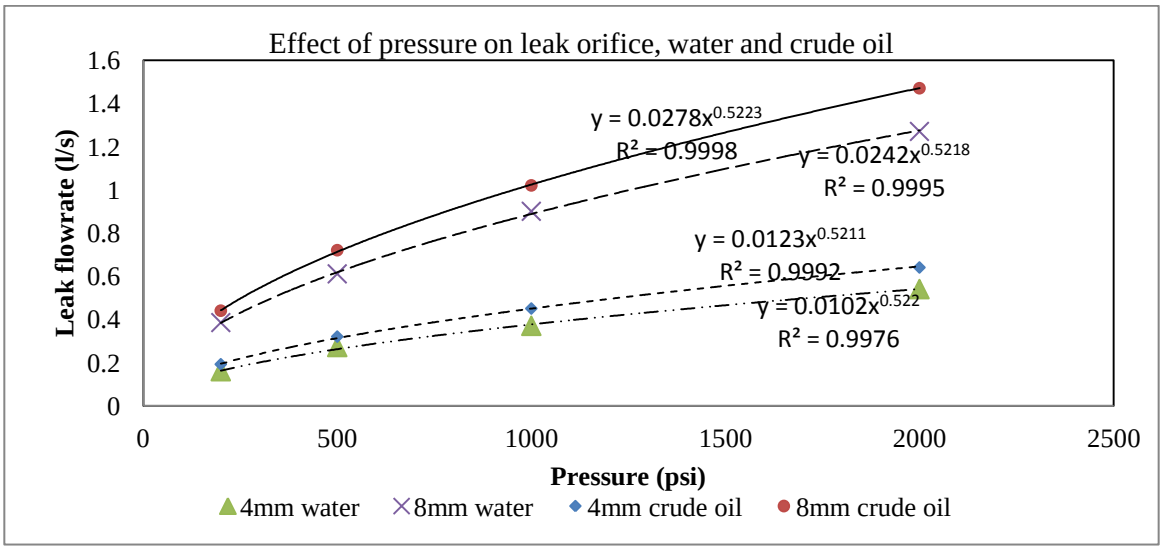

(a) Variation of leak flow rate vs. pressure for water and crude oil for different hole size

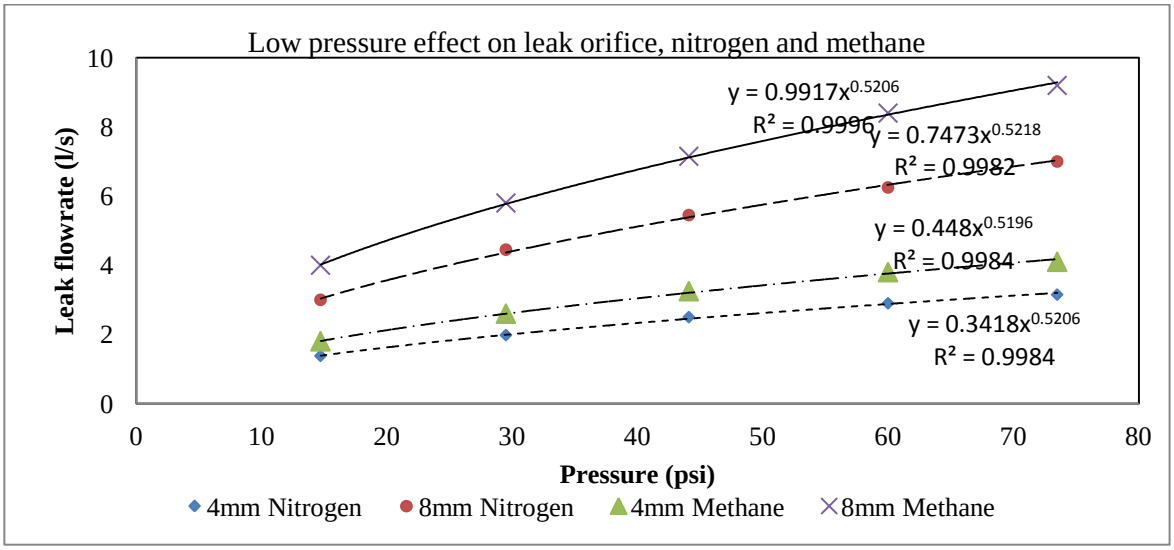

(b) Variation of leak flow rate vs. pressure (at low pressure range) using nitrogen and methane for different hole diameter

Figure 3-5: Effect of pressure on fluids of leak orifice of 8 m pipe length and 0.322 m diameter. Two different leak hole diameters are used, 4mm and 8mm. (a) water and crude oil as fluid, pressure 200-2000 psi, (b) nitrogen and methane as fluid, pressure 15-75 psi.

Two different leak hole sizes and four different fluids have been used. The summary of the results in Figure 3-5 showed that the leak flow rate is a function of the pipeline pressure. It can be represented as [30]:

$$Q_{leak} = A(\Delta P)^n \tag{3-32}$$

where, Q_{leak} is the leak rate in l/s, ΔP is the differential pressure in psi and A is the constant based on the fluid type and operating conditions. The value of coefficient n = 0.52 and it agrees with the results reported by [30]. However, according to R. Ben-Mansour et al. (2012) the single orifice equation states the value of n = 0.5, which is 3.5% different than the result obtained from the simulation. Moreover, the field data referred at the same literature, on the effect of pressure on the leak flow rate have shown the value of the coefficient n varies from 0.25 to 2. Equation 3-32 indicates there are two variables, leak orifice are A and pressure difference ΔP might be accountable for this variation. In case of high pressure of the pipeline, the pressure difference ΔP is higher across the leak results increase of the flow rate from the leak. Similarly if the size of the leak orifice increases the pressure drop across the leak decreases which cause the increase of flow rate through the leak [30].

In the case of compressible fluid with high differential pressure, as shown in Figure 3-6, the fluid behave as a real gas and the results can be expressed as:

$$Q_{leak} = A(\Delta P)^{-n} \tag{3-33}$$

where the value of n = 0.055. It has been observed that the flow rate tends to decrease with the increase in line pressure.

Figure 3-5 (b) shows the flow rate of compressible fluids at relatively low pressure whereas Figure 3-6 shows at high pressure and at a same leak orifice size the flow rate decreases as the pressure increases. This is due to the compressible fluids behave like real gases. As the size of the leak orifice increases the flow rate of fluid from the leak orifice at same pressure increases.

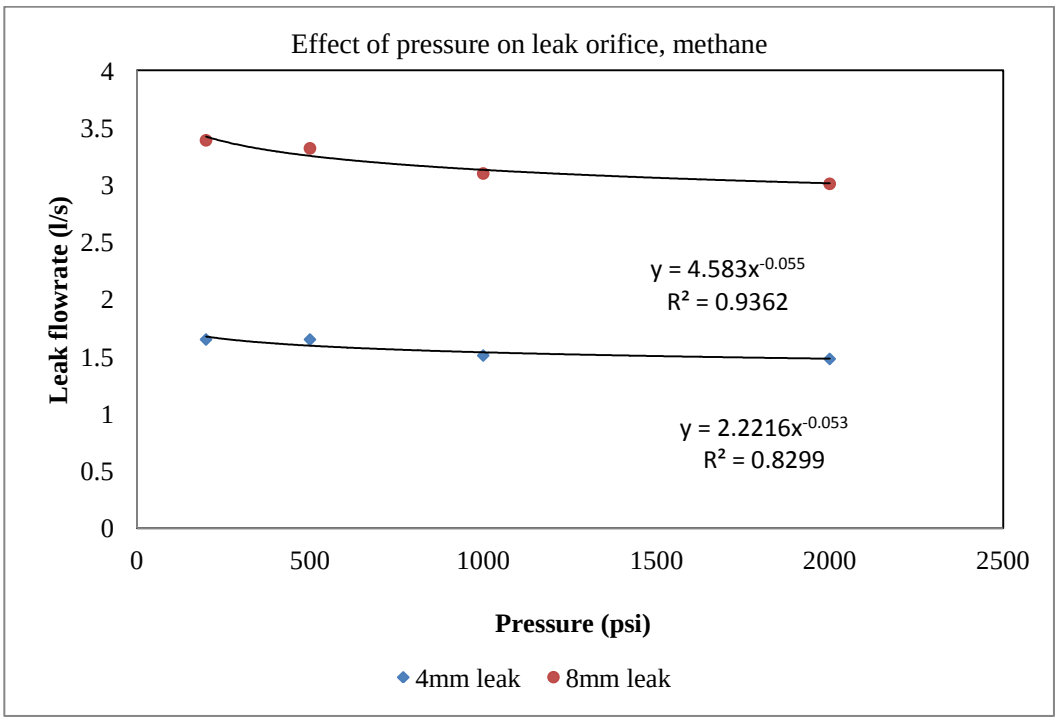

Figure 3-6: Effect of high pressures on compressible fluid (methane). Line pressure 200-2000 psi, hole diameters are 4mm and 8mm.

3.5.1.2 Flow Rate of Different Fluids

The fluid flow inside the pipeline has been simulated for different fluids under same operating conditions in order to predict the flow rate from the leak orifice that released into the subsea water. The selected leak size was 5 mm diameter and the pipe pressure was 5300 psi. At this pressure, the compressible fluids (i.e. nitrogen and methane) behaved like real gases as shown in Figure 3-6. The ambient pressure was 150 psi outside of the leak orifice to simulate hydrostatic head. Figure 3-5 (a) and (b) provide an correlation of the differential pressure and flow rate from the leak for different fluids. The correlation shows that the leak flow rate increases with the differential pressure and the leak orifice diameter. It is observed that for a same fluid, the leak flow rate increased around 2.3 times as the leak diameter increased twice, from 4 mm to 8 mm at a certain differential pressure.

Again, Figure 3-5 (a) shows, for the same operating conditions and leak size, the leak flow rate of crude oil is higher than water; and Figure 3-5 (b) shows, the leak flow rate of methane is higher than nitrogen. The similar phenomena has been observed in the velocity vector profiles of the fluids at Figure 3-7, which presents the behavior of flow velocity for different fluid releases. It should be noted that the velocities at the leak orifice are different for different fluids under same operating conditions. This is due to the properties of the fluids, such as: the jet velocity of methane from the leak orifice is two times more than water; among the fluids, the density of water is the highest whereas the density of methane is the lowest. The velocity of crude oil is slightly higher than the water. Viscosity of crude oil at 300 K is around 0.3 - 0.4 cP and density 790 kg/m^3 at

60^{o}F which is lower than water results higher flow rate at same leak orifice size. The velocity vector profiles also show the leak jet is slightly inclined towards the pipe flow direction. De Sousa et al. (2013) showed for vertical pipeline the leak jet angle towards the pipe flow direction is higher [40]. For horizontally positioned pipeline in this case, the jet angle inclination is lower but greater spread in the leakage with larger angle.

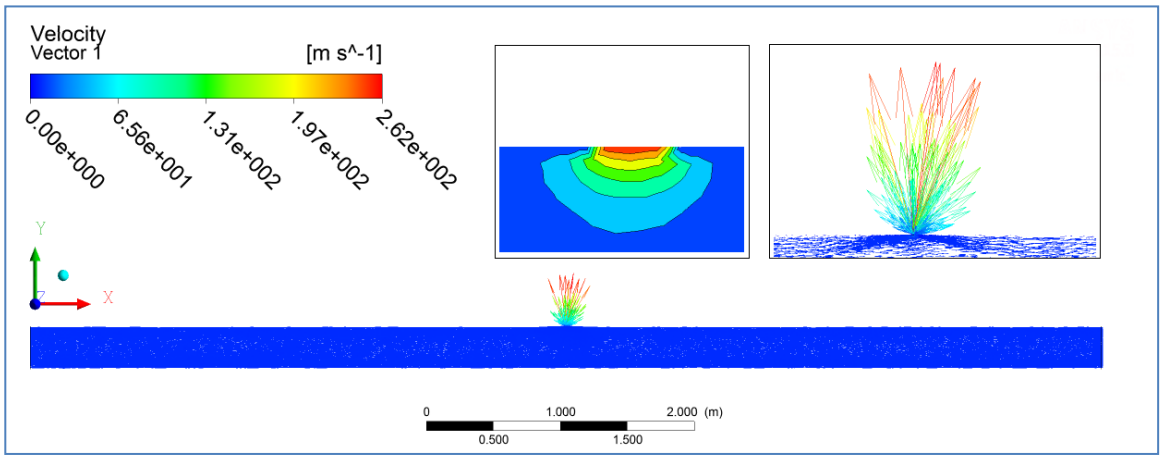

(a) Vector profiles of pipeline and water leak (at pressure 5300 psi and diameter 5mm)

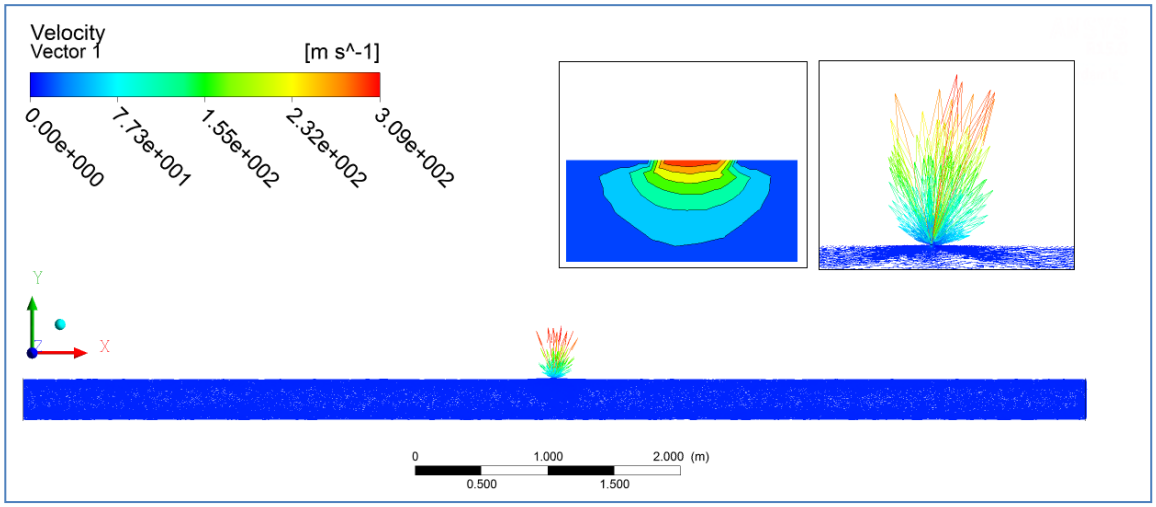

(b) Vector profiles of pipeline and crude oil leak (at pressure 5300 psi and diameter 5mm)

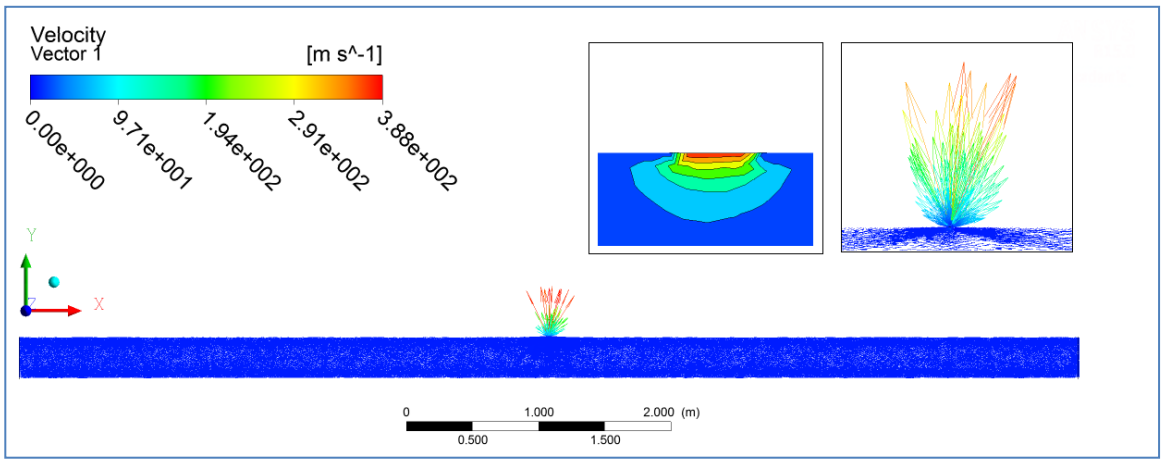

(c) Vector profiles of pipeline and nitrogen leak (at pressure 5300 psi and diameter 5mm)

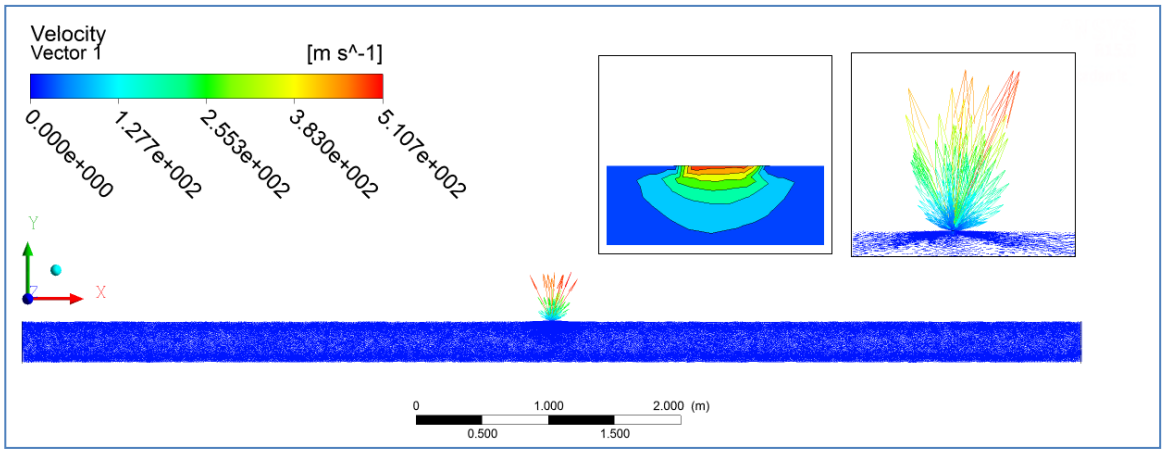

(d) Vector profiles of pipeline and methane leak (at pressure 5300 psi and diameter 5mm)

Figure 3-7: Vector profiles of pipeline with different fluids at pressure 5300 psi and diameter 5mm. (a) water, (b) crude oil, (c) nitrogen and (d) methane.

3.5.1.3 Pressure Variation and Flow Pattern Inside the Pipeline near Leak Orifice

The pressure contours around the 5 mm leak source for different fluids are shown in Figure 3-8. The pressure was the same throughout the pipeline, but a large pressure fluctuation is observed around the leak orifice. This pressure fluctuation is confined to a tiny area around the leak (around 2 mm), and thus a zoomed view of the pipeline around the leak orifice has been taken. The pressure contours showed that the pressure drop was 38.9 MPa for water and crude oil at the vicinity of leak orifice when the line pressure was 40 MPa with an ambient pressure of 1.03 MPa. In the case of nitrogen and methane, the pressure drop was around 37.5 MPa with same line pressure, relatively low when compared to crude oil and water.

The pressure distributions along the axial length of the pipeline at 1mm below at 200 psi line pressure and 5 mm below at 5800 psi line pressure, the leak exhibited a sudden drop in pressure around the leak orifice, as shown in Figure 3-9 and Figure 3-10 respectively. Figure 3-10 also shows that there was a slight pressure drop (around 14 kPa) for water and crude oil throughout the pipeline due to the viscous friction of the fluid, but it is hardly noticeable in case of nitrogen and methane. This small gradual pressure drop for water and crude oil throughout the pipeline maybe due to the roughness of the pipe. However, it is evident that for both cases the pressure kink at the middle section of the pipeline is due to the leak.

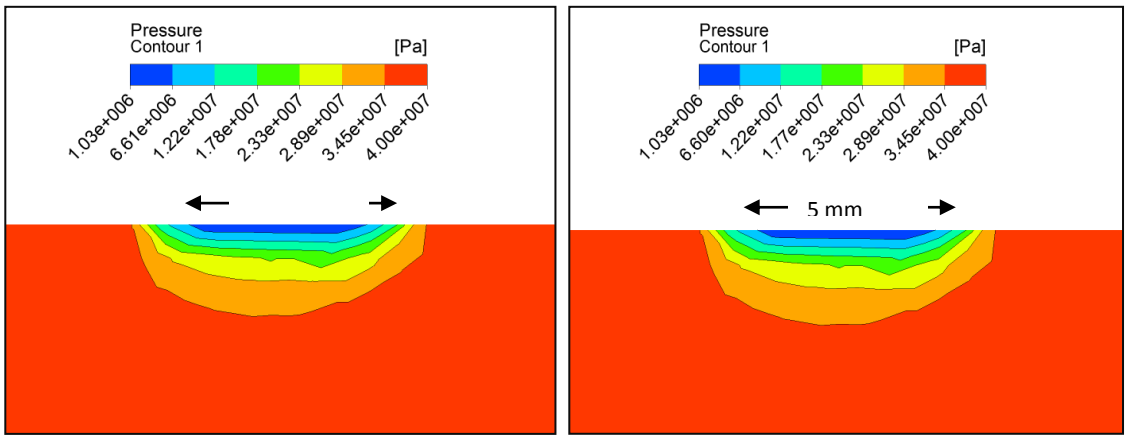

(a) water (b) crude oil

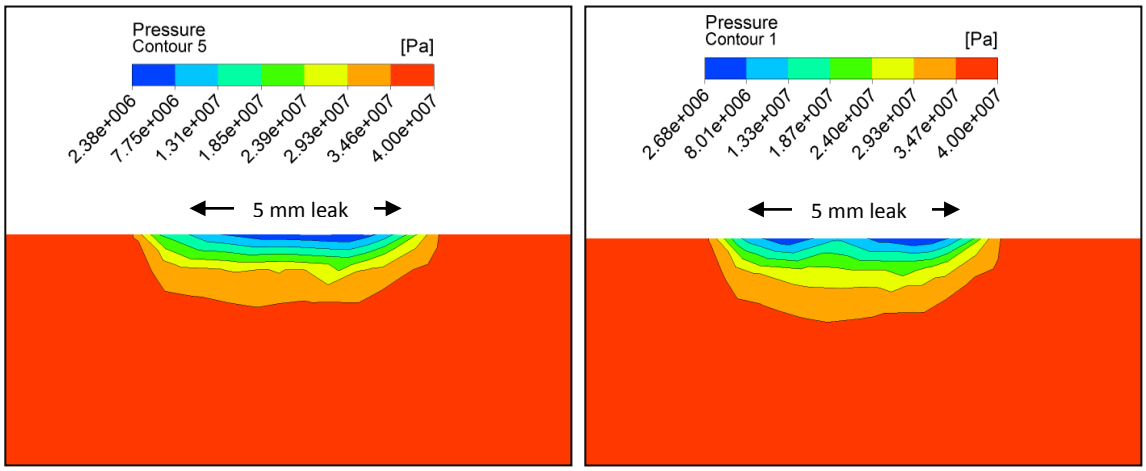

(c) nitrogen (d) methane

Figure 3-8: Zoomed view of local pressure change around the leak orifice. Pressure 40MPa (5800psi), velocity 9m/s, leak orifice 5mm. (a) water, (b) crude oil, (c) nitrogen, (d) methane as fluids.

The pressure kink can be better explained by studying the pressure gradient along the axial length of the pipeline. The pressure gradient profile shows a better evidence for the abrupt change in pressure near leak orifice as shown in Figure 3-11. The Figure 3-11 (a) is the pressure gradient of fluids at 5 mm below the leak. It shows that the pressure gradient is constant throughout the pipeline except at the leak vicinity. The pressure gradient is normal at the upstream of the leak and rapidly increasing at the downstream of the leakage. In this region the pressure gradient values become very steep due to the complex flow pattern near the leak orifice. Figure 3-11 (b) shows a clear signature of pressure gradient at the centerline of the pipeline, which is 0.161 m from the leak orifice. In the case of nitrogen and methane, the pattern is almost similar because the viscous friction is very low for these gases. There are no eddies or turbulence at the laminar sub-layer region of the pipe. Therefore, the pressure gradient of fluids at 5 mm below the leak is shows a smooth transition which is evident at Figure 3-11 (a). The flow velocity and turbulence is high at the turbulent core of the pipe. There is a spatial oscillation of the pressure gradient over the pipe length, which is evident in Figure 3-11 (b), due to the high turbulence at the centerline of the pipe. As suggested by Ben Mansour et al. (2013) [30] the pressure gradient profiles along the centerline would be very helpful to identify the exact location of the leak by using non-intrusive methods. Pipeline leak with high pressure gradient generate higher noise compared to low pressure gradient, which is evident from Figure 3-11. Figure 3-12 shows the zoomed view of pressure gradient contours for different pipe fluids. The pressure gradient decreased from a minimum value (i.e. zero) and then increased to the maximum value. This abrupt change in pressure gradient found to occur near the leak orifice.

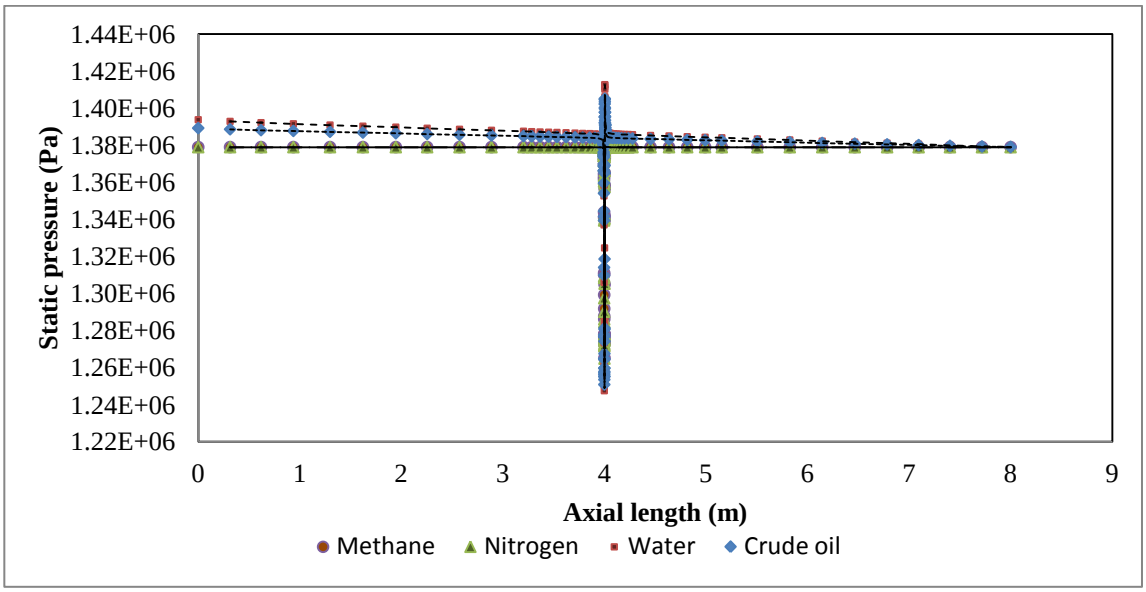

Figure 3-9: Pressure variation of fluids along the axial length of the pipe, 1mm below the leak. Pressure 1.4MPa (200psi), velocity 9m/s and leak orifice 5 mm.

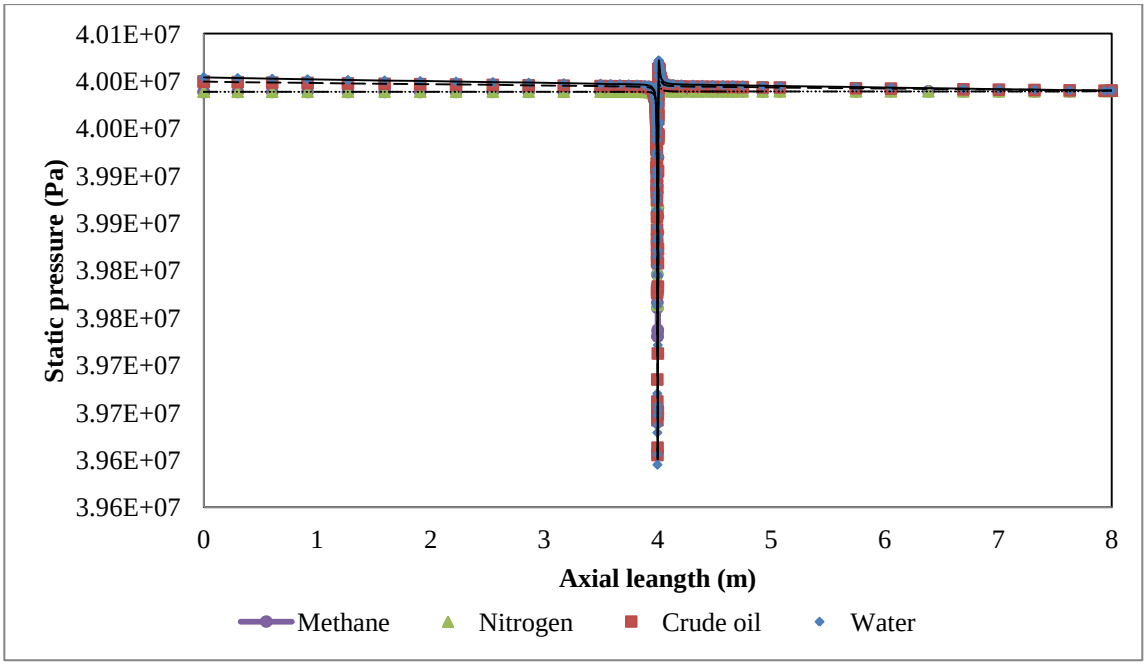

Figure 3-10: Pressure variation of fluids along the axial length of the pipe, 5mm below the leak. Pressure 40MPa (5800psi), velocity 9m/s and leak orifice 5 mm.

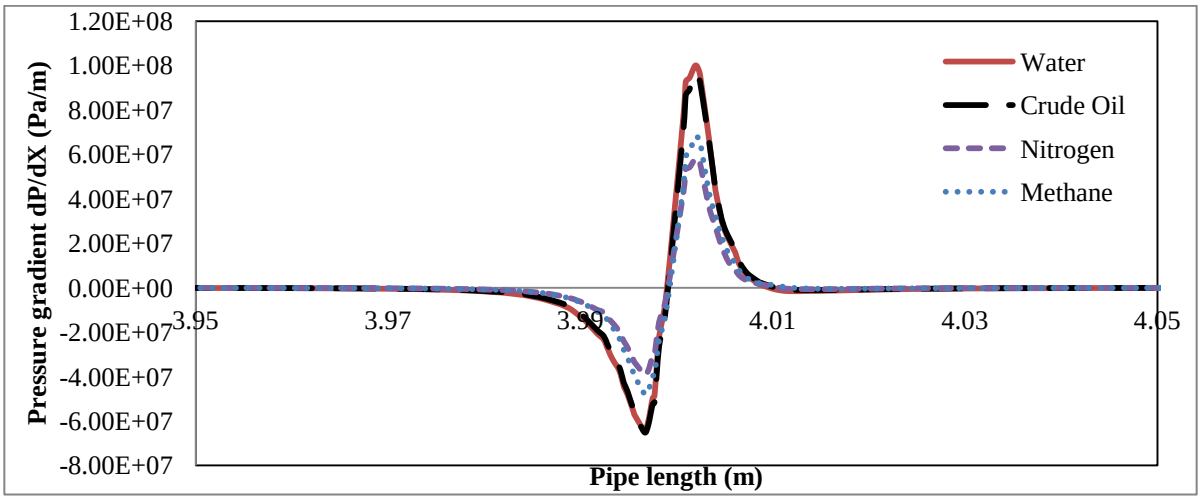

(a) Zoomed view of the pressure gradient along pipe for fluids, 5mm below leak, P=40MPa, v=9m/s, leak orifice=5mm

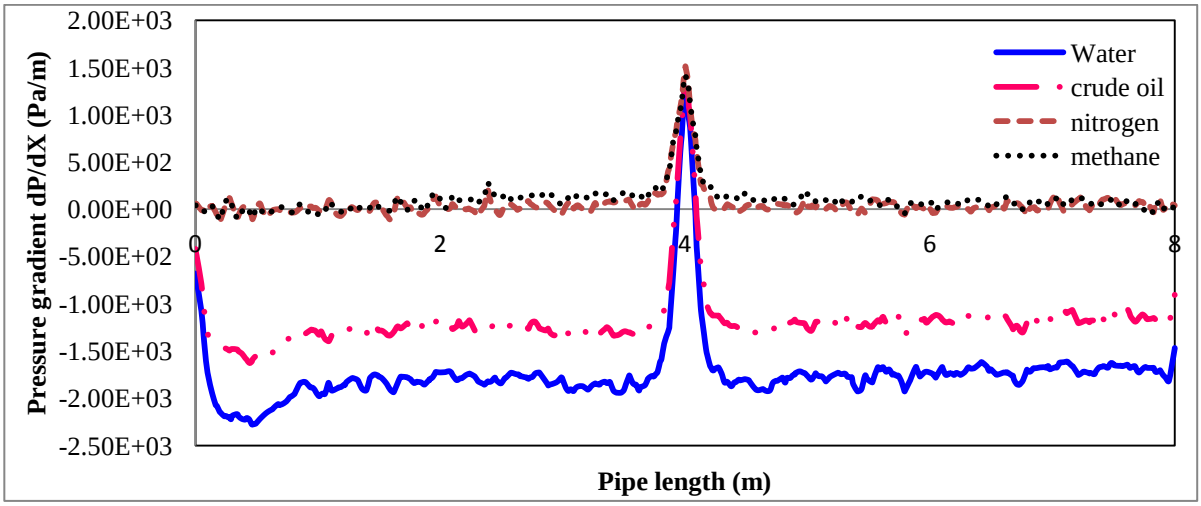

(b) Pressure gradient along pipe of fluids, centerline, P=40MPa, v=9m/s, leak orifice=5mm

Figure 3-11: Pressure gradient variation of different fluids along pipe length. Leak orifice 5mm, line pressure 40 MPa (5800 psi), velocity 9 m/s (a) zoomed view at 5mm below the leak (b) centerline of the pipeline.

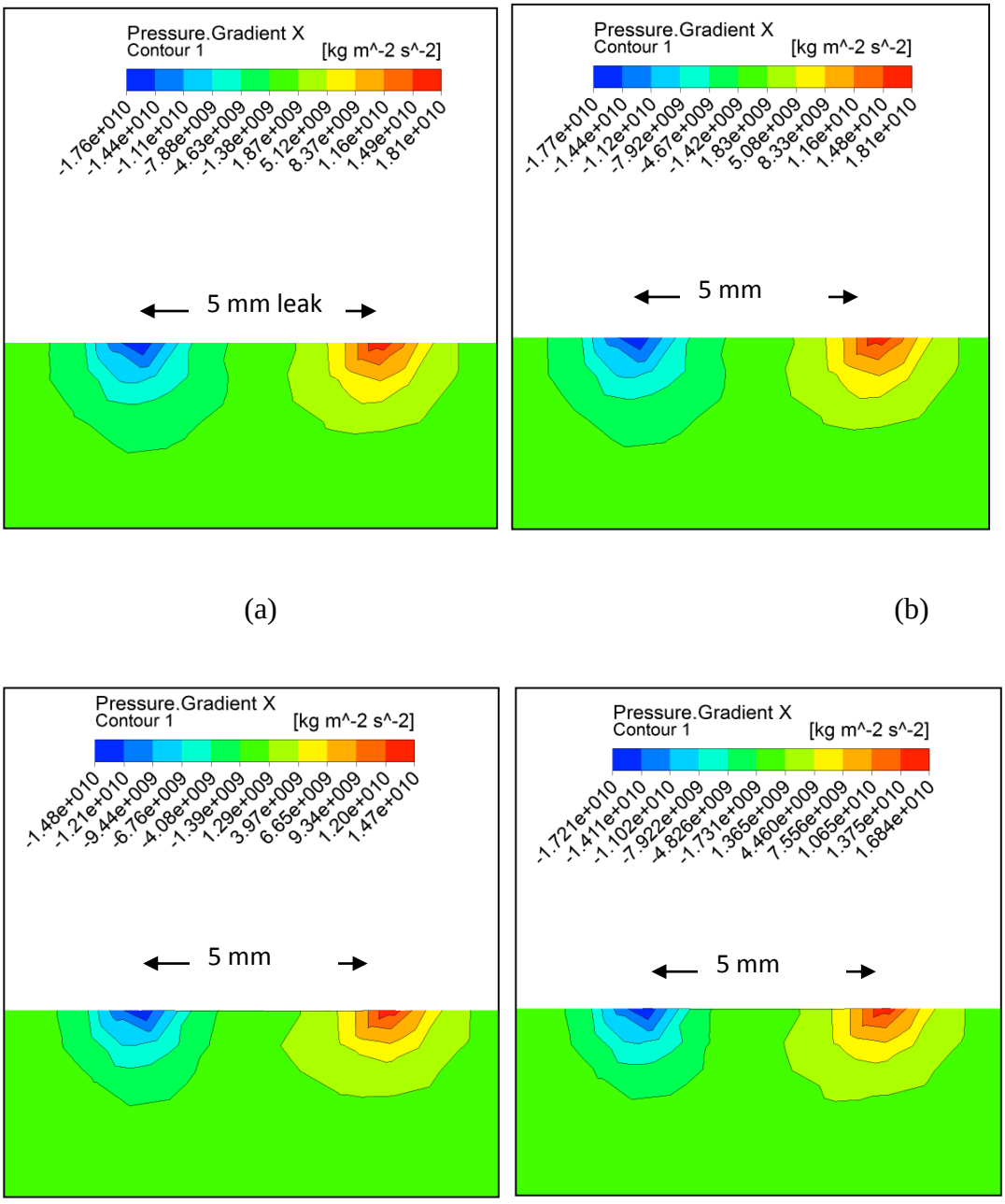

Figure 3-12: Zoomed view of pressure gradient contours of fluids along the pipe axial length. Pressure 40MPa (5800psi), velocity 9m/s and leak orifice 5mm. (a) water, (b) crude oil, (c) nitrogen, (d) methane as fluid.

3.5.1.4 Influence of Turbulence

Turbulent kinetic energy (TKE) and the Turbulent Eddy Dissipation (TED) of the pipe fluids have been estimated in order to observe its influence. Figure 3-13 shows the kinetic energy near the leak area for water and crude oil. It is evident that kinetic energy due to the turbulence is very high near leak area compared to remaining sections of the pipeline. Figure 3-14 shows the eddy dissipation contours of nitrogen and methane. These contours show similar pattern, which is very high eddy dissipation near the leak area, compared to remaining sections the pipeline. Eddies carry momentum, mass and energy of the fluids. The highly turbulent flow has ability to generate noise in low frequency which is explained in section 3.5.2.

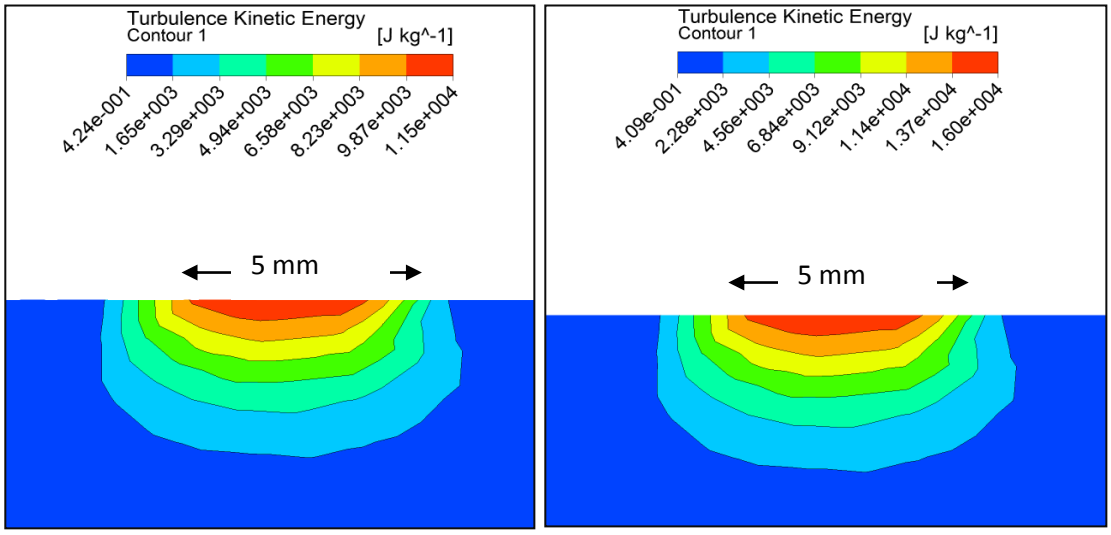

(a) (b)

Figure 3-13: Turbulence kinetic energy (TKE) contours around the fluid leakage (a) water, (b) crude oil.

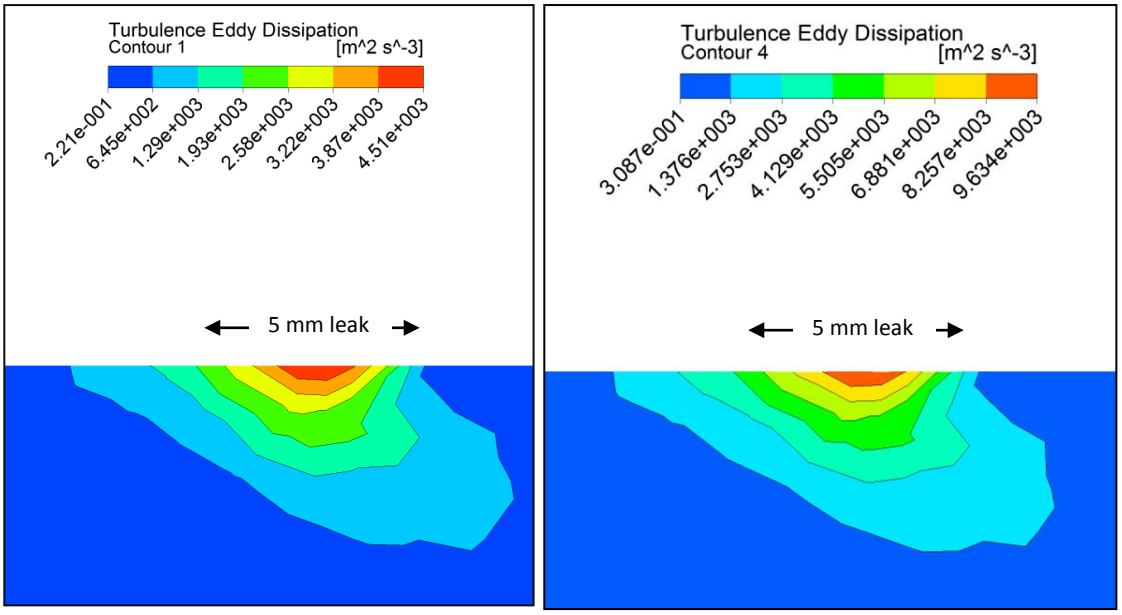

(a) (b)

Figure 3-14: Turbulence eddy dissipation (TED) contours around the leakage (a) nitrogen, (b) methane.

3.5.1.5 Temperature Variation Near Leak Vicinity

The temperature contours are plotted to determine the influence of temperature at the leak orifice. Two different test conditions were presented. Figure 3-15 (a) and (b) shows the temperature profiles for water and crude oil at leak point, at 300 K (27^{o}C) operating temperature. In the case of water and crude oil, the leak produced warm environment surrounding the leak orifice. The temperature rise is around 15 K (15^{o}C) for water and 40

K (40^{o}C) in case of crude oil. Figure 3-15 (c) and (d) shows the temperature contours of nitrogen and methane near leak area at 277 K (4^{o}C) operating temperature. In both cases, temperature drops around the leak orifice. This local cooling effect can be explained by the Joules-Thompson effect during gas decompression [29]. Near the leak vicinity strong vortices exists and results complex flow field around the leak [30]. Due to this complex flow field around the leak small eddies dissipate, and the energy turns from kinetic energy to thermal energy, cause local warming effect near leak for water and crude oil shows at Figure 3-15 (a) and (b) respectively. Temperature has an impact on the viscosity of the fluid. High viscous fluids have ability to generate acoustic signal noise in low frequency range which is discussed in section 3.5.2.

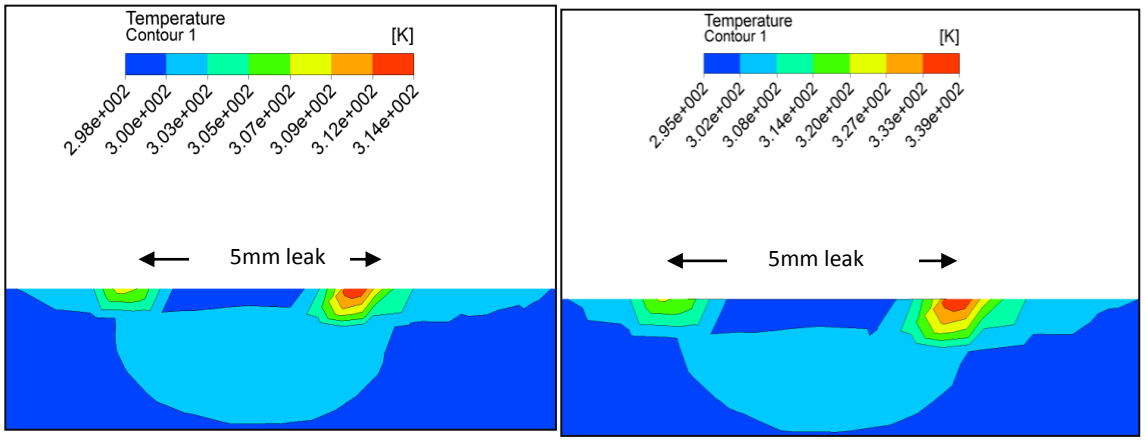

(a) water (operating temperature 300 K) (b) crude oil (operating temperature 300 K)

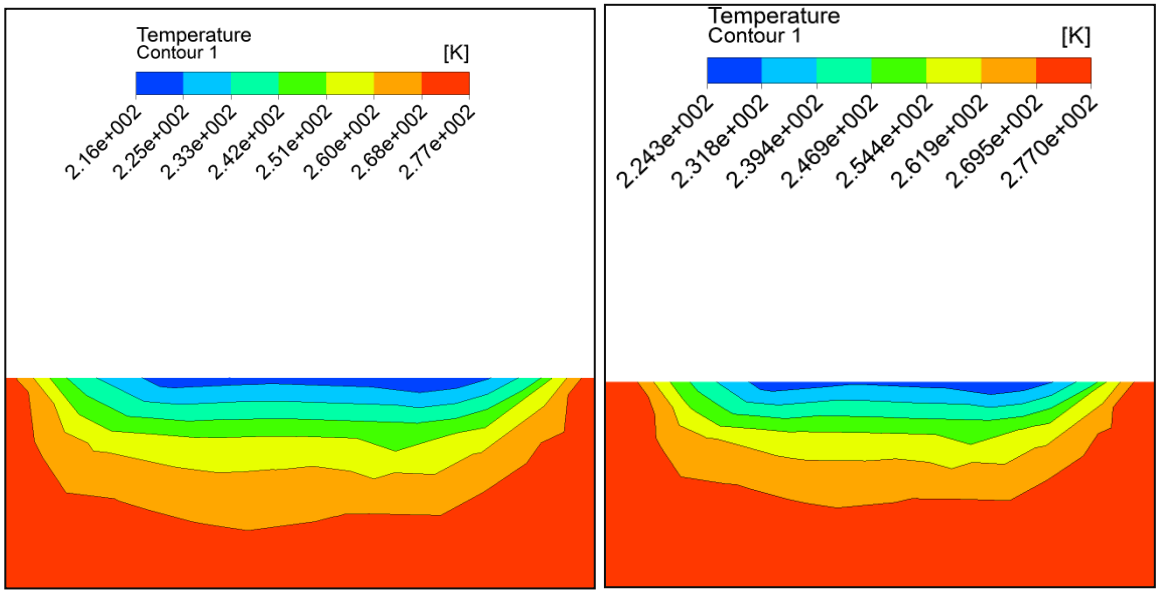

(c) nitrogen (operating temperature 277 K) (d) methane (operating temperature 277 K)

Figure 3-15: Zoomed view of local temperature change around the leak orifice. Pressure 40MPa (5800psi), velocity 9m/s, leak orifice 5mm. (a) water, (b) crude oil, (c) nitrogen, (d) methane as fluid.

3.5.2 Transient Simulations

3.5.2.1 Acoustic Signal Generation from Leak

In order to capture the turbulent feature of the flow inside the pipeline, a transient simulation has been performed. Flow velocity inside the pipeline was set as 9 m/s for 8 m long and 0.322 m diameter pipe. Large eddy simulation has been used to model the turbulence. To generate the acoustic data, FW-H model in FLUENT has been activated. Further, to obtain the higher frequency components, the time step of the simulation (Δt) is

selected as 0.0005 s and the number of iterations as 20000. The flow time must be at least 10 times of the time-period corresponding to the lowest frequency to obtain good results for low frequencies using FW-H method. In this scenario, the total flow time is 10 seconds which satisfies the requirement of having good results for low frequency. The write frequency (in number of time steps) was specified to 500, the write frequency allows to control how often the source data will be written. In order to save computational cost and resources the write frequency can be coarsened [36]. The wall of the pipe at the leak area has been selected as the source of the acoustic pressure signal. Six different positions have been selected as the receiver to capture the pressure signals showed in Table 3-3 and Figure 3-16. These locations are selected in such way so that the receivers can cover all directions and orientations around the leakage. Each iteration took around 10 seconds for one iterative time advancement with PISO solver scheme. During the calculation of acoustic field, the far-field sound speed was 1485 m/s, that is the speed of sound in water. The total simulation time was 45 hours with four parallel processors, each consisting of 2.4 GHz and 16 GB RAM.

Table 3-3: Receiver positions to monitor acoustic signals.

Position	**X** (m)	**Y** (m)	**Z** (m)
1	4	0.161	0
2	4.5	0.161	0
3	4.5	0.661	0
4	4	0.161	0.5
5	4	0.661	0.5
6	4	2.161	2

The contours of power spectral density (PSD) of the pressure signals measured at any arbitrary point contains information regarding the pipe condition. The PSD results a wide spectrum of frequencies for the turbulence of the flow. Figure 3-17 shows that the peak is higher at the leak vicinity. This should not be surprising because there is a very complex flow field creates near at the leak results high turbulence. This high turbulence pressure variations near leak area are responsible to creates high noise [31]. The acoustic noise signal attenuates as it moves far from the leakage.

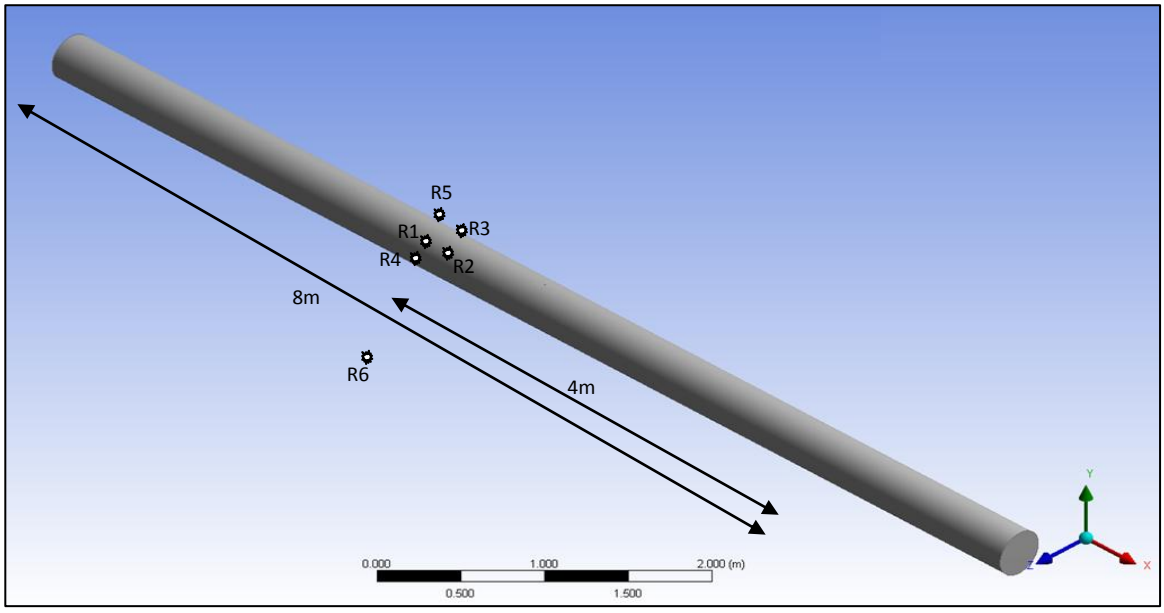

Figure 3-16: Receivers position at the pipeline.

Two different operating conditions were selected to generate the pressure signals. First case was with 5800 psi (40 MPa) line pressure and second case was with 200 psi (1.4 MPa). The PSD responses of the both signals are shown in Figures 3-18 and 3-19.

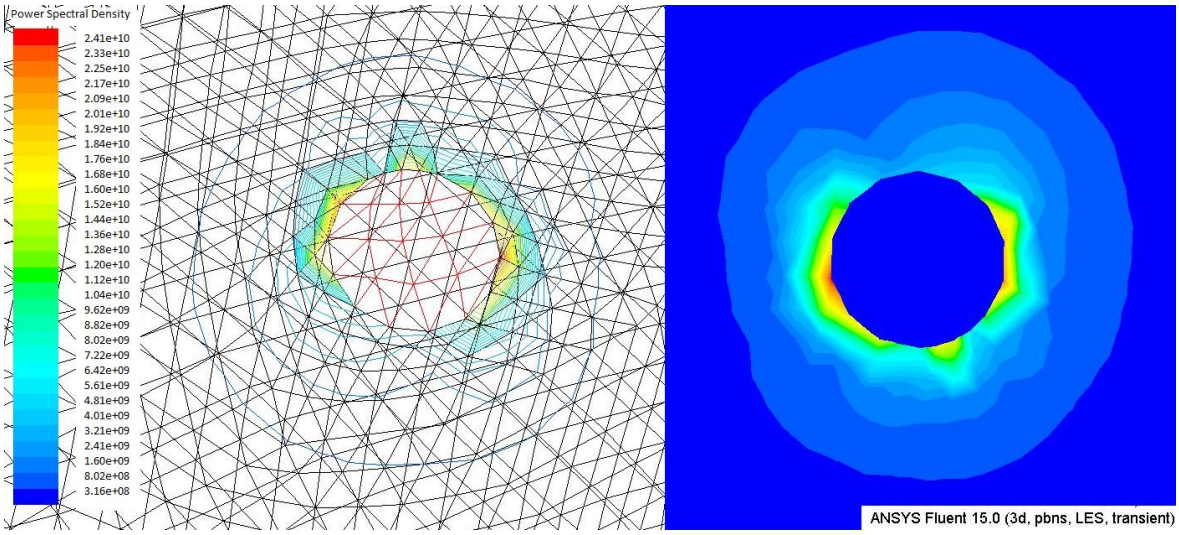

Figure 3-17: Attenuation of acoustic pressure signal response near leak orifice (5 mm).

The acoustic signal data near the leak orifice showed that noise is exists in the low frequency region. Figure 3-18 (a) shows that the maximum PSD is 7×10^{10} at 70-80 Hz frequency range at receiver 1 position, which is near the leak. Whereas Figure 3-18 (a) shows that the maximum PSD is 4.5×10^{5} at 40-50 Hz frequency range at the same receiver position. From these data, it is evident that the noise is clearly influenced by the pipeline pressure. The PSD also provides information about at which frequency range the maximum peaks are located. For example, Figure 3-18 shows the acoustic signal PSD at 0.5 m distance from the leak (i.e. receiver 4) is 3000 at 650-680 Hz, where at the same frequency range, the PSD at 2 m distance from the leak (i.e. receiver 6) was only 200.

The power spectral density gives information about where the maximum peaks are located. From the figures it is clear that the overall intensity of the signal is lower for the low pressure pipes. There is an advantage of having high pressure pipes to increase the noise from the leak. The leak orifice creates high turbulence with small eddies and the

flow pattern is very complex near leak vicinity. This high turbulence creates flow disturbance and it transmits across the pipe which creates acoustic signals, i.e. noise a distance from the leak vicinity. The unwanted noise signals due to turbulence are evident in Figures 3-18 and 3-19. It is important to nullify the unwanted noise signal generated, to determine the actual maximum value of PSD and the corresponding frequency ranges. There are many methods to filter out such noise signals; however, that not addressed in this present work. However, it is important to conduct a sensitivity study in order to get more insights. Only the effect of pressure to the acoustics signature is studied but there are other parameters such as: temperature, leak size, flow velocity and pipe geometry could effect the acoustic signal.

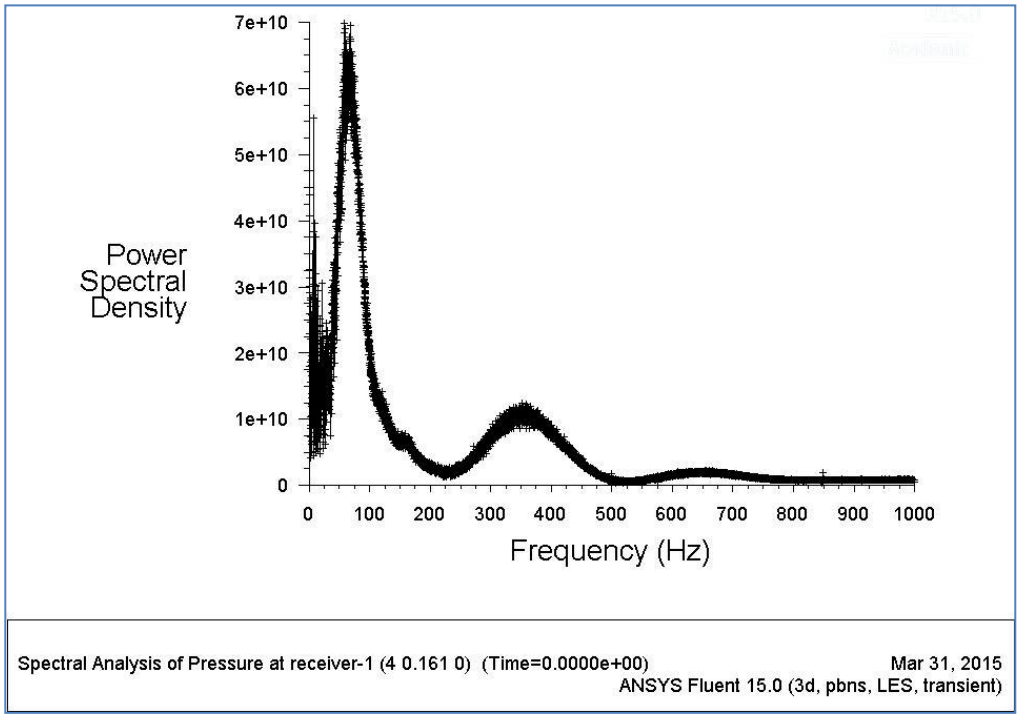

Figure (a) Fast Fourier Transformation of the pressure signals at 6 different leak positions. Water, 5800 psi, velocity 9 m/s, receiver 1

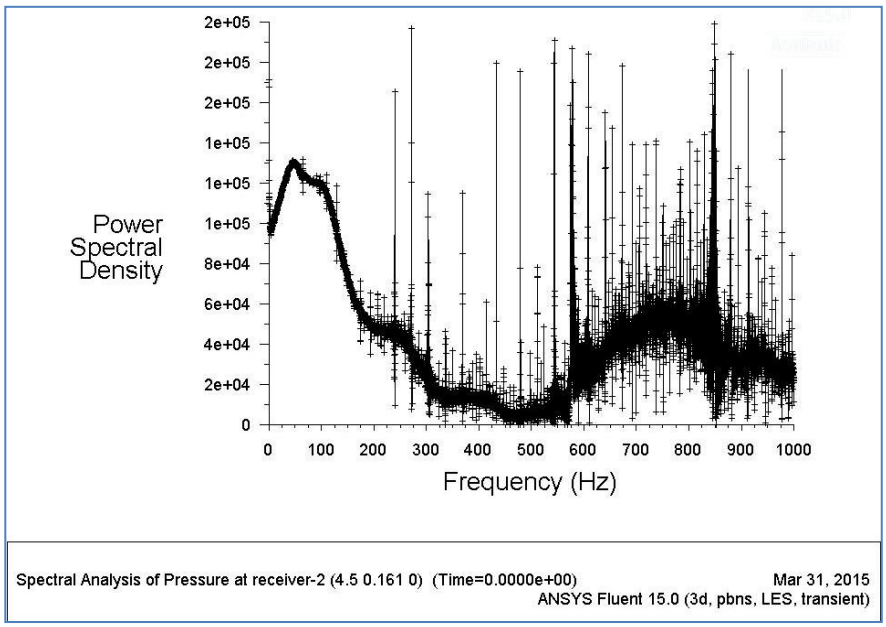

Figure (b) Fast Fourier Transformation of the pressure signals at 6 different leak positions. Water, 5800 psi, velocity 9 m/s, receiver 2

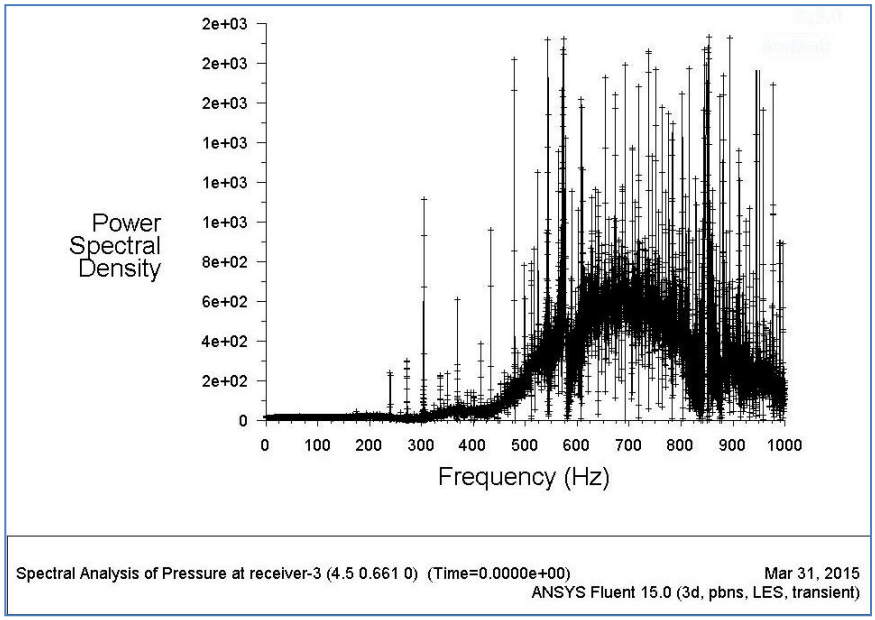

Figure (c) Fast Fourier Transformation of the pressure signals at 6 different leak positions. Water, 5800 psi, velocity 9 m/s, receiver 3

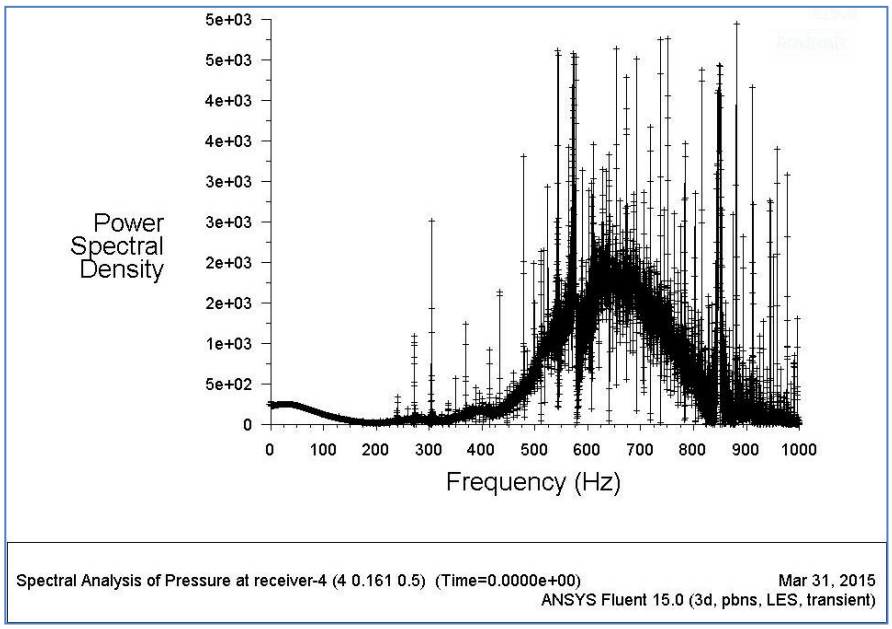

Figure (d) Fast Fourier Transformation of the pressure signals at 6 different leak positions. Water, 5800 psi, velocity 9 m/s, receiver 4

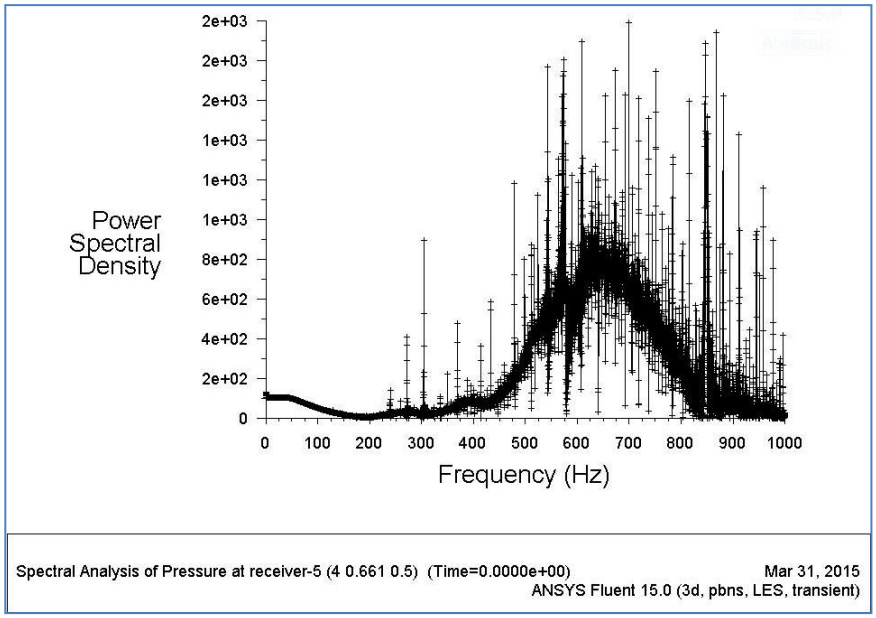

Figure (e) Fast Fourier Transformation of the pressure signals at 6 different leak positions. Water, 5800 psi, velocity 9 m/s, receiver 5

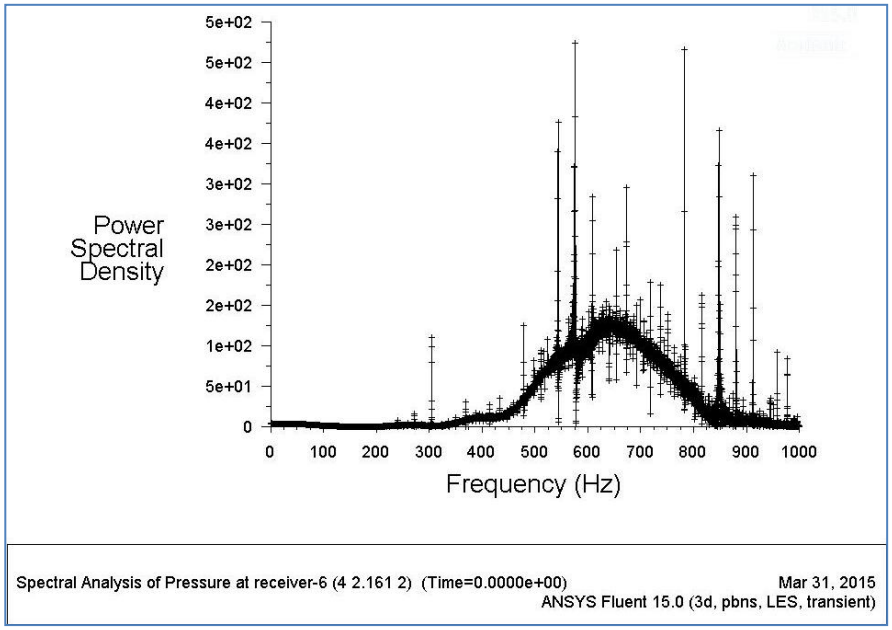

Figure (f) Fast Fourier Transformation of the pressure signals at 6 different leak positions. Water, 5800 psi, velocity 9 m/s, receiver 6

Figure 3-18: Fast Fourier Transformation (FFT) of the pressure signals at 6 different leak positions. Water, 5800 psi, velocity 9 m/s. (a) receiver 1 [x,y,z = 4, 0.161, 0], (b) receiver 2 [x,y,z = 4.5, 0.161, 0], (c) receiver 3 [x,y,z = 4.5, 0.661, 0], (d) receiver 4 [x,y,z = 4, 0.161, 0.5], (e) receiver 5 [x,y,z = 4, 0.661, 0.5], (f) receiver 6 [x,y,z = 4, 0.261, 2].

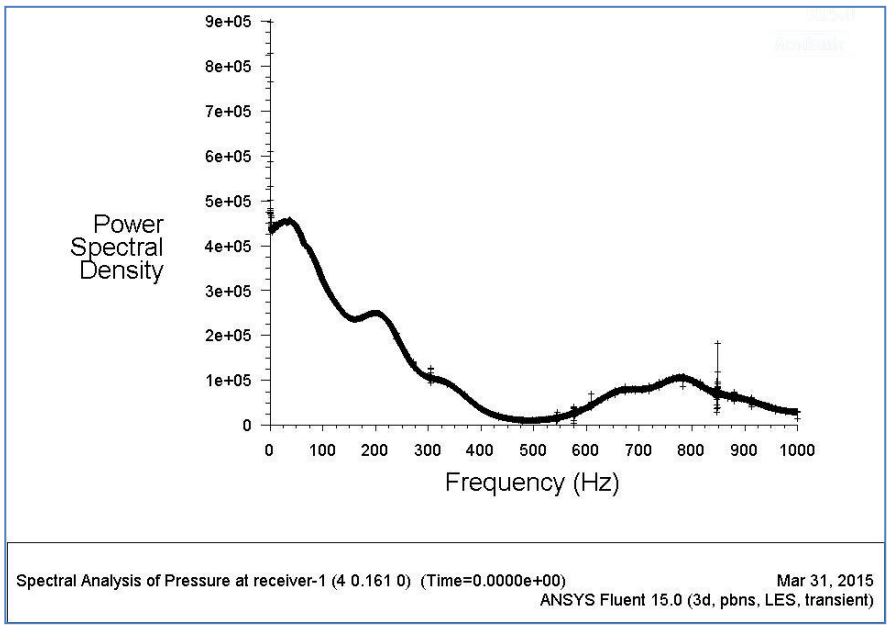

Figure (a) Fast Fourier Transformation of the pressure signals at 6 different leak positions. Water, 200 psi, velocity 9 m/s, receiver 1.

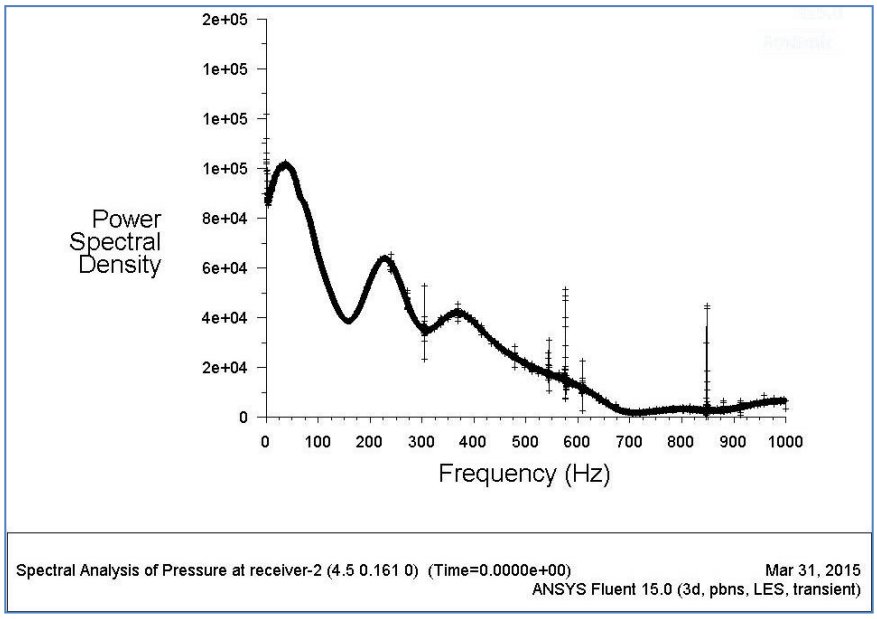

Figure (b) Fast Fourier Transformation of the pressure signals at 6 different leak positions. Water, 200 psi, velocity 9 m/s, receiver 2.

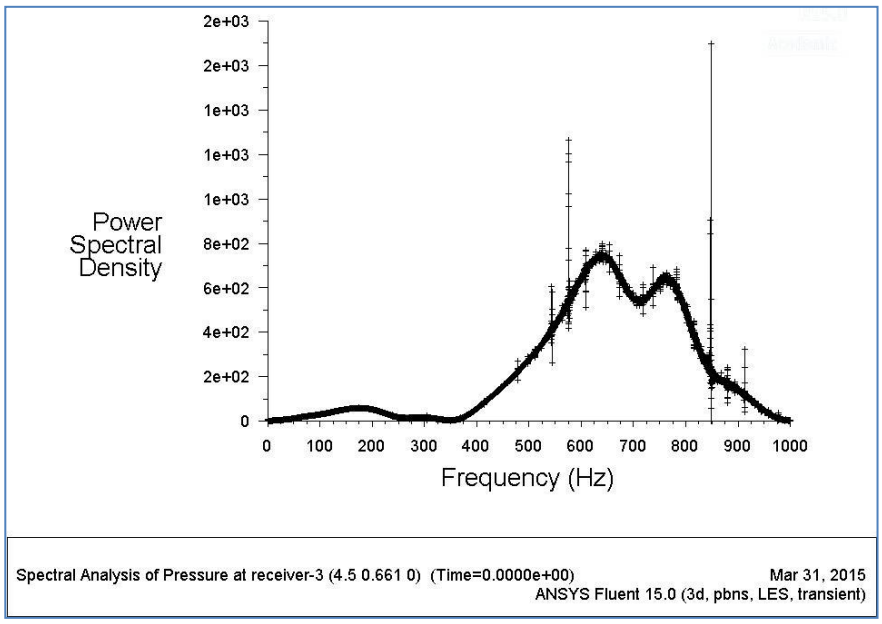

Figure (c) Fast Fourier Transformation of the pressure signals at 6 different leak positions. Water, 200 psi, velocity 9 m/s, receiver 3.

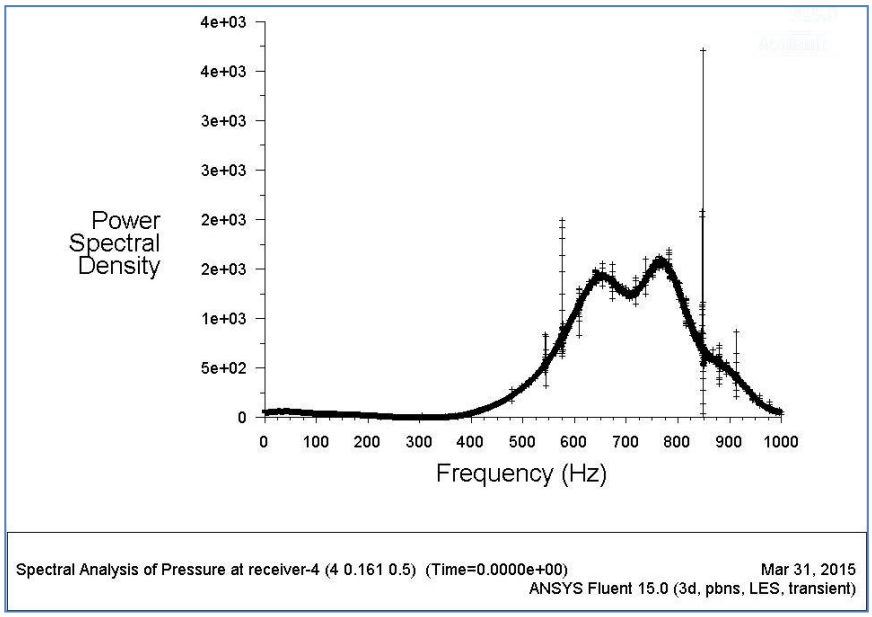

Figure (d) Fast Fourier Transformation of the pressure signals at 6 different leak positions. Water, 200 psi, velocity 9 m/s, receiver 4.

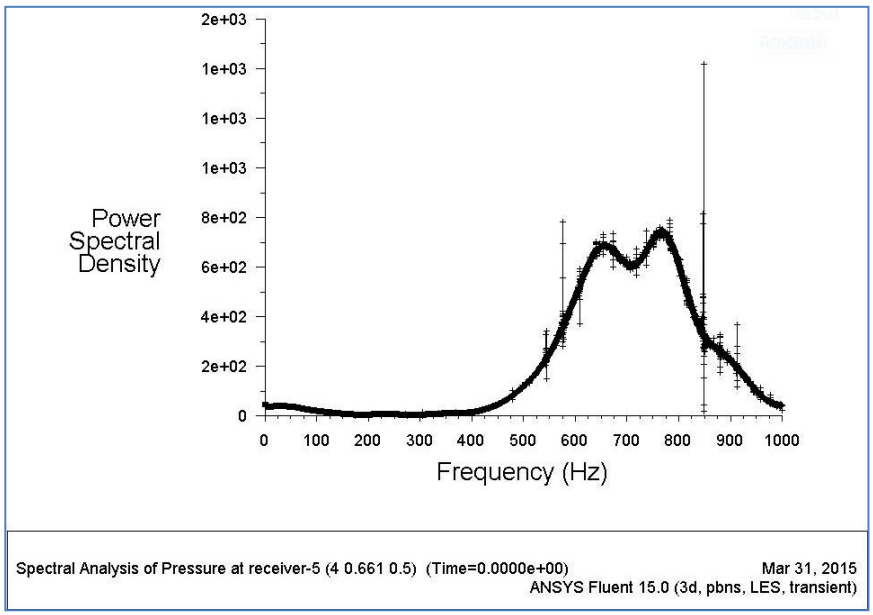

Figure (e) Fast Fourier Transformation of the pressure signals at 6 different leak positions. Water, 200 psi, velocity 9 m/s, receiver 5.

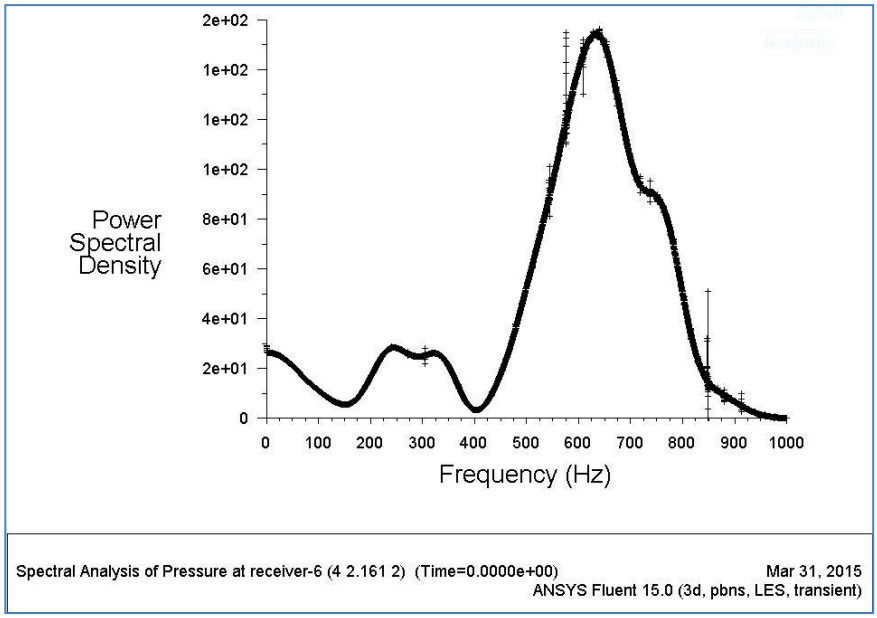

Figure (f) Fast Fourier Transformation of the pressure signals at 6 different leak positions. Water, 200 psi, velocity 9 m/s, receiver 6.

Figure 3-19: Fast Fourier Transformation of the pressure signals at 6 different leak positions. Pressure 200 psi, velocity 9 m/s. (a) receiver 1 [x,y,z = 4, 0.161, 0], (b) receiver 2 [x,y,z = 4.5, 0.161, 0], (c) receiver 3 [x,y,z = 4.5, 0.661, 0], (d) receiver 4 [x,y,z = 4, 0.161, 0.5], (e) receiver 5 [x,y,z = 4, 0.661, 0.5], (f) receiver 6 [x,y,z = 4, 0.261, 2].

3.5.2.2 Fluid Dispersion Model

The transient simulation is performed to obtain the flow trajectories for crude oil and gases. The simulation time for crude oil ran for 15 seconds, but for gases it ran for 1 second due to the high jet velocity. Figure 3-20 and 3-21 shows the fraction of volume of the fluids in water. There was a continuous oil flow pattern observed, which was originated from the leak source and dispersed at subsea. At t = 5 seconds, a small plume of crude oil can be seen, Figure 3-20 (a). This plume continued its growth with the time elapsed and at t = 15 seconds the plume almost covered half portion of the domain, as depicted in Figure 3-20 (b). From this simulation, it was also evident that initially the crude oil created a jet flow with the height of about 5 m but then the jet dispersed and started spreading under the joint influence of gravity, inertia force, buoyancy and shear stress. At t= 15 seconds the crude oil became more dispersed due to the low density and high viscosity of the crude oil compared to water. In case of gases, the plume is observed to be a jet, which is shown in Figure 3-21. The jet was sharp in the case of both nitrogen and methane. This was due to the higher velocity of gases and low density and viscosity.

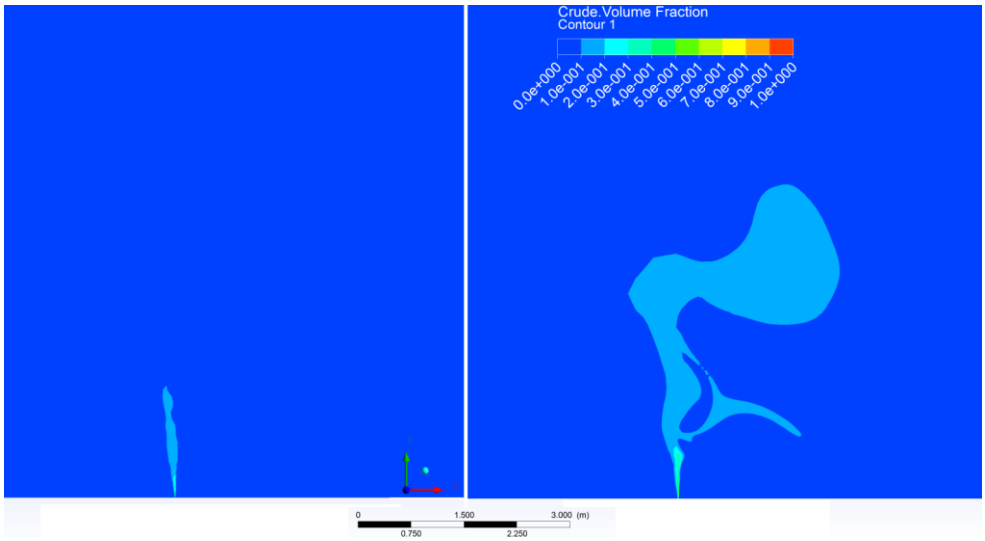

(a) (b)

Figure 3-20: Volume fraction of crude oil after dispersion at the subsea. Pressure 5800 psi. (a) at t = 5 seconds, (b) at t = 15 seconds.

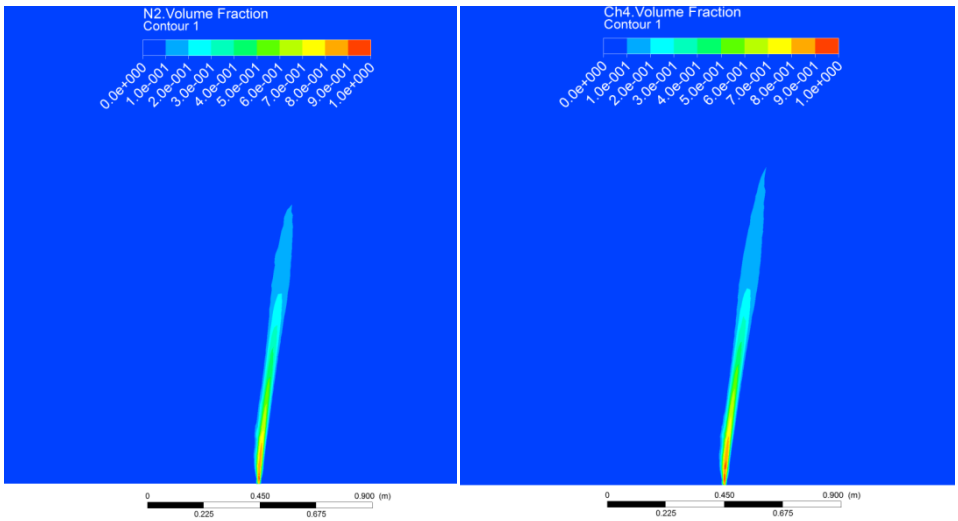

(a) (b)

Figure 3-21: Zoomed view of the volume fraction of nitrogen and methane after dispersion at the subsea (at t = 1 second). Pressure 5800 psi. (a) nitrogen, (b) methane.

3.6. Conclusions and Future Works

In this study, both steady state and transient simulations have been performed to determine the influence of the leakage from subsea pipelines. There are numbers of methods available for leak detection of the pipeline including, infrared thermography, ground penetrating radar, chemical tracer inducing method, free-swimming smart ball sensor inducing etc. From above, the most cost efficient with high accuracy method is the acoustic method; especially at the remote place like offshore and arctic pipelines. The model used in this study provided promising results in terms of the acoustics analysis. A single phase flow has been considered in this study for the simplification of the model, which might differ in real case scenario. There is a possibility of hydrate formation for high pressure and low temperature condition around the leakage which is also not considered in this model. Also, no sensitivity study has been performed to observe the influence of critical parameters (e.g. fluid velocity, pipe diameter) to the acoustic signatures. However, in the future works these crucial issues should be taken care of. The following conclusions can be drawn from this study:

- The steady state simulation results provided the local pressure and temperature change contours for different conditions and pipe fluids. The contours showed the pressure and temperature fluctuations were highly localized at the leakage zone.

- The effect of pipeline pressure on different leak orifice has been studied. A general correlation of the pressure, leak size and flow rate from leak orifice for different fluids have been established.

- The pressure gradient profiles showed better evidence of abrupt change of pressure near leak orifice and at the centerline of the pipeline, which is far from the leak vicinity. Pipe line leak with high pressure gradient generate higher noise compared to low pressure gradient.

- The acoustic signatures were generated from the transient simulation. The acoustic signals for different test conditions have been generated and compared for six different receiver position and four different type of fluids. The PSD data showed that the noise is clearly influenced by the line pressure. It also gave information about at which frequency range the maximum peaks are located. The acoustic signal attenuation with the distance is also measured from the PSD data of different receiver position.

- The dispersion pattern of leak fluid in the subsea condition from the pipeline leakage has been studied. The volume fraction and temperature change for different fluids and operating conditions were analyzed. The fluid dispersion pattern with time showed the trajectory of the plume.

- Based on these results an experimental study could be designed and performed which will provide more insights of detecting leak at the sub-sea oil and gas pipelines.

Acknowledgement

Authors gratefully acknowledge the support provided by INTECSEA Canada, MITACS at Memorial University of Newfoundland, Petroleum Research Newfoundland & Labrador (PRNL), RDC and NSERC.

Chapter 4

LNG Pool Fire Simulation for Domino Effect Analysis

Muhammad Masum Jujuly, Aziz Rahman, Salim Ahmed, and Faisal Khan

Safety and Risk Engineering Group
Faculty of Engineering & Applied Science,
Memorial University of Newfoundland, NL, St. John's, A1B 3X5, Canada.

Preface

A version of this manuscript has been published in 'Reliability Engineering and System Safety' journal on March, 2015 (Ref. No.: RESS-D-14-00570R1). The co-authors of this research work, Dr. Rahman and Dr. Ahmed supervised the author M. Masum Jujuly to develop the research methodology on the entitled topic and helped him to conceptualize the techniques and theories available for this topic. Corresponding author Dr. Khan was the principal supervisor of this work and provided knowledgebase support to the author and co-authors.

Abstract

A three dimensional computational fluid dynamics (CFD) simulation of liquefied natural gas (LNG) pool fire has been performed using ANSYS CFX-14. The CFD model solves

the fundamental governing equations of fluid dynamics, namely, the continuity, momentum and energy equations. Several built-in sub-models are used to capture the characteristics of pool fire. The Reynolds-Averaged Navier–Stokes (RANS) equation for turbulence and the eddy-dissipation model for non-premixed combustion are used. For thermal radiation, the Monte Carlo (MC) radiation model is used with the Magnussen soot model. The CFD results are compared with a set of experimental data for validation; the results are consistent with experimental data. CFD results show that the wind speed has significant contribution on the behavior of pool fire and its domino effects. The radiation contours are also obtained from CFD post processing, which can be applied for risk analysis. The outcome of this study will be helpful for better understanding of the domino effects of pool fire in complex geometrical settings of process industries.

Keywords: pool fire, liquefied natural gas (LNG), computational fluid dynamics (CFD), domino effect.

4.1 Introduction

Fire and explosion are among the most dangerous accidents in process facilities; especially pool fire is the most frequent incidents. Several catastrophic accidents e.g. Buncefield, UK (2005), Puerto Rico, USA (2009), Sitapura, India (2009) and Bucheon LPG filling station, Korea (1998) were caused by pool fire [41, 42]. Pool fire is an

uncontrolled combustion of vapor generated from a flammable liquid pool such as, liquefied natural gas, gasoline, jet fuel and so on. The chain of accidents, termed as 'domino effect' may lead to extremely severe consequences. Analyzing past accidental scenarios it is observed that more than half of the industrial domino accidents involved fire as a primary event. Pool fire is responsible for triggering 44% of all physical accidental scenario which escalates domino effect [48]. The direct flame engulfment and steady radiation from the pool fire is the reason for the escalation of this kind of accidents. In order to avoid such calamity a detail study on pool fire is required to save human lives and prohibit the destruction of a facility. To quantify the risk involved with pool fire, it is important to understand its characteristics. Pool fire characteristics largely depend on the fuel mass burning rate which is a function of the fuel properties, pool diameter and the wind speed. Several methods are available in the literature to calculate surface emitting power of a pool fire [43, 44].

There are two major types of models available to calculate pool fire characteristics, analytical models and numerical models, such as computational fluid dynamics (CFD) models. The point source model and the solid flame model are two examples of analytical models which have been used to analyze fire radiation hazard for a long time. The point source thermal radiation models are based on the assumptions that the flame is a single point source of thermal energy and the thermal radiation intensity varies inversely with the square of the distance. The point source model can predict radiation in larger distances from the flame but in closer distances it underestimates the thermal radiation. The reason behind this is that the thermal radiation is considered a single point source

where as in closer distances flame radiation depends on the size, shape and the orientation of the flame [59]. Another major limitation of the point source model is that it does not consider the effect of smoke. This model also does not consider the wind velocity and direction. For these limitations, point source model is not recommended for modeling large pool fire [46].

Solid flame models and the modified solid flame models are widely used as alternatives of the point source model. In the solid flame model a cylindrical shaped flame zone is considered as a radiating object. In the modified solid flame model two zones are considered: a clear zone and a soot zone with different irradiance power. Although solid flame and modified solid flame models are well established and validated by experimental results, there are still some drawbacks of using these models. These models assume similar irradiance of fire throughout the solid circle zone. Advanced turbulence model is not used in these models to capture the full dynamics of pool fire in eddy scale. During the wind scenario the tilt of the flame as a solid cylinder is practically not valid. In case of complex geometries these models cannot predict the exact behavior of pool fire [47].

Analytical methods are very convenient to calculate the radiation hazard because of their simplicity and accuracy. However, analytical methods are case specific and cannot be applied to complex geometries. Moreover, with analytical methods the domino effect cannot be fully captured.

Although numerical methods are relatively complex, they can reliably predict radiation hazard. Few studies have been performed using computational fluid dynamics (CFD) for numerical investigation of fire related hazard [47, 50-57]. CFD models have much better temporal and spatial fidelity than point source or solid flame models. However, valid assumptions and boundary conditions are required to analyze pool fire using numerical approach at the pre-processing stage. The simulation time of CFD for a complex geometry may be high. Apart from these constraints, CFD is the most reliable and realistic method for fire simulation. Detailed assessment of the domino effect scenarios require advanced three dimensional fire and explosion or dispersion scenarios and their interaction with structures [48]. CFD codes give the advantage to simulate such scenarios. Khan et al. [49] suggested a mechanism to calculate the probability of occurrence of domino effects and forecast the impacts of such chain accidents. The probability of domino effect occurrence depends not only on the damage potential of the primary accident, but also on a number of other factors of the secondary unit. The post processing results obtained from a CFD simulation can accurately predict the probability of domino effect occurrence. Several studies have modeled the pool fire and the consequences involved in case of the release of hydrocarbons. Hyunjoo et al. [50] used ANSYS CFX-11 to predict the instantaneous and time-averaged flame temperature and thermal radiation intensity of organic peroxide pool fire. Alireza et al. [51] performed a similar study with organic pool fire using ANSYS FLUENT to predict the safety distance from the pool. Schalike et al. [52] simulated LNG pool fires using ANSYS FLUENT: three different diameters (d = 1 m, 6.1 m, 30 m) were used to simulate the flame temperature and thermal radiation intensity. In their study, large eddy simulation (LES) is used as the

turbulence model. For modeling combustion, the laminar flamelet approach was taken. The discrete ordinates (DO) model is used for radiation and the Moos-Brookes model is used to model soot formation. The objective of their study is to predict the mass burning rate of LNG. Some consequence analysis studies were also performed to predict and quantify the probability to cause serious injury to personnel, major damage to equipment and structure and disruption of operations. Pula et al. [53] used a grid based approach to analyze the consequences for fire and explosion. Mohammad et al. [54] proposed an integrated approach to model the entire sequenced involved in a potential accident; an integrated accident scenario of liquid and gas release was modeled using FLACS and FDS codes. Hansen et al. [55] used FLACS codes in order to simulate the release and dispersion of LNG and compared the result with experimental data to confirm that FLACS is suitable for modeling LNG dispersion. Gavelli et al. [56] analyzed the consequences resulting from the ignition of LNG vapor cloud dispersion during the offloading process. FLACS CFD codes were used to model the vapor cloud dispersion and ignition. The study showed that the sequences of events led to a pool fire after the release of LNG and ignition. Currently ANSYS CFX and FLUENT are becoming more popular for the numerical investigation of fire, explosion, fluid dispersion and consequence analysis. Ruifeng et al. [57] used ANSYS CFX-11 to perform simulations of LNG vapour dispersion and its consequences; a parametric study was performed to study the effects of atmospheric conditions, LNG pool diameter and turbulence intensity, and the presence of obstacles. Sun, B. et al. [47] conducted a 3-D CFD simulation of LNG pool fire using ANSYS FLUENT-14; an advanced turbulence model large eddy simulation (LES) was used to simulate the pool fire with additional sub-models for

combustion and radiation. The model outcomes were then compared with experimental results for validation.

In this work, a CFD study is performed to evaluate the effects of environmental conditions on the domino effects of an LNG pool fire. The most important feature of this study is analysis of the effects of pool fire on the surrounding processing units using the CFD post-processing results. From the effect of local temperature of the processing units the safe distance of the adjacent tank with flammable liquids can be determined. The maximum thermal radiation intensity and the temperature received by the processing units can be used to perform hazard analysis.

4.2 Theoretical Framework for CFD Simulation

The numerical simulations in this study are carried out with the commercial computational fluid dynamics (CFD) code ANSYS CFX-14. It uses element based finite volume method (FVM) to discretize computational domain utilizing finer meshing [57]. The mesh creates finite volumes which are used to solve mass, momentum, energy equations. Discretization helps to linearize a large system of non-linear algebraic conservation and transport equations [58]. A general solution strategy of ANSYS CFX-14 solver for a steady-state simulation of combustion-radiation model is given in Figure 4-1.

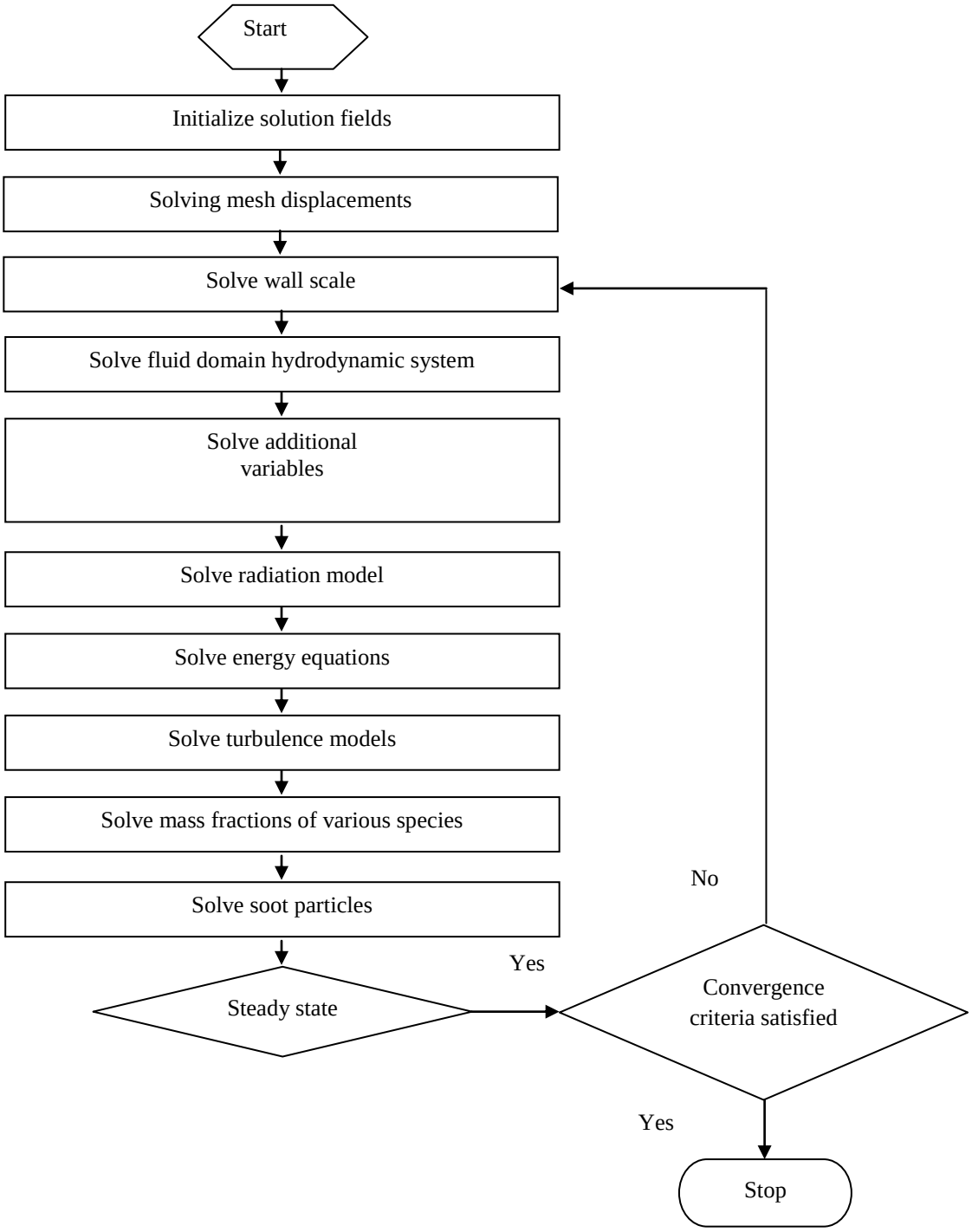

Figure 4-1: Solution procedure for a steady-state simulation by ANSYS CFX-14.

Heat transfer through combustion is complex and consists of various physical and chemical processes. These include buoyancy driven flow, turbulence, fuel evaporation, fuel combustion, radiation heat transfer and the interaction between solid structures and radiant heat. These physical and chemical processes are modeled as a set of partial differential equations with boundary conditions. The theoretical framework of a CFD simulation is based on the solution of the conservation equations, namely, mass, energy and momentum conservations [59].

The overall conservation equation is:

$$\frac{\partial(\rho\Phi)}{\partial t} + \nabla.(\Phi\rho\vec{v}) = \nabla.\left(D^{(\Phi)}\nabla\Phi\right) + S_{\Phi} \quad (4\text{-}1)$$

where ρ (kg/m^3) is the density of the fluid and $\vec{v}$ is the velocity vector. The general exchange coefficient $D^{(\Phi)}$ is determined through local sources S_{Φ} and the temporal change of variable property Φ. Pool fire simulation requires the conservation equation of reactive mixture of fuel [60, 61]. These equations are given bellow:

Continuity equation ($\Phi = 1$)

$$\frac{\partial\rho}{\partial t} = -\nabla.(\rho\vec{v}) \quad (4\text{-}2)$$

Momentum conservation equation ($\Phi = \vec{v}$)

$$\frac{\partial(\rho\vec{v})}{\partial t} + \nabla.(\rho\vec{v}\vec{v}) = -\nabla p + \nabla.\tau + S_{\mathrm{M}} \quad (4\text{-}3)$$

$$\tau = \mu(\nabla\vec{v} + \nabla(\vec{v})^T - \frac{2}{3}\delta\nabla.\vec{v}) \quad (4\text{-}4)$$

where τ is stress tensor, p is pressure, and μ is dynamic viscosity.

Energy conservation equation ($\Phi = E$)

$$\frac{\partial(\rho \mathrm{E})}{\partial t} - \frac{\partial p}{\partial t} + \nabla.(\mathrm{E}\rho\vec{v}) = \nabla.(\lambda \nabla T) + \nabla.(\vec{v}.\tau) + \vec{v}.S_{\mathrm{M}} + S_E \quad (4\text{-}5)$$

$$E = h + \frac{v^2}{2} \quad (4\text{-}6)$$

where E is total energy, λ is conductivity and S_E is energy source term. The term $\vec{v}.S_{\mathrm{M}}$ is the work due to external moment source and is often ignored.

4.2.1 Sub-models in Fire Modeling

To simulate thermal radiation of a pool fire using ANSYS CFX-14, different sub-models are used, which are presented as follows:

- Turbulence model
- Non-premixed combustion model
- Radiation model
- Soot model

4.2.1.1Turbulence Model

Reynolds-Averaged Navier–Stokes (RANS) equation based turbulence model is selected to simulate pool fire in this paper. This approach is more commonly used compared to its

alternative large eddy simulation (LES) [62]. RANS equation based models are the only modeling approach for steady-state turbulent flow simulation [75]. Two equations model such as the standard $k-\epsilon$ model is most widely used in engineering turbulence modeling for industrial applications based on RANS turbulence equation. In this model, two transport equations, turbulent kinetic energy, k, and the dissipation rate of turbulent kinetic energy,ϵ, are solved. The $k-\epsilon$ model is based on the eddy viscosity concept where the effective viscosity, μ_{eff}, accountable for turbulence is modeled as:

$$\mu_{eff} = \mu + \mu_t \tag{4-7}$$

where μ_t is the turbulent viscosity and $k-\epsilon$ model assumes that the turbulent viscosity is linked to the turbulence kinetic energy and dissipation via this relation: $\mu_t = C_\mu \rho \frac{k^2}{\epsilon}$. Fluid density ρ and $C_\mu$is a constant [58]. The $k-\epsilon$ model is numerically robust and proven to be stable. It has well established regime of predictive capability and it offers good accuracy [63]. The implementation of RANS turbulence model into CFD is easy and computationally least expensive with satisfactory results for engineering applications [64, 69].

4.2.1.2 Non-premixed Combustion Models

The combustion is a very rapid and complex mechanism by which different species are formed as well as destroyed. In a premixed combustion process, the molecules of reactant are partially or fully premixed with the oxidant. Most of the natural diffusion flame

scenarios (including pool fire) are non-premixed where two distinct separated flows of gasified fuel is mixed with air and creates a reactant mixture for combustion. The mixture fraction f is a scalar variable defined as the mass fraction of burned and unburned fuel.

$$f = \frac{Y_\alpha - Y_{\alpha_{ox}}}{Y_{\alpha_{fu}} - Y_\alpha} \tag{4-8}$$

Where Y_α is the mass fraction of the species α and the subscripts ox and fu represents oxidizer and air, respectively. The transport equation for f is expressed as similar to that of the multi-component fluids with additional reaction term in ANSYS CFX when $k-\epsilon$ turbulence model is used in the RANS equation [65].

$$\frac{\partial(\rho f)}{\partial t} + \nabla.(\rho f \vec{v}) = \nabla.\left(\Gamma_{i_{eff}} \nabla f\right) + S_i \tag{4-9}$$

where $\Gamma_{i_{eff}}$ is the molecular diffusivity coefficient and S_i is the chemical reaction rate of species i.

The eddy-dissipation model developed by Magnussen and Hjertager [66] is used in this simulation. This model is based on the interaction between chemistry and turbulence. In this model the turbulence is treated via RANS equation based $k-\epsilon$ model and the chemical kinetics coupled with turbulence model by eddy-dissipation concept [76]. Mixing time of the reactants at molecular level is directly related to the reaction rate. This mixing time is directly proportional to the eddy properties in turbulent flows.

$$Reaction\ rate \propto \frac{\epsilon}{k} \tag{4-10}$$

The eddy-dissipation model is widely used in industrial combustion problems due to its simplicity and reasonably good correlation with measured data [63].

4.2.1.3 Modeling of Thermal Radiation

The radiative transfer equation (RTE) is a complex integral-differential equation. The combustion process consists of highly non-isothermal and non-homogeneous medium where taking account of the spectral variation of the radiative properties of the medium is important [63]. The RTE considering absorption, emission and scattering effect can be expressed as:

$$\frac{dI_\nu(\vec{r},\vec{s})}{ds} = -(\alpha_\nu + \sigma_{s\nu})I_\nu(\vec{r},\vec{s}) + \alpha_\nu I_b(\nu,T) + \frac{\sigma_{s\nu}}{4\pi}\int_{4\pi} dI_\nu(\vec{r},\vec{s}')\Phi\,(\vec{s}.\vec{s}')d\Omega' + S \quad (4\text{-}11)$$

where ν is the frequency, $\vec{r}$ and$\vec{s}$ are the position and the direction vector, s is the path length, α is the absorption coefficient, σ is the Stefan-Boltzmann constant ($5.67 \times 10^{-11} kW/m^2K^4$), I_ν is the spectral radiation intensity, I_b is the black body radiation intensity, T is the local temperature, Φ is the in-scattering phase function, Ω' is the solid angle and S is the radiation intensity source term.

There are several ways to solve the radiation equation, such as, statistical method, zonal method, flux method and hybrid method. Among these, the statistical method (Monte Carlo) is widely used because of its convergence properties [62]. In this simulation solid media is used as objects to determine the radiation effect on the solid. For solid-fluid media interfaces in the model, the same radiation interface model need to be used. Monte

Carlo is the only suitable model in this case. Another benefit of the use of Monte Carlo simulation is, during simulations with different solid objects each radiation model can be chosen independently [59].

4.2.1.4 Modeling of Soot Formation

The Magnussen soot model is used as soot formation model in a combustion system. It is assumed that soot is formed in two different stages from a gaseous fuel. The first stage represents the formation of radical nuclei and the soot particle formation from these nuclei is presented at the second stage [63]. The transport equations for the soot mass fraction $\widetilde{Y}_s$(kg/kg) and specific concentration of radical nuclei X_N(mol/kg) are:

$$\frac{\partial(\bar{\rho}\widetilde{Y}_s)}{\partial t} + \nabla.\left(\bar{\rho}\widetilde{Y}_s\vec{v}\right) = \left(\bar{\mu} + \frac{\mu_t}{Pr_t}\right)\nabla\widetilde{Y}_s + \tilde{S}_{soot,f} + \tilde{S}_{soot,c} \quad (4\text{-}12)$$

$$\frac{\partial(\bar{\rho}X_N)}{\partial t} + \nabla.\left(\bar{\rho}X_N\vec{v}\right) = \left(\bar{\mu} + \frac{\mu_t}{Pr_t}\right)\nabla X_N + \tilde{S}_{nuclei,f} + \tilde{S}_{nuclei,c} \quad (4\text{-}13)$$

In fire scenario calculations in CFD the soot variables are assigned to one of the fluids because soot variables cannot be a separate phase from the fluid. The formation of soot particles is computed empirically using the Tenser model [70]. Magnussen's eddy dissipation concept is used for modeling the effect of turbulence at the formation of nuclei and soot particles [50, 59].

4.3 CFD Simulation Procedure

The main purpose of CFD simulation in this study is to predict the flame and subsequent wall temperature (T), thermal radiation intensity or the surface emitting power (SEP) of the pool fire and the effect of these parameters on the solid units. In this simulation multiple step reaction set with different sub-models are used as discussed in Section 4.2.1. The computational domain of this simulation consists of 3-D rectangular hexahedral mesh. The dimension of the domain length and width is 100 m×100 m and 70 m high. The pool is placed at the center of the domain surrounded by a low rim and adiabatic ground surface. Pool diameter is selected as 15 m and burning rate is assumed 0.177 kg/m^{2}s which are the same as the China Lake test [67, 68]. The other wider boundary conditions are set as pressure outlet. These remaining boundaries are placed relatively distant from the fire source so that the physical features can be fully developed to achieve open boundary conditions. Solid units such as tanks and other installations are placed inside of the domain and solid-fluid domain interfaces are created to connect multiple unmatched meshes within the domain. The rectangular hexahedral cells are computationally more efficient and non-uniform mesh structure at the pool inlet is used. Total number of elements used is 358,452 with finer mesh close to the center of the pool in order to capture all necessary macroscopic features of the fire.

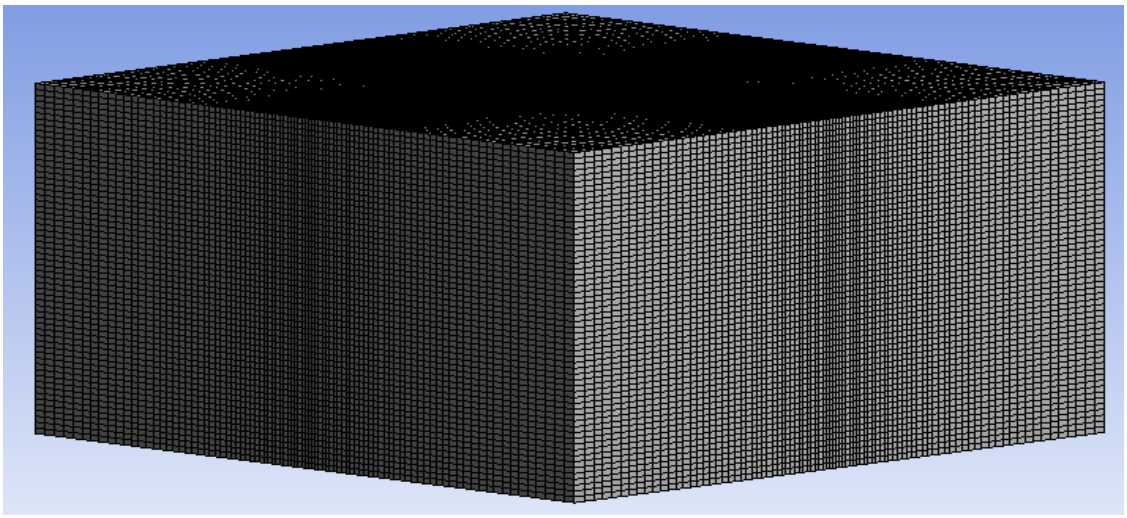

(a) Mesh of the external domain.

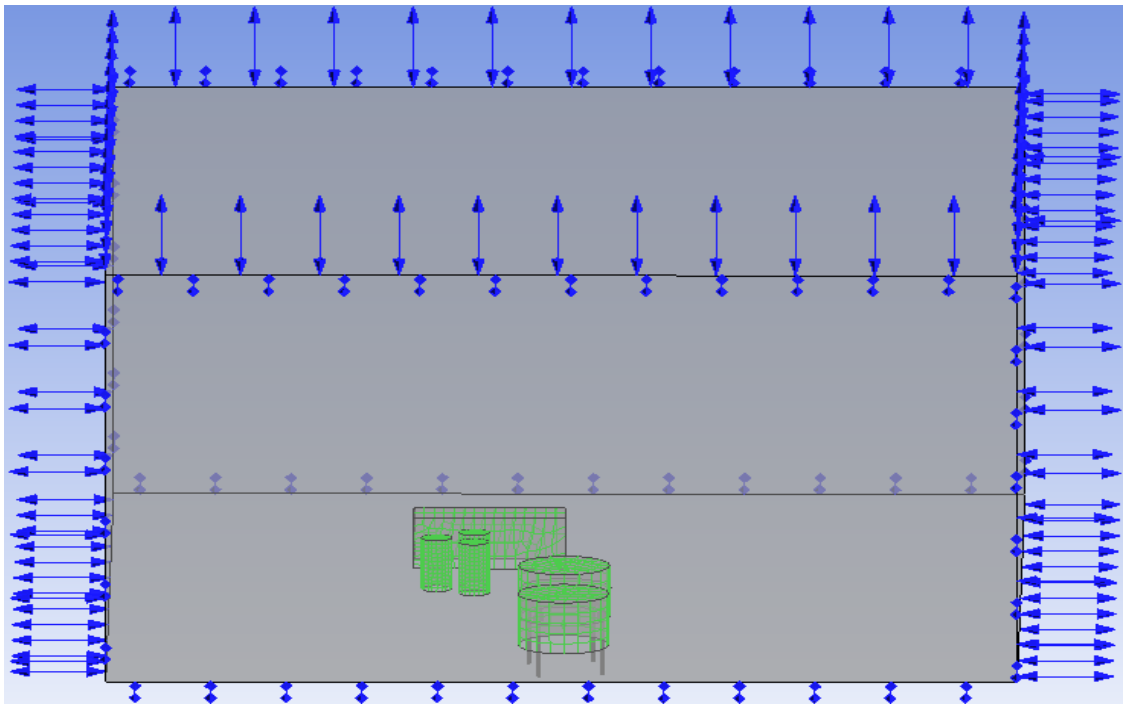

(b) Mesh of the internal elements (solid objects) domain.

Figure 4-2: A schematic diagram of 3-D rectangular hexahedral mesh applied in this simulation. (a) Mesh of the external domain. (b) Mesh of the internal elements.

In order to make sure the numerical solution of the simulation is independent on mesh size, a mesh-independency study is also performed. The different grid sizes are used to vary the total number of grids shown in Table 4-1. The time averaged flame temperature of the pool fire is observed for LNG pool fire with 15 m pool diameter. The results presented in Figure 4-3 show the pool fire temperature distribution has insignificant effect on grid 4 and grid 3. Hence, grid 4 is chosen to make sure the simulations are independent with the number of mesh.

Table 4-1: Mesh-independency study by selecting different grid sizes.

Grid no.	Number of nodes	Number of elements
1	156079	177338
2	258135	290825
3	351278	391658
4	320887	358452

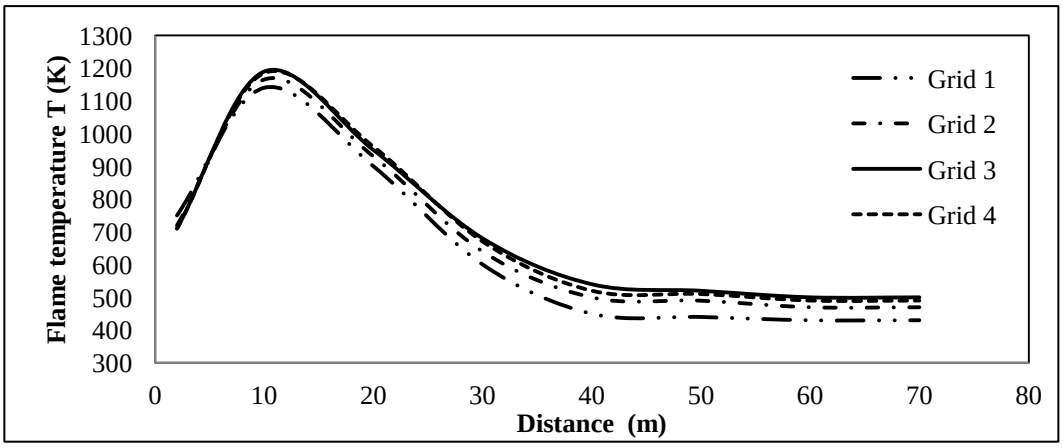

Figure 4-3: Mesh-independency study by selecting different grid sizes.

Table 4-2: Initial conditions for the CFD simulation of pool fire.

Initial conditions	
parameter	**Value**
$\boldsymbol{N_2}$ **mass fraction**	0.748
$\boldsymbol{O_2}$ **mass fraction**	0.232
$\boldsymbol{CO_2}$ **mass** fraction	0.01
vapour mass fraction	0.01
domain pressure	$1\ bar$
relative pressure	0
domain temperature	$298K$
wind velocity	$0\ m/s, 3\ m/s, 5\ m/s, 9m/s$
gravitational force	$9.8m/s^2$
mixing fraction	non premixed

The initial computational domain contains air consists of nitrogen, oxygen and carbon dioxide at ambient condition, T = 300 K and P = 101.3 kPa. The fuel source is defined as an inlet to the pool. It is assumed that the fuel is already evaporated and the evaporated fuel vapor is coming through the inlet to the domain. The evaporated fuel creates a reacting mixture slightly at the top of the pool rim from the ground at the vaporization temperature of the fuel [50, 52]. The burning rate of 15 m diameter LNG pool fire is 0.177 kg/m^{2}s, obtained from the experimental results of China Lake LNG test [67]. It was assumed that the mass burning rate of the fuel for 15 m pool diameter is equal to the pool inlet mass flow rate. The initial conditions and the boundary conditions are presented in Table 4-2 and Table 4-3 respectively. Thermal radiation and the soot generation are coupled by using gray gas approach [52]. Simulation with cross-wind is performed to predict the radiation with wind and without wind velocity.

Table 4-3: Boundary conditions for the CFD simulation of pool fire.

Boundary conditions	
Surface area	adiabatic
Outlet (4 walls and top)	pressure outlet
Inlet	mass flow rate of fuel

The simulation started with the RANS equation based $k-\epsilon$ model. The automatic time scale shows that the size of the flame grows from the time initially it started until the full size is reached. The convergence accuracy level set as 10^{-4}, however, the convergence level depends on sub-models used in this simulation. Total simulation time was 27 minutes with Intel Xeon 3.40 GHz CPU with 8GB RAM. The simulation performed on the 'double precision parallel environment'. The simulation running mode was 'platform MPI local parallel' with four partitions. The solver's memory allocation factor for the simulation was 3.

4.4 Result and Discussions

4.4.1 Experimental Result from Literature

A field test of LNG pool fire experimental data available in the literature [67, 68, 74] are used to validate CFD results. The LNG spill volume in 'China Lake' LNG pool fire experiment was ranged to 3 m^3 - 5 $m^3$and the spill was controlled in 50 m × 50 m × 1 m depth pond as shown in Figure 4-4. The diameter of the pool was 15 m [68]. The total duration of burning was 75 sec. The test result 6 of this series of experiment is summarized at Table 4-4 [67, 68].

Table 4-4: Test result of LNG pool fire experiment in China Lake test (test 6) [67].

LNG spill volume m^3	Spill duration sec	Pool diameter m	Duration of burning sec	Burning rate m/s	Wind speed m/s	Visible flame length m	Mean SEP (field test) kW/m^2	Mean SEP analytical model kW/m^2
5.7	52	15	40	8.06	3.1	42±6.4	185±6	172

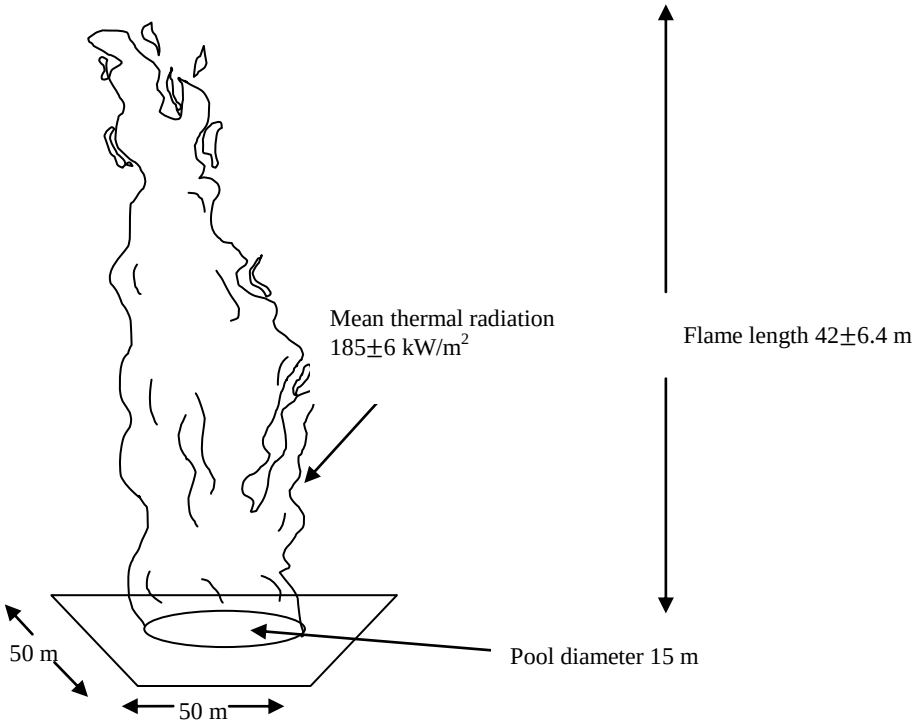

Figure 4-4: Illustration of LNG pool fire experiment (d = 15 m) in China Lake test.

4.4.2 CFD Result Validation

The experimental value from China Lake test (test number 6) is compared with the CFD post processing results for 3 m/s wind. The summery is given in Table 4-5. The CFD result shows close match with experimentally obtained value.

Table 4-5: Experimental value from China Lake test (d = 15 m) and CFD result for 3 m/s wind condition [68].

Parameters	Field test data	CFD result	Analytical method
Pool diameter (m)	15.4	15	15
Wind speed (m/s)	3.1	3	3
Flame length (m)	42 ± 6.4	40 (at visible flame range T > 550 K)	-
Mean ratio (L/D)	2.8	2.6	-
Radiating surface area (m^2) [74]	1980[#]	1767	-
Mean SEP (kW/m^2)	185 ± 6	174.4[*]	172

[#] Radiating surface area is calculated using pool diameter and average length of the visible flame considering cylindrical surface.
[*]Radiation intensity calculated from 0.5 m above ground.

The CFD post-processing results are compared with the field test values obtained from the China Lake NLG test [68]. The China lake test is carried out on water which is a non-adiabatic surface. This simulation for the model validation is also performed in a non-adiabatic surface condition. The thermal radiation is 185 ± 6 kW/m^2 and flame length is 42 ± 6.4 m, according to the test results. Analytically obtained result [67] of this experiment is 172 kW/m^2. CFD simulations results from this study are 174.4 kW/m^2 for thermal radiation and 40 m for the flame height. The relative error of the mean SEP or thermal radiation intensity is 2.56% from the field test data to CFD result and 1.37% from the result produced in analytical method. The dimensionless number length to diameter ratio (L/D) which dominates the flame geometry [43] is a very close match with the CFD and field test data and the relative error is only 0.71%. A narrow angle radiometer (NAR) is used to measure the fire radiative emissive power in China lake test. In case of test number 6, the narrow angle of NAR was projected in 12.1 ± 0.4 degree which gave the local thermal radiation value of the flame. The distance between the NAR and the center of the fire was 60 m [74]. Placement of the radiometer is very important to get accurate results from pool fire experiment. The distance from the fire source and the radiometer is high which might lead to the moderate level of inaccuracy to the measured data [74]. Table 4-5 shows that the CFD result of average surface emitting power got an acceptable match with the field test data and close match with the analytical model developed by Raj et al. [67]. There is only significant difference at the radiation surface area from the experimental to CFD data. This is because in experimental work the fire was considered as a solid cylindrical object where this assumption is not valid.

4.4.3 Pool Fire Characteristics and Hazard Analysis

In this study two simulations of unconfined pool fire are performed with different wind conditions, u_w = 0 m/s and 5 m/s, as the average wind speed of the region is about 5 m/s. Two engulfed pool fire scenario was simulated with complex geometry. The temperature and thermal radiation of the receptor units were also observed with different wind speeds. The CFD simulation showed that the low temperature zone exists right above of the pool surface. The temperature near the pool surface was low because LNG is very frigid and it condenses moisture from the atmosphere resulting gas-vapor cloud which acts as heat barrier from the higher temperature zone at the top. It burned as oxygen diffuses into the LNG vapor above the spill pool. The inner flame temperature of the pool fire was lower than the outer flame. For large pool diameter there was a lack of oxygen inside of the pool resulting partial combustion of the fuel at the lower end of the combustion zone of the flame. The unburned reactive mixture of gas burned at the upper end of the combustion zone. Thus, the temperature of the plume zone of the flame got higher.

Wind played an important role in pool fire. Figure 4-5 (a) and (b) showed the effect of the wind on an unconfined LNG pool of 15m diameter. As shown in Figure 4-5 (a), there was no tilt of flame at 0 m/s velocity of wind. The angle of the flame tilts increases with wind velocity. The tilted angle of the flame for 5 m/s wind at Figure 4-5 (b) was around 65 degree from the ground. It's also found from the simulation that for a higher wind speed the flame drag was also high. Figure 4-5 (a) showed no flame drag while in Figure 4-5 (b) it showed the flame drag due to the high wind speed (5 m/s). Maximum flame temperature and the hot plume zone were reduced with the increment of wind speed. The

radiation contours showed that the radiation hazard increased at the upwind direction in the presence of wind. The radiation affected area for 50 kW/m^2 in Figure 4-5 (a) was increased by around 50% at the crosswind direction compared to Figure 4-5 (b) with wind speed 5m/s. National Fire Protection Association (NFPA) have specific guidelines for LNG standard at NFPA 59A. These standards are applicable for all on-shore LNG facilities. According to NFPA 59 A, a property line that can be built upon for ignition of a design spill within 5 kW/m^2 thermal radiation and a property line that can be built upon for a fire over an impounding area within 15 kW/m^2 [71]. However, according to the health and safety executive (HSE), UK the human fatality limit is 37.5 kW/m^2 of thermal radiation exposure. An instantaneous death will happen from exposure to this level of thermal radiation over a very short duration.

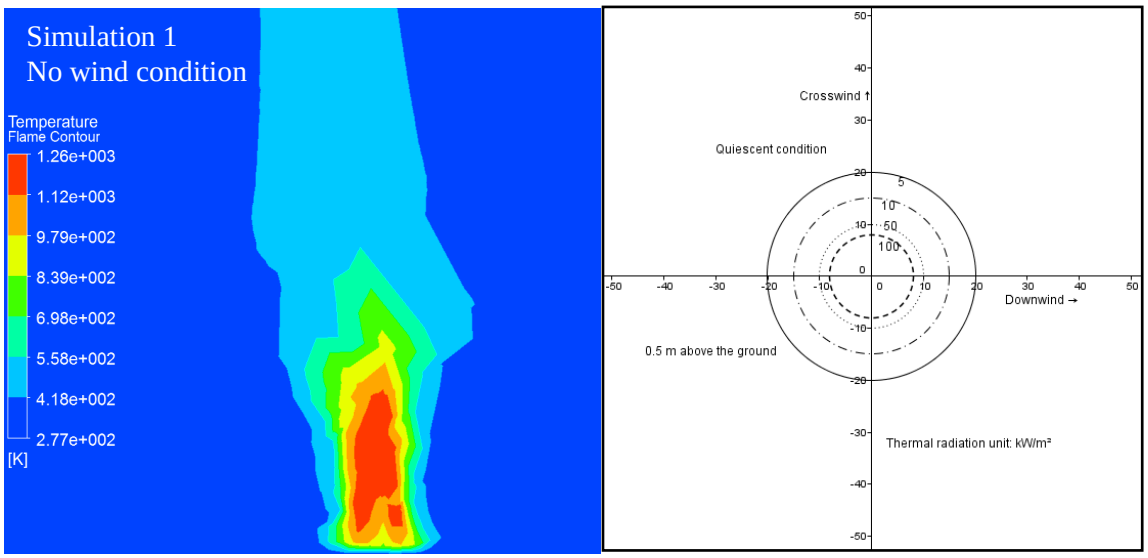

(a) CFD simulations of unconfined pool fire in quiescent condition

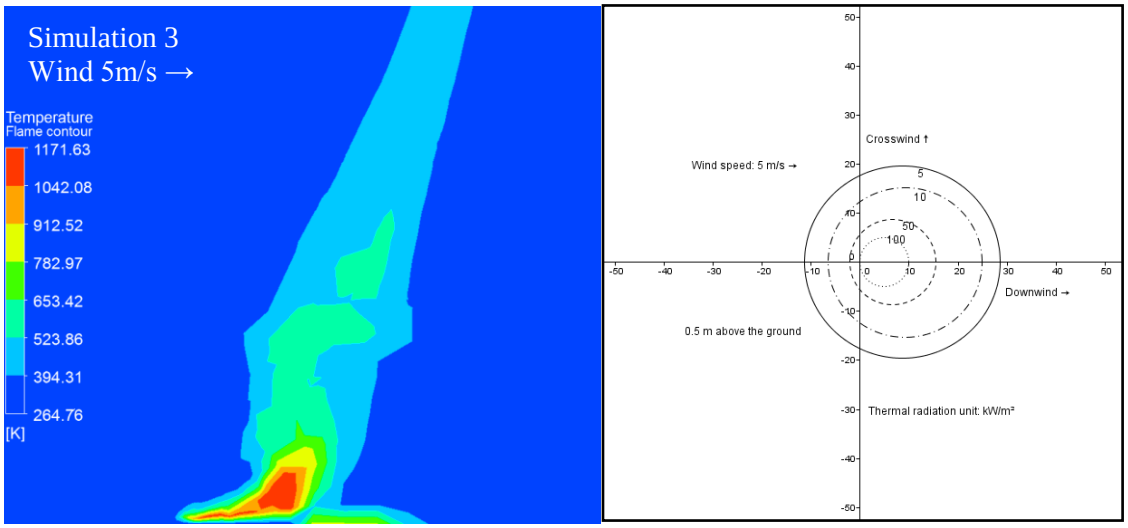

(b) CFD simulations of unconfined pool fire in wind speed 5 m/s.

Figure 4-5: CFD simulations of unconfined pool fire with temperature and thermal radiation profiles of the flame. (a) in quiescent condition (b) in wind speed 5 m/s.

4.4.4 Domino Effect Accident Scenario

A LNG fuelled power plant layout [77] is selected to study the domino effects. The plant is divided into three parts, LNG tanks, property lines and process units as shown in Figure 4-6. The process units are assumed far enough for the flame to reach. The LNG tanks are made with metals having emissivity of surface paint is 0.9. The tank walls boundary conditions are considered adiabatic. The dynamics of the fluid inside the tank due to the tank wall temperature rise such as, pressure and temperature build up are not considered in this simulation. The large tanks have a capacity of 1767 m^3 (height 10 m, diameter 15 m) and the small tanks have that of 195 m^3 (height 10 m, diameter 5 m). The pool area, a

tank with 15 m dike diameter is the source of fire. The distance between the tanks are consistence with NFPA 59 A (2013 edition) which is one fourth of the sum of the diameters of neighboring tanks. The nearest property line is also placed according to the NFPA guideline which is 7.6 m (25 ft) from the nearest tank [73].

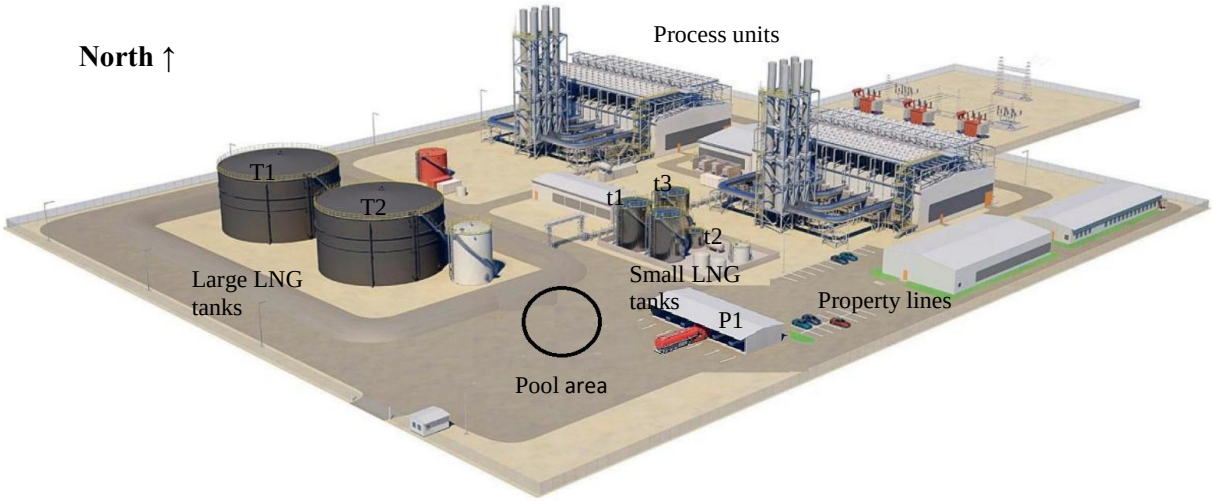

Figure 4-6: Layout of the LNG fuelled power plant [77].

Two case studies are simulated in this accident scenario. The first case study is in quiescent condition, without any wind effect on the pool fire. The second case study is with wind speed at 3 m/s from the south-west side.

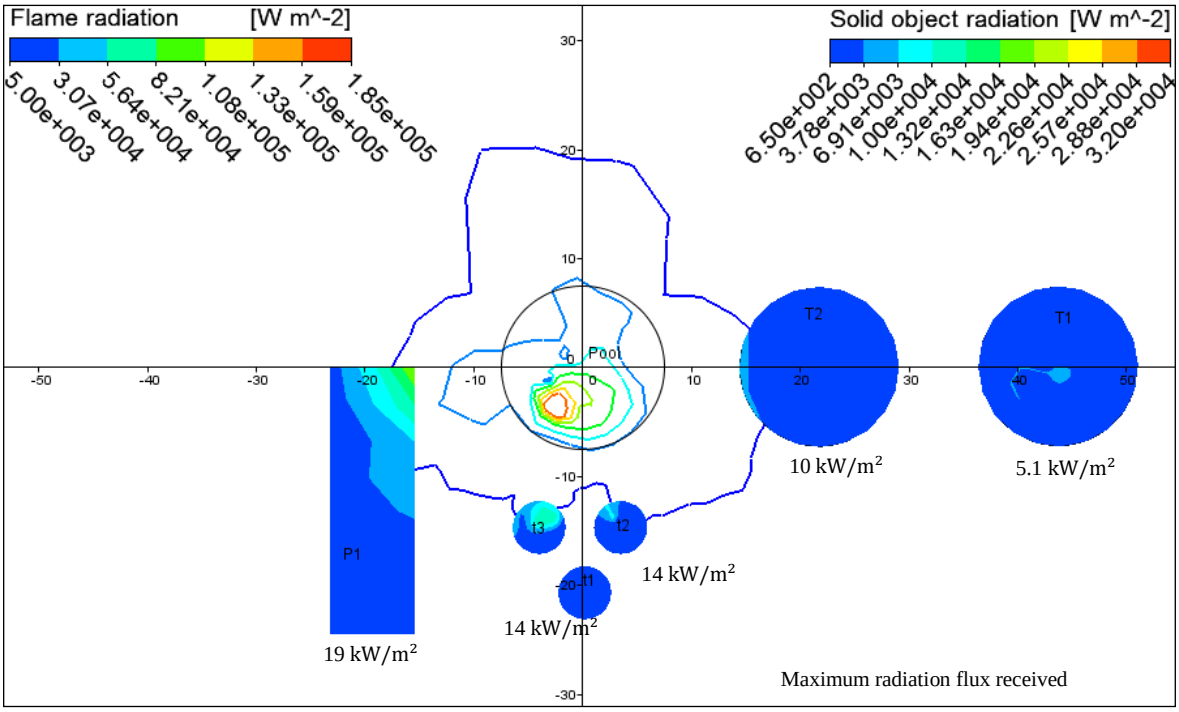

(a) Thermal radiation contour plot of the pool and maximum heat flux received by the units in quiescent condition.

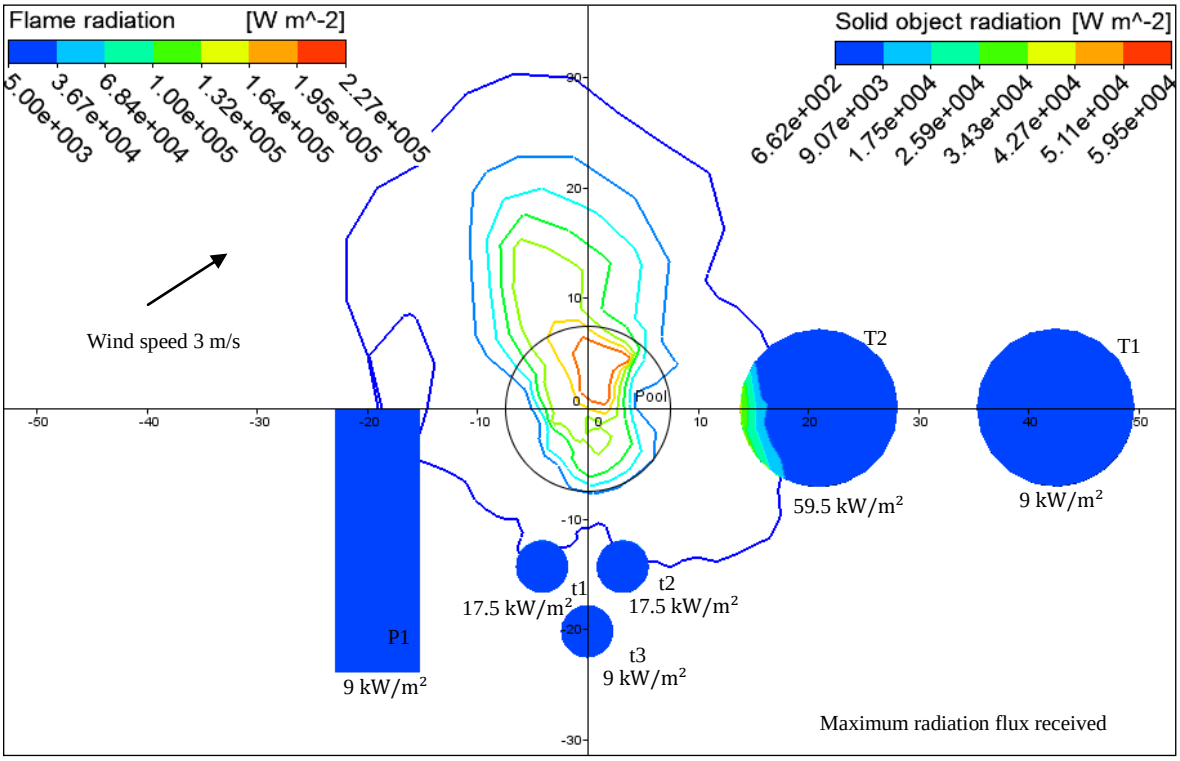

(b) Thermal radiation contour plot of the pool and maximum heat flux received by the units, wind speed 3 m/s.

Figure 4-7: Thermal radiation contour plot of the pool and maximum heat flux received by the units. The reference plane is taken 0.5 m above the pool surface. (a) Quiescent condition. (b) Wind speed 3 m/s.

CFD simulation in this study the time-averaged value of the temperature and thermal radiation of the flame and adjacent tanks is predicted. The maximum thermal radiation received at the nearest target unit in Figure 4-7 (a) in quiescent condition is 19 kW/m^2

which satisfies the NFPA 59 A (2013 edition) of 30 kW/m^2 [72]. In Figure 4-7 (b) the maximum thermal radiation received by the tank T2 is 59.5 kW/m^2. The presence of wind tilted the flame towards the tank. The threshold radiation value for all equipment failure suggested by Khan and Abbasi [49] is 37 kW/m^2. Cozzini et al. (2007) suggested for a tank with atmospheric pressure, the threshold value for the failure of the tank due to the thermal radiation is 15 kW/m^2 and 45 kW/m^2 for pressurized vessel in case of pool fire [84].

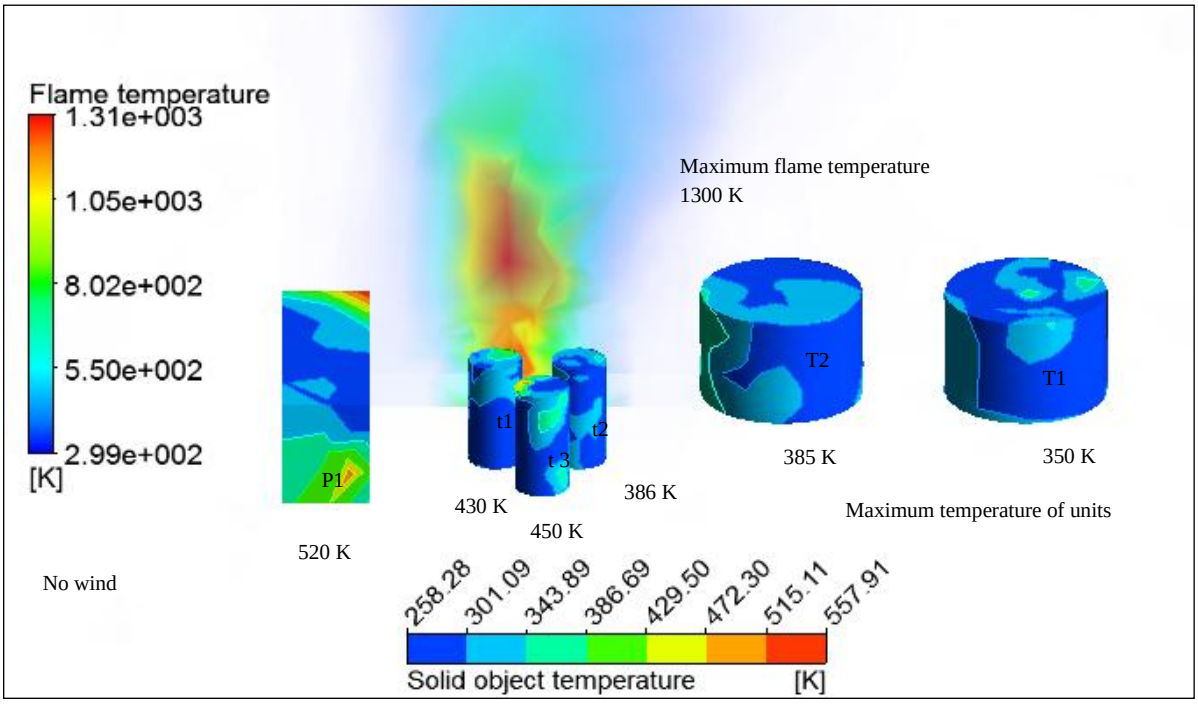

(a) Maximum temperature distribution of flame and solid units in quiescent condition.

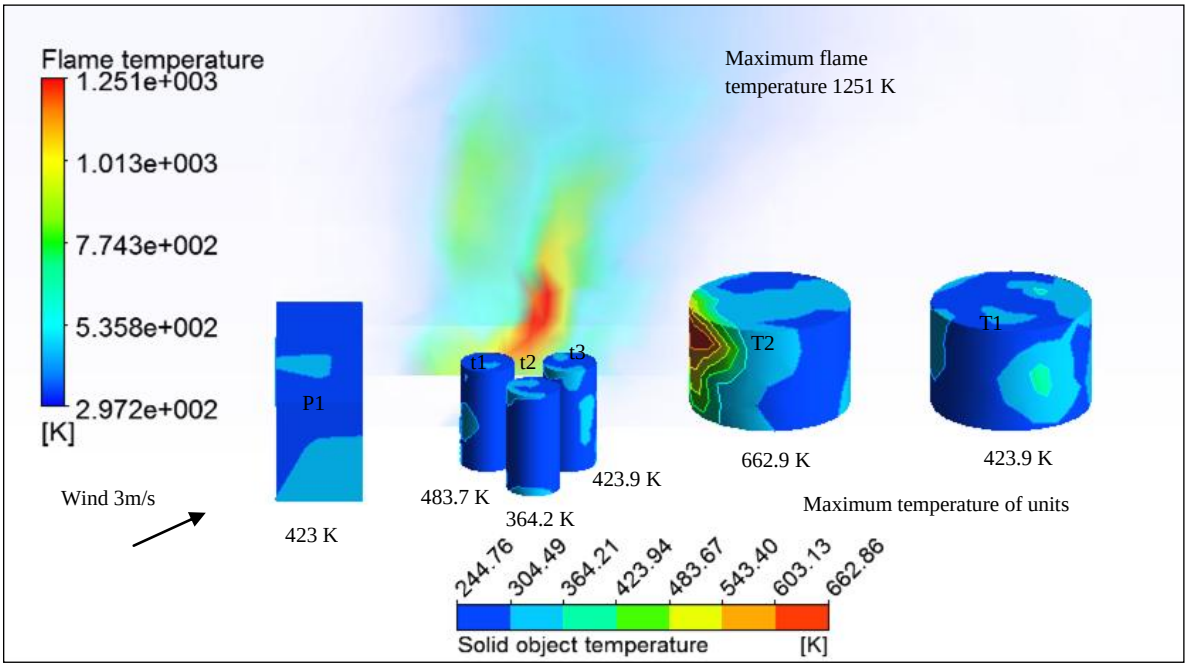

(b) Maximum temperature distribution of flame and solid units, wind speed 3 m/s.

Figure 4-8: Maximum temperature distribution of flame and solid units. (a) Quiescent condition. (b) Wind speed 3 m/s.

High temperature of the fire between 1000 K to 1500 K can escalate gas phase wall temperature higher than 700 K which severely weakens the shell materials by decreasing their resistance. The heat up process of the pool fire takes few minute and the vessel shell temperature rise up to 850 K to 950 K and vessel shell lose its structural integrity quickly [85]. The heat load of a pool fire is a combination of radiation and convection received by the target units. The heat radiated by the pool fire also increases the temperature of the internal fluid of the tank which leads to the increment of vapor pressure of the liquid phase that maybe presented at the target unit. These conditions create the escalation of

targeted vessel failure and propagate the domino effect. Sun et al. (2013) showed in a dynamic simulation of 35 m diameter LNG pool fire that the burning duration was 10 minutes [83].

The property area receives the maximum temperature in Figure 4-8 (a) which is around 520 K. For most of the common types of construction materials used for process industries, lose 40% of its strength at temperature higher than 670 K. Below 570 K strength of the material are not affected drastically but at temperatures above 850 K leads to the loss of 80-90% of its structural strength [85]. NFPA 2013 regulation 59 A states that for "LNG containers larger than 265 m^3 shall be separated from adjoining LNG storage containers such that a fire in one container or impoundment will not cause loss of containment from adjacent containers. This shall be accomplished by ensuring that no part of the adjacent storage container roof, walls, or its impoundment structure reaches a temperature at which the strength of the material of the container roof, wall, or its impoundment is reduced to a level where the LNG tank, roof, or impoundment loses its structural integrity".

In Figure 4-8 (b) the maximum temperature of Tank T2 is around 663 K. Pressure vessel steel plate such as P460NH lose its 40% structural integrity which can lead to the failure of the tank. P460NH is a high yield carbon steel used to design LPG tankers [86]. At this high temperature exposed to the tank, the internal fluid temperature will increase and this will lead the increase of internal pressure and escalate the tank failure [85]. Heymes et al. (2013) conducted an experiment to study the a small pressurized vessel of low filling level (15%) LPG heated by a remote wall fire. The volume of the cylindrical shaped tank

was 2300 L with 1 m diameter and the tank was made of steel. The tank surface emissivity was 0.9, which value is also used in this study. Initial pressure of the tank was around 9 bar. The experimental result shows that at peak wall temperature of 659 K the internal temperature of vapor build up was 531 K. The internal pressure of the tank raised 17 bar after 11 minutes of the test duration and the tank failed at that time. The average radiation intensity at the tank surface was 43 kW/m^2 which is near the threshold value of the pressurized vessel failure 45 kW/m^2 mentioned by Cozzini et al. (2007) [82, 84]. If the tank T2 is a pressurized vessel for an exposure of 10 minutes with an average radiation flux of 59.5 kW/m^2 and 663 K surface temperature seems sufficient enough to fail the vessel made of steel. If it is assumed that the vessel is not a pressurized vessel, the pressure build-up at the inside of the vessel for the exposure of 663 K temperature is 278.3 kPa by employing Khan and Abbasi method to calculate overpressure of the tank for internal fluid boil-up [49]. The set point of the reliving pressure of pressure relieving valve (PRV) must be designed to relieve this extra build-up pressure. This extra pressure and the mechanical properties of the construction material of the vessel would bear upon the severity of the accident. Over-pressure created inside the tank is 177 kPa or 1.75 atm. The pressure relieving device of the tank should be larger than the overpressure to prevent the secondary accident. An overpressure of 0.7 atm can destroy a unit by blast wave impact, a heat load of 37 kW/m^2 is sufficient to induce vessel failure, and a missile (sharp edged) having a velocity higher than 75 m/s has sufficient potential to penetrate the target unit provided that it collides with the unit [73].

4.4.5 Discussion on the Influence of the Wind on Domino Effect Escalation

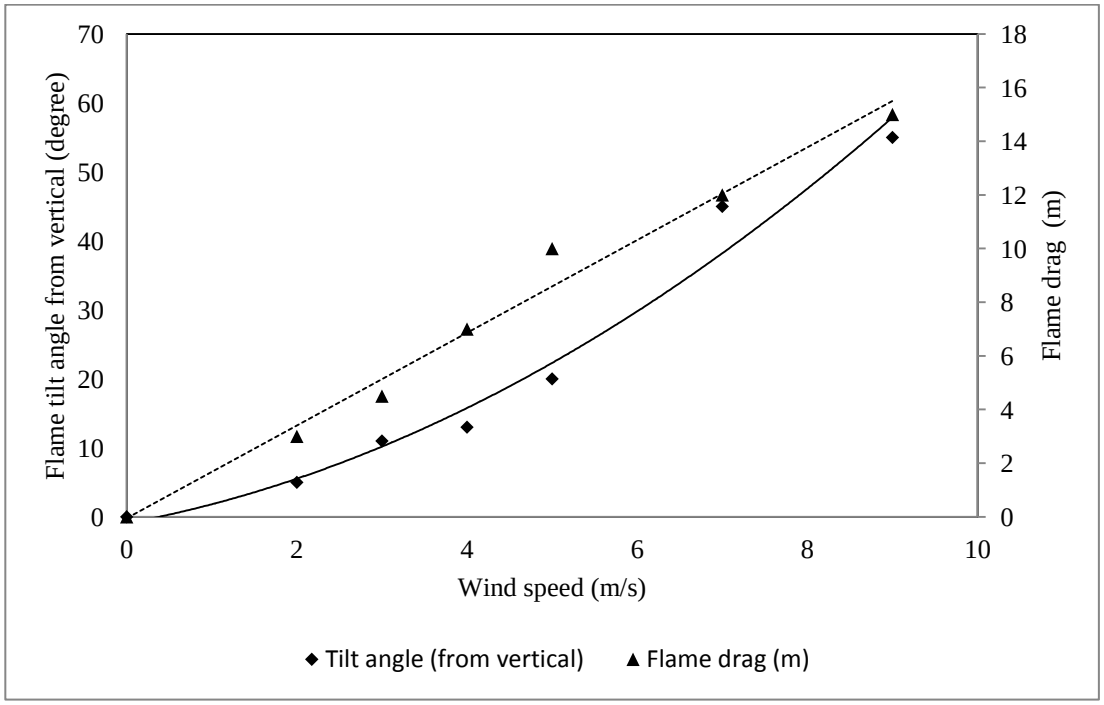

Figure 4-9: Relation between the flame tilt angles (from vertical) and the flame drag with wind speed.

The CFD simulation results for the effect of the wind speed to the escalation of domino effect are comprised in Figure 4-9 and Figure 4-10. The tilting angle of the flame due to the wind presented in Figure 4-9 shows a linear relationship. The flame drag due to the wind is presented in Figure 4-9 and the flame drag increase with the wind speed. In case of circular pool fire, which is used in this study, under the influence of the wind the pool become more elliptical shape [79]. For a high wind speed the wind is more tend to tilt

with the ground and the angle of the flame with the vertical axis will increase and these result more elliptical shape of the circular pool at the direction of the wind. Consequently, the view factor of the flame on the receiver surface changes due to the flame tilt and drag [59]. The maximum temperature and thermal radiation intensity received by the nearest tank of the pool at different wind conditions are showed in Figure 4-10. Wind direction is towards the nearest tank of the pool T2 as shown in Figure 4-8 (b). The flame inclined more towards the nearest tank T2 as the wind speed goes high, results the increase of the exposure are of the flame to the targeted nearest tank T2 and consequently the increase of temperature and thermal radiation of the nearest tank T2. This behavior of the pool fire at the presence of wind will escalate the domino effect. For example, at 4 m/s wind speed the tank receives thermal radiation intensity of 98.5 kW/m^2. It will take only 90 seconds to fail the tank if the vessel is in atmospheric pressure and for pressurized vessel it will take 120 seconds [78]. Thus the wind direction and speed largely effect on escalating the domino effect in case of pool fire.

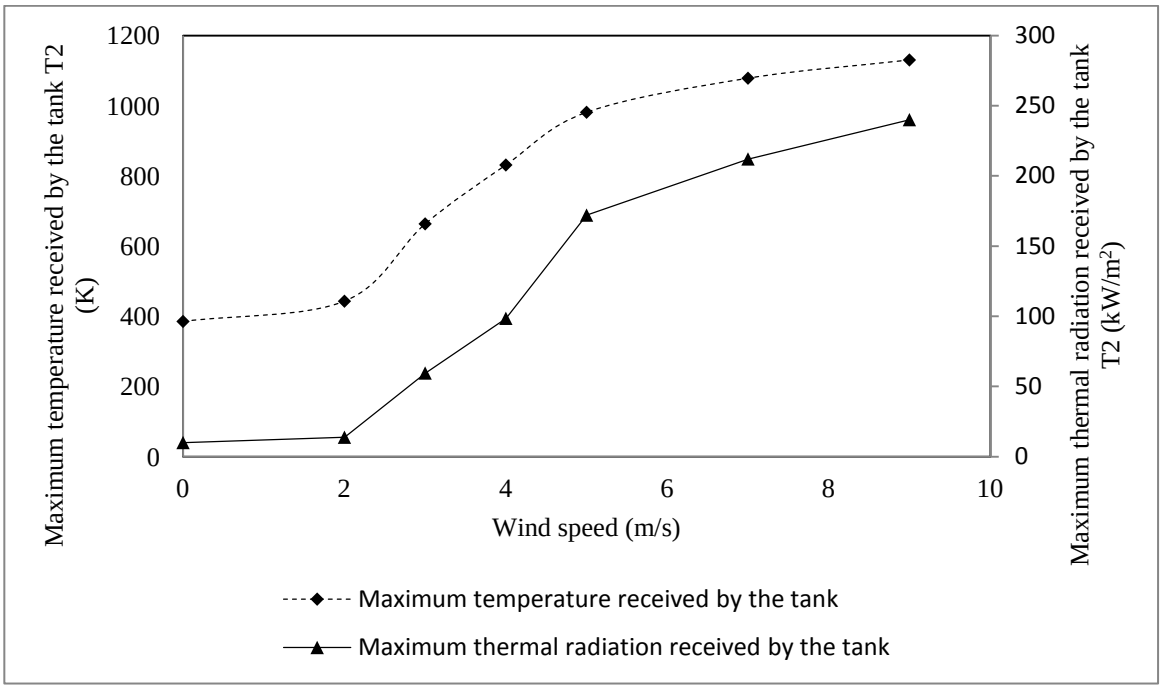

Figure 4-10: Maximum temperature and thermal radiation received by the nearest tank (T2) in different wind speed.

CFD results from Figure 4-5 (a), 4-5(b), 4-9, and 4-10 showed that the influence of the increment of wind speed leads to the following observations:

i. Flame tilt from the vertical.

ii. Increasing of temperatures and irradiances received by the vessel.

iii. In a case of wind velocity of 2 m/s no noticeable change of maximum temperature or thermal radiation received are observed in CFD results.

iv. With increasing wind velocity to 2 m/s to 5 m/s there is a noticeable rise on the temperature and thermal radiation received by the vessel. The flame tilt from the vertical and flame drag formation at horizontal direction became significant in CFD results at this range of the wind speed.

v. With increasing wind velocity to 5 m/s to 9 m/s a flame tilt and drag became more significant in CFD. This results also showed that the maximum temperature and thermal radiation received by the vessel is slightly reduce than the 2 m/s to 5m/s wind range.

Taking all these consideration, a remote impounding is suggested. It is clear from the Figure 4-7 (a) and Figure 4-8 (a) that the distance between vessels filled with flammable material with a property value needs to be higher than 7.6 m (25 ft). In order to prevent the secondary accident scenario the impounding between vessels are necessary. The safety distance of the tanks suggested by Cozzani et al. for the pool fire incident to prevent domino effect is 50 m from the pool border for an atmospheric pressure tank and 15 m from the pool border for a pressurized vessel [80]. It can be either done by increasing the spacing between the neighboring vessels or using a dike. However, the simulation result at Figure 4-8 (b) shows that the temperature is higher at the upper portion of the tank as the flame tilted by the wind. Thus the height of the dike, painted with thermal radiation reflective colors, should be higher which not only control the spill, also resist from the thermal radiation of any accident scenario.

4.6 Conclusions

The CFD model of LNG pool fire is successfully simulated using ANSYS CFX-14. This study will help for better understanding the domino effect related work. From this study the following conclusions can be drawn:

- The three dimensional CFD simulation provides the local temperature and radiation distributions of the units and encompassed area which can predict accident scenario better than any existing analytical model.
- The CFD simulation result is validated with the experimental field test data. The close match of thermal radiation (with 2.56% error) and flame geometry (with 0.71% error) demonstrates the rationale of the CFD model in this study.
- Wind has a significant effect on pool fire. The unconfined pool fire CFD simulations with different wind conditions provided additional insights of the characteristics of pool fire such as, wind effect on flame tilt and drag. The radiation contour of the unconfined pool fire is drawn for quiescent and 5 m/s wind speed.
- Two domino effect accident scenarios have been discussed. The radiation contours and the local temperature distribution from the CFD post-processing result can be used to calculate risk of the domino effect.
- The influence of the wind speed on domino effect escalation is investigated. The maximum temperature and thermal radiation received by the nearest tank at the downwind is studied.

Acknowledgements

Authors gratefully acknowledge the financial support provided by Vale Research Chair Grant, Research & Development Corporation (RDC) of Newfoundland & Labrador and Natural Sciences and Engineering Research Council (NSERC) of Canada.

Chapter 5

Summary, Conclusions and Recommendations

5.1 Summary

Numerical simulations have been performed to describe different hazard scenarios related to hydrocarbon storage and transportation. Transportation of hydrocarbons from offshore platforms to onshore storage tanks through subsea pipelines involves greater risks of release of hydrocarbons through pipeline leakage. A leak detection methodology has been developed utilizing acoustic signal in order to prevent such catastrophe. Research findings on this topic can be summarized as below:

- Simulations results show that pressure and temperature fluctuations were highly localized at the leakage zone.
- The leakage of the pipeline has influence on the pressure gradient.
- Pipe line leak with high pressure gradient generate higher acoustic noise signals compared to low pressure gradient.
- The power spectral density (PSD) data showed that the noise is clearly influenced by the line pressure of the pipe.

- PSD data also provided information about the frequency range at which the maximum peaks of the acoustic signals are observed.
- The fluid dispersion pattern with time showed the trajectory of the plume and the ultimate fate of escaped fluids.
- Experimental setups for pipeline leakage identification can be designed and built by using data generated by this current study.

An accidental release of hydrocarbon from the storage tank can lead to pool fire and further it could be escalated to domino chain effect. This chain of accidents may lead to extremely severe consequences. A pool fire model is developed to calculate the radiation intensity, maximum temperature received by the units, and evaluated risks in case of complex three dimensional geometry, which is discussed in chapter 4. The research findings are:

- 3-D CFD simulation models provide a better understanding of domino chain caused by pool fire accident scenario.
- The effect of wind in terms of flame tilt and drag provided additional insights of the characteristics of pool fire.
- The radiation contours and the local temperature distributions from the CFD post-processing results can be used to calculate risk of the domino effect.

- The influence of the wind speed on domino effect escalation is investigated.
- Based on maximum thermal radiation and temperature, a remote impounding is suggested.
- The simulation results showed that the temperature is higher at the upper portion of the tank as the flame tilted by the wind.

5.2 Conclusions

The proposed CFD models will help to prevent the unanticipated events which can lead a major incident during hydrocarbon handling. Leakage is the major risk of transportation of fluids through pipeline, especially in submarine pipelines. Leakage modeling of subsea pipelines and the detection of very small chronic leak using the acoustic signature of the leak will help to detect the leak in timely manner and prevent losses and save wildlife, environment, and most importantly the reputation of the company. However, pool fire is accountable for the major accident of the industries and pool fire can escalate into domino chain which leads to severe disaster. The LNG pool fire simulation for domino effect analysis will be helpful for the industries to understand the escalation of domino chain and how to prevent it. The main contribution of this study can be summarized as follows:

- The numerical approach of dealing with risk scenarios provides new insight on the flexibility of simulating the consequences under valid assumptions. A computational fluid dynamics software ANSYS is used to quantify the risks involved and it gives wide degree of freedom to the users regarding on the three dimensional hazard scenario for actual visualization and numerical methods provide more accurate results than analytical solutions.

- Leak modeling of oil and gas sub-sea pipeline using acoustic model (FW-H method) is a unique method to detect small leakage at the pipeline.

- The novelty of the CFD simulation of pool fire is to predict the domino effect the effect of the wind to the domino chain escalation.
- These simulation results are very important to quantify the risk associated with the process where the experimental data are either unavailable or very expensive.

5.3 Future Works

At the pipeline simulation model a single phase flow has been considered, which might differ in real case scenario. At low temperature and high pressure there is a possibility of hydrate formation around the leakage which is also not considered in this model. There is no sensitivity study has been performed to observe the influence of critical parameters (e.g. fluid velocity, pipe diameter) to the acoustic signatures. The acoustic frequency data from the simulation is required to filter out the background noise components, a low pass filter could be introduced to serve this purpose. The acoustic signal generated from the leak hole is a function of the leak size, fluid properties and flow conditions (i.e. pressure, temperature and flow rate). A leak characterization model can be developed to understand the influence of the leak size and shape to the pressure signals.

In case of LNG pool fire simulation, a transient simulation is very important to analyze the growth of the flame and the time to failure of the units due to the radiation intensity. In this present study, a simple turbulence $k - \epsilon$ model is used. It is highly recommended to use more advanced turbulence model like LES. A better mitigation plan for hindering the escalation of domino effect is also important.

Bibliography

1. Mannan, S. (Ed.). (2012). *Lees' Loss prevention in the process industries: Hazard identification, assessment and control*. Butterworth-Heinemann, pp. 22/20 - 23/40.
2. Audunsson, T. H. (2006). Risk analysis of the oil depot in Örfirisey. *Ph.D. Thesis*, Lund University, ISSN: 1402-3504.
3. Meiwes, K. C., Erdelen-Peppler, M., & Brauer, H. (2014, September). Impact of small-scale reeling simulation on mechanical properties on line pipe steel. In *2014 10th International Pipeline Conference* (pp. V004T10A003- V004T10A003). American Society of Mechanical Engineers.
4. Palmer, A. (2000, January). Are we ready to construct submarine pipelines in the Arctic?. In *Offshore Technology Conference*. Offshore Technology Conference.
5. Persson, H., & Lzonnermark, A. (2004). *Tank fires: Review of fire incidents 1951-2003: BRANDFORSK Project 513-021*. SP Sveriges Provnings-och Forskningsinstitut.
6. Khan, F. I., Sadiq, R., & Husain, T. (2002). Risk-based process safety assessment and control measures design for offshore process facilities. *Journal of hazardous materials*, *94*(1), pp. 1-36.
7. Khan, F. I., & Abbasi, S. A. (1999). Major accidents in process industries and an analysis of causes and consequences. *Journal of Loss Prevention in the process Industries*, *12*(5), pp. 361-378.

8. Middha, P., Hansen, O. R., & Storvik, I. E. (2009). Validation of CFD-model for hydrogen dispersion. *Journal of Loss Prevention in the Process Industries*,*22*(6), pp. 1034-1038.

9. Koo, J., Kim, H., So, W., Kim, K., & Yoon, E. (2009, January). Safety assessment of LNG terminal focused on the consequence analysis of LNG spills. In *Proceedings of the 1st annual gas processing symposium*.

10. Ben-Mansour, R., Habib, M. A., Khalifa, A., Youcef-Toumi, K., & Chatzigeorgiou, D. (2012). Computational fluid dynamic simulation of small leaks in water pipelines for direct leak pressure transduction. *Computers & Fluids*, *57*, pp. 110-123.

11. Olivares, P. A. V. (2009). Acoustic wave propagation and modeling turbulent water flow with acoustics for district heating pipes (Doctoral dissertation, Ph. D. dissertation, Uppsala University).

12. Xu, Q., Zhang, L., & Liang, W. (2013). Acoustic detection technology for gas pipeline leakage. *Process Safety and Environmental Protection, 91(4),* pp. 253-261.

13. De Vasconcellos Araújo, M., de Farias Neto, S. R., de Lima, A. G. B., & de Luna, F. D. T. (2014). Hydrodynamic study of oil leakage in pipeline via CFD. *Advances in Mechanical Engineering*, *6*, pp. 170-178.

14. Zhu, H., Lin, P., & Pan, Q. (2014). A CFD (computational fluid dynamic) simulation for oil leakage from damaged submarine pipeline. *Energy*, *64*, pp. 887-899.

15. Cloete, S., Olsen, J. E., & Skjetne, P. (2009). CFD modeling of plume and free surface behavior resulting from a sub-sea gas release. *Applied Ocean Research, 31(3)*, pp. 220-225.

16. Reniers, G., & Cozzani, V. (Eds.). (2013). *Domino Effects in the Process Industries: Modelling, Prevention and Managing*. Newnes.

17. Zabetakis, M. G., & Burgess, D. S. (1961). *Research on hazards associated with production and handling of liquid hydrogen. [Fire hazards and formation of shock-sensitive condensed mixtures]* (No. BM-RI-5707). Bureau of Mines, Washington, DC (USA).

18. Mudan, K. S. (1984). Thermal radiation hazards from hydrocarbon pool fires. *Progress in Energy and Combustion Science, 10(1),* pp. 59-80.

19. Fay, J. A. (2006). *Model of large pool fires. Journal of hazardous materials,136(2),* pp. 219-232.

20. Koseki, H., Iwata, Y., Natsume, Y., Takahashi, T., & Hirano, T. (2000). Tomakomai large scale crude oil fire experiments. *Fire technology, 36(1),* pp. 24-38.

21. Chatris, J. M., Quintela, J., Folch, J., Planas, E., Arnaldos, J., & Casal, J. (2001). *Experimental study of burning rate in hydrocarbon pool fires. Combustion and flame, 126(1),* pp. 1373-1383.

22. Blanchat, T. K., Brown, A. L., Figueroa, V., & Yoon, S. S. (2008, February). Benchmark enclosure fire suppression experiments and modeling. In *Suppression*

and detection research and application - A technical working conference SUPDET 2008, pp. 11-13.

23. Mishra, K. B., Wehrstedt, K. D., & Schoenbucher, A. (2009, December). Prediction of burning rate of an accidentally released flammable fuel by means of CFD simulation. In *Proceedings of 7th International conference on CFD in the minerals and process industries, 9–11 December 2009*, CSIRO, Melbourne.

24. Moorhouse, J., & Pritchard, M. J. (1982). Thermal radiation hazards from large pool fires and fireballs-a literature review. In *IChemE Symp. Series No. 71*, pp. 397-428.

25. Sun, B., Guo, K., & Pareek, V. K. (2014). Computational fluid dynamics simulation of LNG pool fire radiation for hazard analysis. *Journal of Loss Prevention in the Process Industries, 29*, pp. 92-102.

26. Comfort, G., Dinovitzer, A., Lazor, R., & Hinnah, D. (2004, January). Offshore arctic pipeline oil spill risk assessment. In *2004 International Pipeline Conference*. American Society of Mechanical Engineers, pp. 2535-2542.

27. Li, W., Pang, Y., Lin, J., & Liang, X. (2013). Computational modelling of submarine oil spill with current and wave by FLUENT. *Research Journal of Applied Sciences, Eng. Technol, 5*, pp. 5077-5082.

28. Palmer, A. (2000, January). Are we ready to construct submarine pipelines in the arctic?. In *Offshore Technology Conference. Offshore Technology Conference, Huston, Texas*.

29. Thodi, P., Paulin, M., Forster, L., Burke, J., & Lanan, G. (2014, February). Arctic pipeline leak detection using fiber optic cable distributed sensing systems. In *OTC arctic Technology Conference. Offshore Technology Conference, Huston, Texas*.

30. Ben-Mansour, R., Habib, M. A., Khalifa, A., Youcef-Toumi, K., & Chatzigeorgiou, D. (2012). Computational fluid dynamic simulation of small leaks in water pipelines for direct leak pressure transduction. *Computers & Fluids, 57*, pp. 110-123.

31. Olivares, P. A. V. (2009). Acoustic wave propagation and modeling turbulent water flow with acoustics for district heating pipes. *Doctoral dissertation, Ph. D. dissertation, Uppsala University*.

32. Liang, W., Zhang, L., Xu, Q., & Yan, C. (2013). Gas pipeline leakage detection based on acoustic technology. *Engineering Failure Analysis, 31*, pp. 1-7.

33. De Vasconcellos Araújo, M., de Luna, F. D. T., Barbosa, E. S., de Farias Neto, S. R., & de Lima, A. G. B. (2013). Numerical study of oil flow in tee junction with leaks. *Advances in Petroleum Exploration and Development, 6(2)*, pp. 1-11.

34. Zhu, H., Lin, P., & Pan, Q. (2014). A CFD (computational fluid dynamic) simulation for oil leakage from damaged submarine pipeline. *Energy, 64*, pp. 887-899.

35. Cloete, S., Olsen, J. E., & Skjetne, P. (2009). CFD modeling of plume and free surface behavior resulting from a sub-sea gas release. *Applied Ocean Research, 31(3),*pp. 220-225.

36. ANSYS FLUENT-Solver Theory Guide. Release 12.1. ANSYS, Inc. April 2009.

37. Yang, X., Gupta, S., Kuo, T. W., & Gopalakrishnan, V. (2014). RANS and Large Eddy Simulation of Internal Combustion Engine Flows—A Comparative Study. *Journal of Engineering for Gas Turbines and Power, 136(5)*, p. 051507.

38. Wearden, G. (Jan 10, 2011), BP shuts Alaska pipeline after leak, The Guardian. Retrieved from: http://www.theguardian.com/business/2011/jan/10/bp-shuts-alaska-pipeline-after-leak

39. Wang, Y., Wang, S. X., Liu, Y. H., & Chen, C. Y. (2011). Influence of cavity shape on hydrodynamic noise by a hybrid LES-FW-H method. *China Ocean Engineering, 25*, pp. 381-394.

40. Sodré, C. H., de Lima, A. G. B., & de Farias Neto, S. R. (2013). Numerical analysis of heavy oil-water flow and leak detection in vertical pipeline. *Advances in Chemical Engineering and Science, 2013, 3*, pp. 9-15.

41. Mishra, K. B., Wehrstedt, K. D., & Krebs, H. (2013). Lessons learned from recent fuel storage fires. *Fuel Processing Technology, 107,* pp. 166-172.

42. Park, K., Sam Mannan, M., Jo, Y. D., Kim, J. Y., Keren, N., & Wang, Y. (2006). Incident analysis of Bucheon LPG filling station pool fire and BLEVE. *Journal of hazardous materials, 137(1),* pp. 62-67.

43. Mudan, K. S. (1984). Thermal radiation hazards from hydrocarbon pool fires. *Progress in energy and combustion science, 10(1),* pp. 59-80.

44. Fay, J. A. (2006). Model of large pool fires. *Journal of hazardous materials,136(2),* pp. 219-232.

45. Assael, M. J., & Kakosimos, K. E. (2010). *Fires, Explosions, and Toxic Gas Dispersions: Effects Calculation and Risk Analysis*. CRC Press.

46. Raj, P. K. (2007). LNG fires: A review of experimental results, models and hazard prediction challenges. *Journal of hazardous materials, 140(3),* pp. 444-464.

47. Sun, B., Guo, K., & Pareek, V. K. (2014). Computational fluid dynamics simulation of LNG pool fire radiation for hazard analysis. *Journal of Loss Prevention in the Process Industries, 29,* pp. 92-102.

48. Reniers, G., Cozzani, V., (2013). Features of escalation scenarios: Sources of domino accidents and promary scenarios. In Reniers, G., & Cozzani, V. (Eds.*), Domino Effects in the Process Industries: Modelling, Prevention and Managing*, Newnes, p. 33.

49. Khan, F. I., & Abbasi, S. A. (1998). Models for domino effect analysis in chemical process industries. *Process Safety Progress, 17(2),* pp. 107-123.

50. Chun, H., Wehrstedt, K. D., Vela, I., & Schönbucher, A. (2009). Thermal radiation of di-tert-butyl peroxide pool fires—Experimental investigation and CFD simulation. *Journal of hazardous materials, 167(1),* pp. 105-113.

51. Attar, A. A., Pourmahdian, M., & Anvaripour, B. (2013). Experimental study and CFD simulation of pool fires. *International Journal of Computer Applications, 70(11).*

52. Schälike, S., Wehrstedt, K. D., & Schönbucher, A. (2011). CFD simulation to predict the thermal radiation of large LNG pool fires. In *Proceedings of the European combustion meeting*.

53. Pula, R., Khan, F. I., Veitch, B., & Amyotte, P. R. (2006). A grid based approach for fire and explosion consequence analysis. *Process Safety and Environmental Protection, 84(2),* pp. 79-91.

54. Dadashzadeh, M., Khan, F., Hawboldt, K., & Amyotte, P. (2013). An integrated approach for fire and explosion consequence modelling. *Fire Safety Journal,61,* pp. 324-337.

55. Hansen, O. R., Gavelli, F., Ichard, M., & Davis, S. G. (2010). Validation of FLACS against experimental data sets from the model evaluation database for LNG vapor dispersion. *Journal of Loss Prevention in the Process Industries, 23(6),* pp.857-877.

56. Gavelli, F., Davis, S. G., & Hansen, O. R. (2011). Evaluating the potential for overpressures from the ignition of an LNG vapor cloud during offloading. *Journal of Loss Prevention in the process industries, 24(6),* pp. 908-915.

57. Qi, R., Ng, D., Cormier, B. R., & Mannan, M. S. (2010). Numerical simulations of LNG vapor dispersion in Brayton Fire Training Field tests with ANSYS CFX. *Journal of hazardous materials, 183(1),* pp. 51-61.

58. ANSYS CFX-Solver Theory Guide. Release 12.1. ANSYS, Inc. November 2009.

59. Vela, I. (2009). *CFD prediction of thermal radiation of large, sooty, hydrocarbon pool fires.* Doctoral dissertation, Duisburg, Essen, Univ., Diss., 2009.

60. Ferziger, J. H., & Perić, M. (2002). *Computational methods for fluid dynamics, Vol. 3*. Berlin: Springer.

61. Yeoh, G. H., & Yuen, K. K. (2009). *Computational fluid dynamics in fire engineering: Theory, Modelling and Practice*. Butterworth-Heinemann.

62. Karlsson, B., & Quintiere, J. (2002). *Enclosure fire dynamics*. CRC press.

63. ANSYS CFX-Solver Modeling Guide. Release 12.0. ANSYS, Inc. April 2009.

64. Yang, X., Gupta, S., Kuo, T. W., & Gopalakrishnan, V. (2014). RANS and Large Eddy Simulation of internal combustion engine flows—A comparative study. *Journal of Engineering for Gas Turbines and Power, 136(5),* p. 051507.

65. Jones, W., & Whitelaw, J. H. (1982). *Calculation methods for reacting turbulent flows: A review. Combustion and flame, 48,* pp.1-26.

66. Kong, S. C., Han, Z., & Reitz, R. D. (1995). *The development and application of a diesel ignition and combustion model for multidimensional engine simulation (No. 950278).* SAE Technical Paper.

67. Raj, P. K. (2005). Large LNG fire thermal radiation—modeling issues and hazard criteria revisited. *Process safety progress, 24(3),* pp. 192-202.

68. Raj, P. K. (2007). Large hydrocarbon fuel pool fires: Physical characteristics and thermal emission variations with height. *Journal of hazardous materials,140(1),* pp. 280-292.

69. Launder, B. E., Reece, G. J., & Rodi, W. (1975). Progress in the development of a Reynolds-stress turbulence closure. *Journal of fluid mechanics, 68(03),* pp. 537-566.

70. Dalzell, W. H., & Sarofim, A. F. (1969). Optical constants of soot and their application to heat-flux calculations. *Journal of Heat Transfer, 91(1),* pp. 100-104.

71. Raj, P. K. (2008). A review of the criteria for people exposure to radiant heat flux from fires. *Journal of hazardous materials, 159(1),* pp. 61-71.

72. Raj, P. K., & Lemoff, T. (2009). Risk analysis based LNG facility siting standard in NFPA 59A. *Journal of Loss Prevention in the Process Industries,22(6),* pp. 820-829.

73. Khan, F. I., & Abbasi, S. A. (2001). An assessment of the likelihood of occurrence, and the damage potential of domino effect (chain of accidents) in a typical cluster of industries. *Journal of Loss Prevention in the Process Industries, 14(4),* pp. 283-306.

74. Raj, P. P., Moussa, A. N., & Aravamudan, K. (1979). *Experiments involving pool and vapor fires from spills of liquefied natural gas on water*. Little (Arthur D) Inc. Cambridge, MA.

75. Salim, S. M., Ong, K. C., & Cheah, S. C. (2011). Comparison of RANS, URANS and LES in the prediction of airflow and pollutant dispersion. In *Proceedings of the World Congress on Engineering and Computer Science, Vol. 2,* pp. 19-21.

76. Lysenko, D. A., Ertesvåg, I. S., & Rian, K. E. (2014). Numerical simulation of non-premixed turbulent combustion using the Eddy dissipation concept and comparing with the steady laminar flamelet model. Flow, *Turbulence and Combustion, 93(4),* pp. 577-605.

77. Punnonen, K. (2013). *Small and medium size LNG for power production.* Wärtsilä Finland Oy, Finland.

78. Cozzani, V., Gubinelli, G., & Salzano, E. (2006). Escalation thresholds in the assessment of domino accidental events. *Journal of hazardous materials, 129(1),* pp. 1-21.

79. Sinai, Y. L., & Owens, M. P. (1995). Validation of CFD modelling of unconfined pool fires with cross-wind: flame geometry. *Fire Safety Journal, 24(1),* pp. 1-34.

80. Cozzani, V., Tugnoli, A., & Salzano, E. (2007). Prevention of domino effect: From active and passive strategies to inherently safer design. *Journal of hazardous materials, 139(2),* pp. 209-219.

81. Cozzani, V., Gubinelli, G., Antonioni, G., Spadoni, G., & Zanelli, S. (2005). The assessment of risk caused by domino effect in quantitative area risk analysis. *Journal of Hazardous Materials, 127(1),* pp. 14-30.

82. Heymes, F., Aprin, L., Birk, A. M., Slangen, P., Jarry, J. B., François, H., & Dusserre, G. (2013). An experimental study of an LPG tank at low filling level heated by a remote wall fire. *Journal of Loss Prevention in the Process Industries, 26(6),* pp. 1484-1491.

83. Sun, B., & Guo, K. (2013). LNG accident dynamic simulation: Application for hazardous consequence reduction. *Journal of Loss Prevention in the Process Industries, 26(6),* pp. 1246-1256.

84. Cozzani, V., Spadoni, G., & Reniers, G. (2013). Approaches to domino effect prevention and mitigation: Preliminary analysis of domino hazard. In Reniers, G., & Cozzani, V. (Eds.), *Domino Effects in the Process Industries: Modelling, Prevention and Managing.* Newnes. p. 179.

85. Landucci, G., Cozzani, V., & Brik, M. (2013). Heat radiation effects. In Reniers, G., & Cozzani, V. (Eds.), *Domino Effects in the Process Industries: Modelling, Prevention and Managing*. Newnes. pp. 71-86.

86. Paltrinieri, N., Landucci, G., Molag, M., Bonvicini, S., Spadoni, G., & Cozzani, V. (2009). Risk reduction in road and rail LPG transportation by passive fire protection. *Journal of hazardous materials, 167(1),* pp. 332-344.